REVUE ROUMAINE DE CHIMIE (ROUMANIAN JOURNAL OF CHEMISTRY)

Tome 52, N^o 3 **Mars 2007**

REVIEW

PAPERS

Silvia IMRE, Laurian VLASE and Sorin LEUCUȚA

HPLC method for quantification of nizatidine and its N-desmethylmetabolite in human plasma

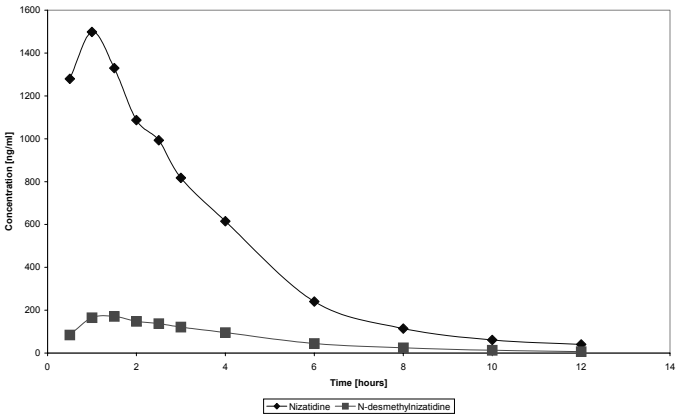

Rev. Roum. Chim., **2007**, *52*(3), 261-266

Key words: nizatidine, N-desmethylnizatine, plasma, HPLC, bioequivalence.

Marcela MIHAI and Ecaterina Stela DRĂGAN

Formation and colloidal stability of some polyelectrolyte complex dispersion based on random copolymers of AMPS

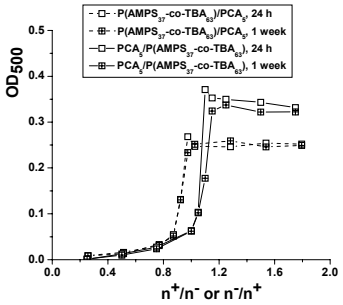

Rev. Roum. Chim., **2007**, *52*(3), 267-273

Key words: polyelectrolyte complex dispersions; polyions concentration; turbidity; specific viscosity; colloidal stability.

Maria Nicoleta GRECU, Gabriela BURDUCEA, Voicu GRECU, Rodica MOLDOVAN, Traian BEICA and Irina ZGURA

Temperature dependence of the alkyl chain ordering in two lyotropic systems

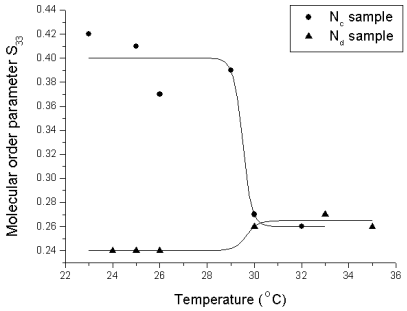

Rev. Roum. Chim., **2007**, *52*(3), 275-281

Key words: liquid crystals, lyotropic nematic, ESR, order parameter.

Mădălina-Nicoleta COBÂRLIE, Adriana IORDĂCHESCU, Ioan SĂNDULESCU et Ioan-Cezar MARCU

Étude de l'oxydeshydrogenation non catalytique de l'isobutane dans un reacteur integral

Study of non catalytic oxidehydrogenation of isobutane in an integral reactor

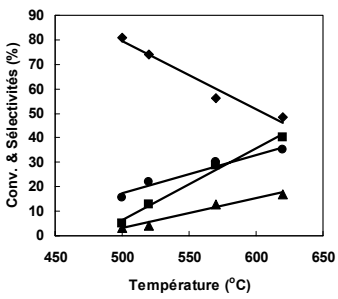

Rev. Roum. Chim., **2007**, *52*(3), 283-291

Key words: isobutane, non catalytic oxidehydrogenation, quartz .

Paul Gabriel ANOAICA and Costinel I. LEPĂDATU

QSAR study for classes with a broad range of biological activity using electronegativity descriptors for OMO-UMO quantum states. Clotrimazole imidazole derivatives with antifungal activity

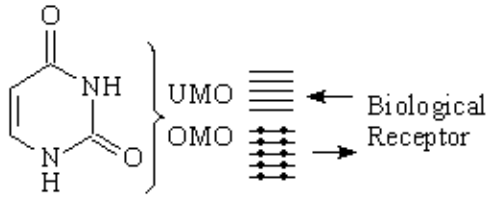

Rev. Roum. Chim., **2007**, *52*(3), 293-297

Key words: QSAR, electronegativity, hardness, OMO – UMO quantum states, fingerprint descriptors.

NOTE

Ludovic SAYTI, Valentin Careja, Simona MUNTEAN, Ramona TUDOSE, Otilia COSTIŞOR and Zeno SIMON

Quantum chemistry computation of stability of cobalt-hexamine ion in aqueous solution. An atempt

$$Co(OH_2)_6^{3+} + 6\ NH_3 \rightleftharpoons Co(HN_3)_6^{3+} + 6\ H_2O$$

ΔG_{calc} = -21.25 kcal/mol
ΔG_{exp} = -31.8 kcal/mol

Rev. Roum. Chim., **2007**, *52*(3), 299-300

Key words: cobalthexamine ion, stability constant, water solution, ab initio 3-21g, polarisable continuum method.

Revue Roumaine de Chimie, **2007**, *52*(3), 219–234

REVIEW

CHEMICAL FLUORINATION OF ORGANIC COMPOUNDS

Vasile DINOIU[a*]

[a]Roumanian Academy, Institute of Organic Chemistry "C. D. Nenitzescu", Spl. Independentei 202B, 77141 Bucharest, Roumania

Received August 3, 2006

This review covers the recent remarkable advances in chemical fluorination of organic compounds such as olefins, aromatic compounds, carbonyl compounds, heteroatom compounds and heterocycles. Mono-, di- and trifluorination are discussed.

INTRODUCTION

Very few fields in chemistry have shown such a considerable interest as fluoroorganic chemistry. Fluorine is perhaps the element that has experienced the greatest recent interest as pointed out by the exceptionally high number of publications and the high percentage of fluorinated new molecules over recent decades.[1] Today, the significant expansion in the use of fluorinated chemicals has attracted the attention of organic, agricultural, medicinal, and material chemists.[2-10] The replacement of hydrogen by fluorine, the most electronegative element, alters sterically and electronically the properties of the molecules, affecting the basicity or acidity of neighboring groups, dipole moment, and overall reactivity and stability. Fluorine is often regarded as an isostere of hydrogen despite the fact that their van der Waals radii are different (1.47 versus 1.20 Å).[11] The carbon-fluorine bond length (1.39 Å) is similar to the carbon-oxygen one (1.43 Å), suggesting an isosteric behavior. The high carbon-fluorine bond energy (485.7 kJ/mol)[12] confers relative stability against metabolic transformations. In addition, fluorine can participate in hydrogen bonding interactions with H-C even if hydrogen bonds to C-F are definitely much weaker than those observed to oxygen or nitrogen.[13,14] Nevertheless, the controversy remains on the existence of hydrogen bonds between the C-F group and -OH or -NH donors.[15-17] With regard to the CF_3 group, its size (van der Waals volume) is relatively large, between those of the *i*-Pr and the *t*-Bu groups.[18] The CF_3 group has an electronegativity similar to that of oxygen[19] and a large hydrophobic parameter.[20] The trifluoromethyl group appears in many biologically active pharmaceutical and agrochemical compounds. The increased lipophilicity and a superior metabolic stability compared to that of the trimethyl analogues, often accounts for an improved activity profile. Higher fluoroalkyl groups, which are the perfluoroalkyl groups, are introduced mainly to increase the lipophilicity, and also in the context of fluorous chemistry.[21]

Partially fluorinated organic compounds are prepared by two different approaches: (i) by insertion of a group already containing C-F bonds into an existing molecule (the building-block approach), or (ii) by creating new C-F bonds by fluorination.

MONOFLUORINATION OF ORGANIC COMPOUNDS

Electrophilic fluorination is one of the most direct methods for selective introduction of fluorine into organic compounds. Elemental fluorine, F_2, itself is one of the most powerful reagents.[22] However, fluoroxy compounds, such as CF_3OF[23], $FClO_3$,[24] CF_3COOF,[25] CH_3COOF,[26] and $CsSO_4F$[27], some of which are generated in situ, are exciting reagents for the introduction of fluorine electrophilically into a wide variety of organic compounds.

* E-mail address: vdinoiu@yahoo.com

The rather hazardous perchloryl fluoride has lost favor to other electrophiles, including xenon difluoride, XeF_2, which has been employed as a particularly interesting and easily handled source of electrophilic fluorine. [28]

More recently, much attention has been given to new N-F, C-F, or S-F compounds that are generally somewhat less reactive than the fluoroxy reagents described above, but nevertheless they have proved to be particularly useful with a wide range of organic nucleophiles.

DAST (Diethylaminosulfur trifluoride), Et_2NSF_3

DAST (Fig. 1) has proven to be an extremely popular reagent for nucleophilic fluorination, due to its ease of handling and versatility. It has regularly been employed in selective fluorination of alcohols, carbohydrates, ketones, sulfides, epoxides, thioethers and cyanohydrins. In addition some novel organic cyclizations are possible when DAST was used as a reagent.[29] For example, 1,2,2-trifluorostyrene can be synthesized using a sequential reaction on the parent α-(trifluoromethyl)phenylethanol with DAST, followed by dehydrohalogenation with lithium bis(trimethylsilyl)amide (LHMDS). This method achieves the trifluorostyrene without requirement of palladium coupling (Scheme 1).[30]

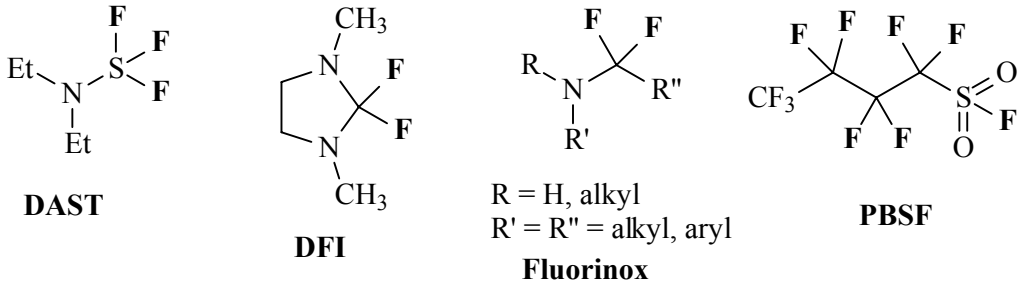

Fig. 1

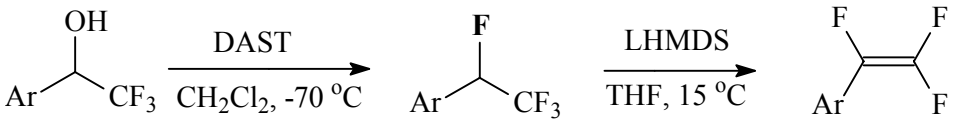

Scheme 1

Because DAST is made from very toxic and corrosive SF_4 and decomposes spontaneously, new milder and more stable fluorinating reagents were developed. Perfluoro-1-butanesulfonyl fluoride (PBSF) is a nontoxic, easily handled reagent used in the stereoselective substitution of an alcohol by fluorine, on a highly functionalized chiral substrate.

Fluorinox and DFI (Fig. 1), like DAST, exchange fluorine for hydroxyl groups but they are more stable.

DEOXOFLUOR $[(CH_3OCH_2CH_2)_2NSF_3]$

The Deoxo-Fluor™ reagent, (Fig. 2), is a versatile, easy-to-use, nucleophilic fluorinating reagent with enhanced safety features. It rapidly "deoxofluorinates" a wide variety of alcohols, aldehydes, ketones and sulfoxides under mild conditions to yield the corresponding fluorinated compounds with high efficiency and selectivity. Various fluorinated chiral compounds were synthesized by the reactions of amino alcohols with bis(2−methoxyethyl)aminosulfur trifluoride (Deoxofluor) (Scheme 2).[31]

SELECTFLUOR

More recently, much attention has been given to the fluoronitrogen compounds. Selectfluor, 1-chloromethyl-4-fluoro-1, 4-diazoniabicyclo[2.2.2] octane bis-(tetrafluoroborate) or F-TEDA (Fig. 2) is a user-friendly, mild, air- and moisture-stable, non-volatile reagent for electrophilic fluorination in one step, with excellent regioselectivity. An example is the regioselective fluorination of pyrimidine bases (Scheme 3).[32]

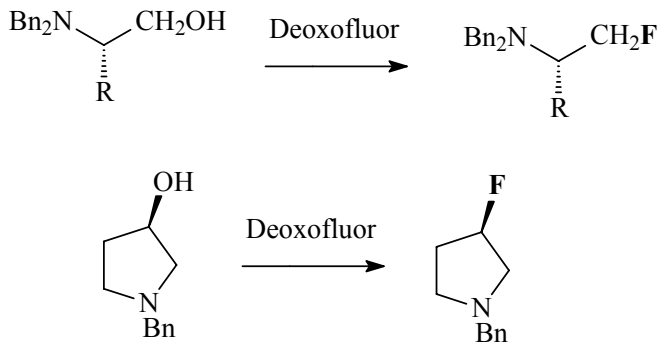

Scheme 2

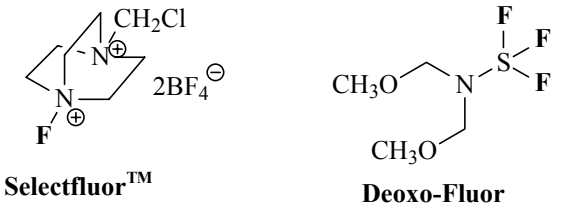

Fig. 2

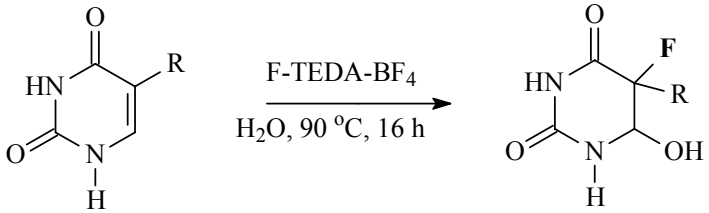

Scheme 3

Recently, a synthesis of a potent and noncytotoxic nucleoside inhibitor of Hepatitis C virus RNA application was accomplished using Selectfluor (Scheme 4). This ribonucleoside shows a significantly improved enzymatic stability profile compared to the parent 2'-C-methyladenosine.[33]

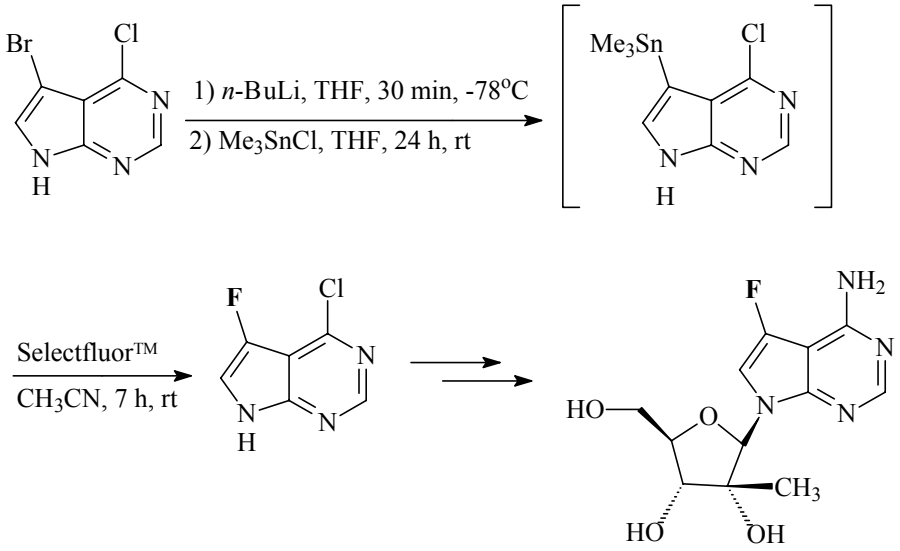

Scheme 4

Selectfluor is considered a good alternative to harsher methods, especially for high-value compounds. The electrophilic reagent acts essentially as a stoichiometric source of F^+ and can fluorinate specific positions in a range of substrates.

Selectfluor and Deoxo-Fluor were created to deliver fluorine to the pharmaceutical industry through a safe and effective material. Deoxo-Fluor is an easy-to-use, stable liquid that is cost-efficient and more amenable than DAST to large-scale applications. Similarly, Selectfluor consists of thermally stable, free-flowing crystals.

IODOTOLUENE DIFLUORIDE - a new and mild fluorination reagent

Elemental fluorine and many electrophilic fluorinating agents have been used in synthesis; however, most of these fluorinating agents are highly aggressive, unstable, and require special equipment and care for safe handling. By contrast, iodotoluene difluoride (tol-IF_2) is easy to handle, and is less toxic than many fluorinating agents.

A new methodology for the synthesis of fluorinated cyclic ethers was recently reported, which utilized tol-IF_2 to achieve a fluorinative ring-expansion of four-, five-, and six-membered rings, an example of which is illustrated below (Scheme 5).[34]

Selective monofluorination of β-ketoesters, β-ketoamides, and β-diketones takes place without requirement of HF-amine complexes under mild conditions (Scheme 6). The formation of difluoro products were not detected in these reactions.[35]

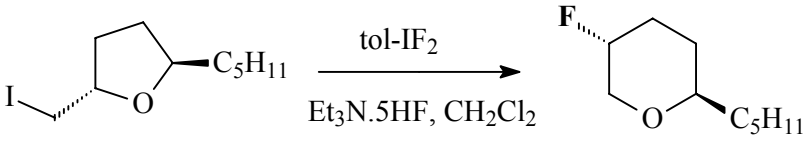

Scheme 5

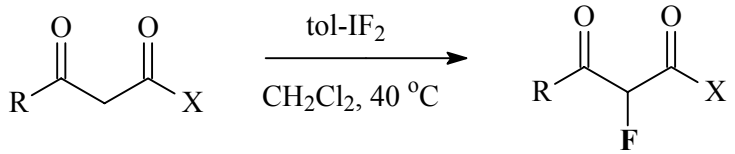

X = R', OR', NR'_2

Scheme 6

N-FLUOROPYRIDINIUM SALTS

The *N*-fluoropyridinium salts are particularly useful as electrophilic fluorinating agents toward organic compounds in terms of easy handling and variability of fluorinating power and selectivity. This variability makes selective fluorination of a wide range of organic compounds differing in reactivity possible. Three classes of power- and selectivity-variable fluorinating agents, non-counterion-bound *N*-fluoropyridinium salt series, counterion-bound *N*-fluoropyridinium-sulfonate series, and dimeric *N,N*'-difluorobipyridinium salt series, were developed and successfully utilized for selective fluorinations of various substrates.

N-Fluoropyridinium trifluoromethanesulfonate (triflate) and its analogs (Fig. 3) are widely applicable, stable fluorinating agents with varying degrees of power and selectivity in fluorinations.[36-45] The reagents are all stable, crystalline materials and thus can be handled routinely. It should be noticed that the relative stability of the *N*-fluropyridinium salts decreases with increasing fluorinating power. Examples of fluorinations which illustrate their use are given in Table I. The weakest reagent, **2**, is most suited for fluorinating reactive or easily oxidized compounds, such as carbanions, enamines, and sulfides, whereas the most potent reagents **4** and **5** are preferred for fluorinating alkenes and aromatic rings.

N-Fluoropyridinium triflate shows high regioselectivity in its fluorinations, as evidenced by the results in Scheme 7.[46] With steroids **6** and **8**, each having two reactive sites, **1** reacts to give exclusively the 6-fluoro steroid **7** and the 16-fluoro steroid **9**, respectively. Thus **1** can distinguish between a conjugated and a nonconjugated vinyl acetate, and between an enol silyl ether and a

conjugated vinyl acetate in its fluorinations. The present procedure for converting estrone enol silyl ether to 16α-fluoroestrone also shows that **1** selectively reacts with an enol silyl ether moiety in the presence of an activated aromatic ring.

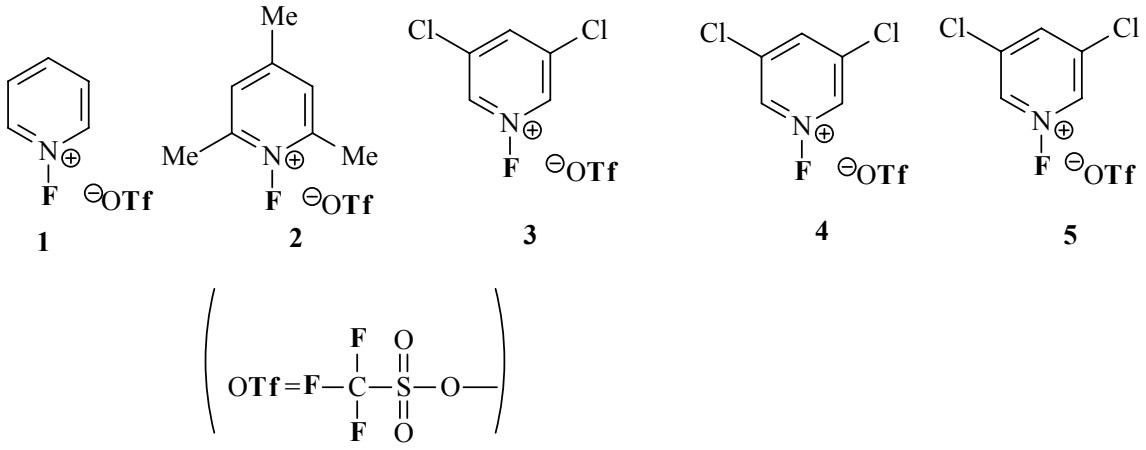

Fig. 3

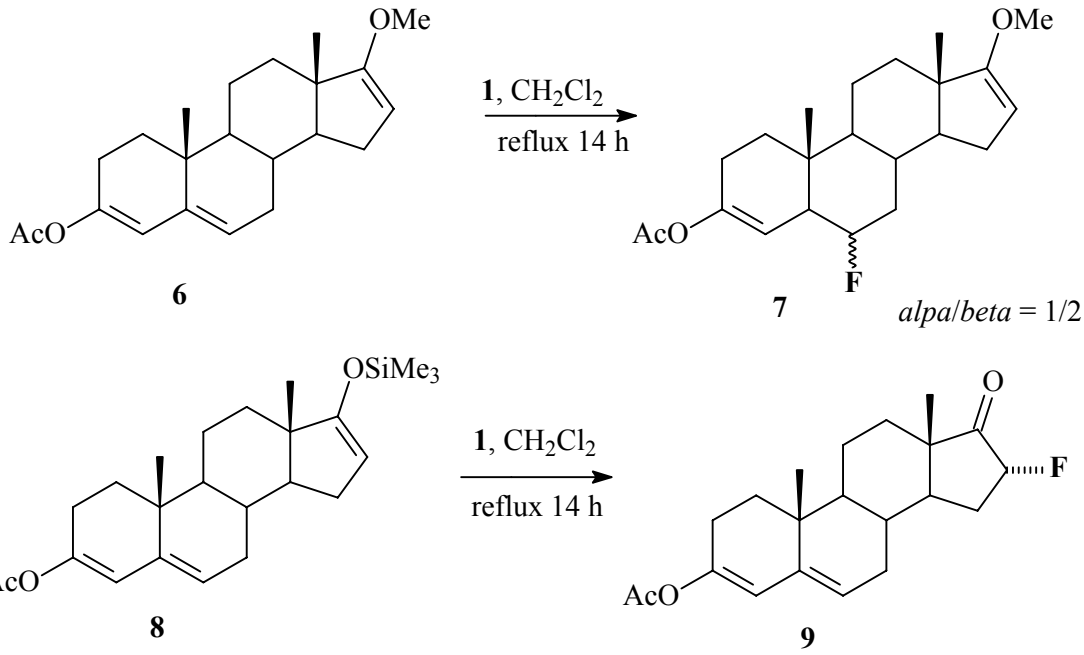

Scheme 7

HALOGEN EXCHANGE, a selective aliphatic fluorination by in mild conditions

Fluorine–chlorine exchange is the most widely used technology to synthesize fluorinated molecules. When this exchange reaction occurs in an aliphatic molecule or at the benzylic position, anhydrous hydrogen fluoride is the most versatile industrial reagent. The limitation of this technology comes from the acidity of anhydrous HF. Its use on fragile or functionalized molecules is limited due to formation of cationic intermediates and undesired side reactions. Alternatives to or improved versions of traditional fluorination reagents are being developed by companies with fluorine chemistry expertise. The early fluorinating reagent pyridinium poly(HF), or Olah's reagent, was discovered by Nobel Laureate George A. Olah

in the late 1970s. Since then, many other nitrogen-based structures have emerged; with the general form $R_2N{-}F$ or $R_3N^+{-}F$, they are often called the N-F or $[N\text{-}F]^+$ reagents, respectively.

Daikin Industries offers several derivatized pyridinium compounds in lab and bulk scale, including *N,N′*-difluoro-2,2′-bipyridinium bis(tetrafluoroborate). DuPont makes *N,N*-dimethyl-1,1,2,2-tetrafluoroethylamine (TFEDMA), the dimethylamine adduct of tetrafluoroethylene (TFE), available on a research scale. Mitsui Chemicals, which makes fluorinated materials for electronics applications, also sells 2,2,-difluoro-1,3-dimethylimidazolidine (DFI), which exchanges hydroxyl groups and carbonyls for fluorine, as a low-cost and more stable alternative to DAST.

In a paper published in 2006, Laurent Saint-Jalmes[47] reported new fluorinating reagents based on HF-Base media, in particular $(HF)_{10}$-pyridine or $(HF)_3$-triethylamine that allow aliphatic chlorine–fluorine exchanges on acid-sensitive molecules without side reactions involving carbocation intermediates. Depending on the nature (pyridine or triethylamine), stoichiometry of the base and temperature, selective mono-, di-, or tri-chlorine–fluorine exchanges on trichloromethyl groups alpha to sulfur, oxygen and carbon atoms can be obtained. For example the use of $(HF)_{10}$-pyridine and $(HF)_3$-triethylamine on trichloromethylbenzyl sulfide **1** give the results shown in Scheme. Trichloromethylbenzyl sulfide **1** is totally fluorinated at 20 °C in 18 h in $(HF)_{10}$-pyridine (40 molar equivalents of HF) and leads to trifluoromethylbenzyl sulfide **2** with 94% selectivity (^{19}F NMR assay) and 85% isolated yield. Surprisingly $(HF)_3$-triethylamine (50 molar equivalents of HF) leads to selective fluorination on trichloromethylbenzyl sulfide **1** through exchange of one or two chlorine atoms depending on the temperature; at 20 °C in 4 h monofluorodichlorobenzyl sulfide **3** is obtained with 90% selectivity, at 50 °C in 10 h difluorochlorobenzyl sulfide **4** is obtained with 88% selectivity (Scheme 8). These results are in accordance with the lower acidity of $(HF)_3$-triethylamine compared to $(HF)_{10}$-pyridine; the less acidic is the medium of fluorination the lower is the rate of chlorine–fluorine exchange.

Recently, chemistry Professor Stephen G. DiMagno at the University of Nebraska, Lincoln, USA, has used tetrabutylammonium fluoride (TBAF) for Halex and fluorodenitration reactions.[48] His group found that anhydrous $TBAF_{anh}$ in dimethylsulfoxide works well under mild conditions as a fluorinating reagent for activated ring systems (Scheme 9). The results suggest that ion pairing and solvation are the factors that limit the impressive nucleophilicity of the fluoride ion under conditions typically employed for nucleophilic aromatic substitution.

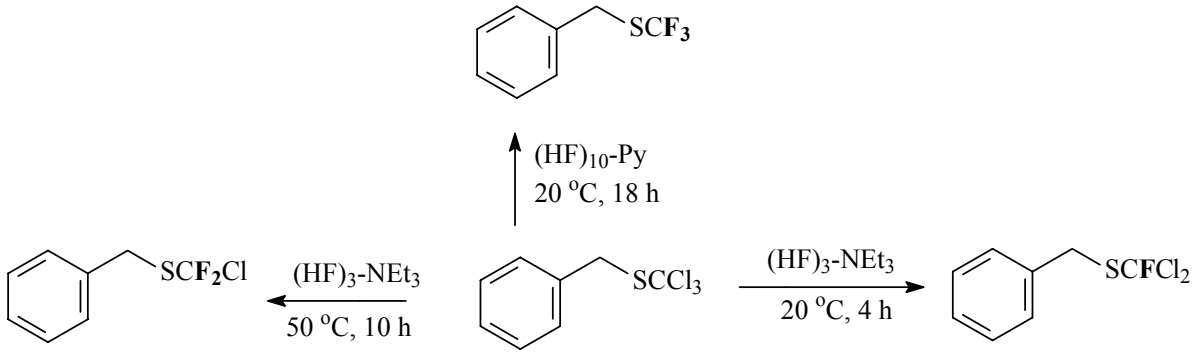

Scheme 8

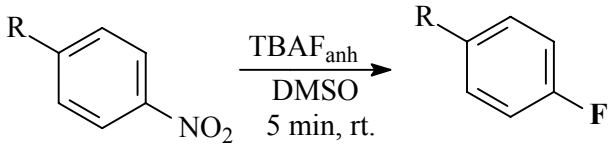

R = COOEt, CN, CF_3, F, H, Me

Scheme 9

In 2005, Satoshi Takei from Daiichi Pharmaceutical Company, Research Center, presented at ACS Meeting, San Diego, California, March 13-17, an interesting fluorination with TBAF as fluorinating reagent in synthesis of DC-756, a new potent quinolone antibacterial agent.[49] The synthesis of DC-756 required the development of the preparation of the key building block pyrrolodine. Carbamateon 3-amino group was suitable for fluorination by TBAF (Scheme 10).

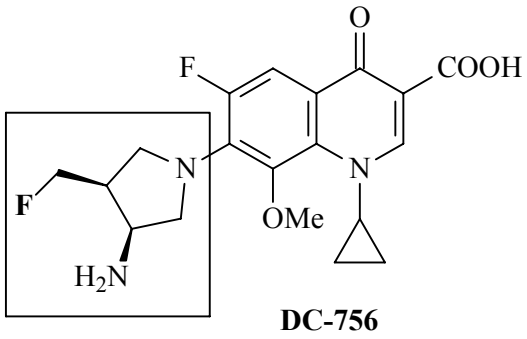

DC-756

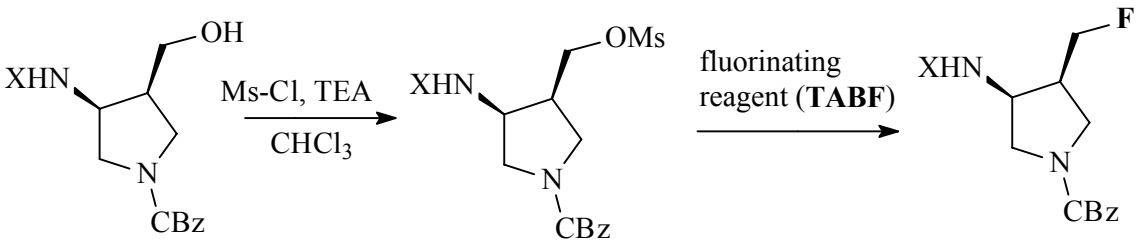

Scheme 10

ELECTROPHILIC ENANTIOSELECTIVE FLUORINATION

An important part of the advances in fluorination of organic compounds was the development of the enantioselective fluorination reactions, especially those that proceed by electrophilic mechanisms. Since the initial report over 10 years ago of the first examples of enantioselective halogenating reagents crystalline, optically pure N-fluoro sultams, these have been studied extensively. An asymmetric fluorination of enolates[50] is presented in Scheme 11.

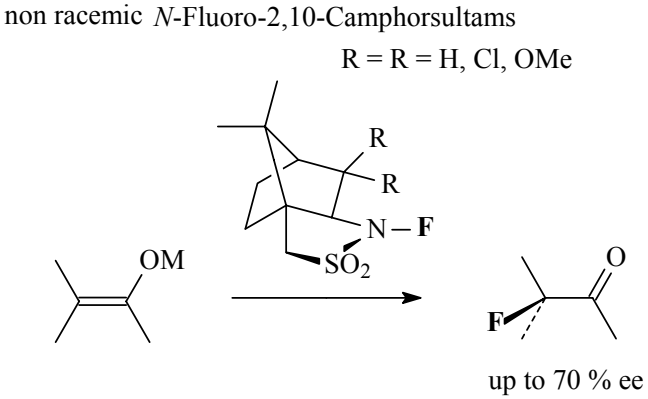

Asymmetric Fluorination of Enolates with Nonracemic N-Fluoro-2,10-Camphorsultams

Scheme 11

Thus unprecedented enantiomeric excesses up to 70% are observed when various prochiral metal enolates are fluorinated by using these new reagents. These initial efforts revealed several limitations in both the chemical yields and enantioselectivities of the fluorinated products using these first-generation chiral reagents. Recent advances in methodology of electrophilic enantioselective fluorinations have led to significant improvements over the past few years, and now enantioselectivities of 90% ee have been reached. In 1999, Takeuchi et al. used *N*-Fluoro-3-cyclohexyl-3-methyl-2,3- dihydrobenzo[1,2-*d*]isothiazole 1,1-Dioxide as an efficient agent for electrophilic asymmetric fluorination of enolates (Scheme 12).[51]

In the last years, reactions in which chiral stoichiometric reagents generated stereogenic centers in achiral substrates were performed. More recently, transition-metal catalysts and organocatalysts have emerged for enantioselective reactions.[52]

In 2003, the first practical application of enantioselective fluorination systems for the synthesis of chiral medically important fluorinated compounds was reported by Japanesse chemists.[53] They synthesized fluorooxindole ***S*-1** using as catalyst *N*F-$(DHQD)_2$PYR and tests for treatment of acute ischemic stroke are currently in progress. Fluorination occurred to produce ***S*-1** with 84% ee, and recrystallization produced enantiomerically pure (>99% ee) product (Scheme 13). (***S*-1**) is a chiral, nonracemic compound, a key structural feature of which is the fluorine atom bonded to the asymmetric quaternary carbon center at C3 in the oxindole ring.

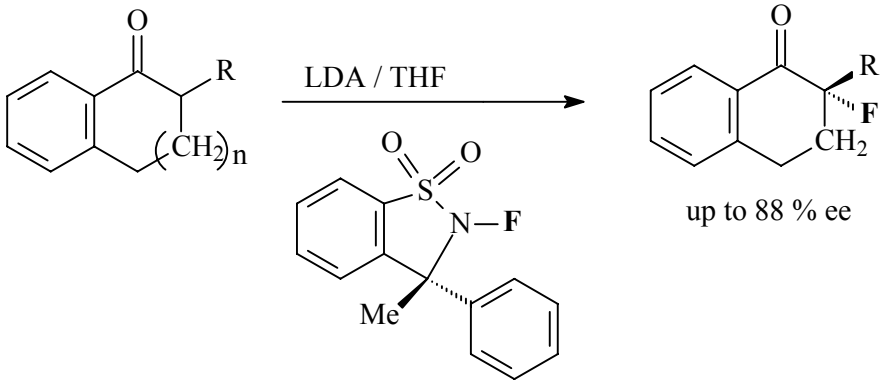

Scheme 12

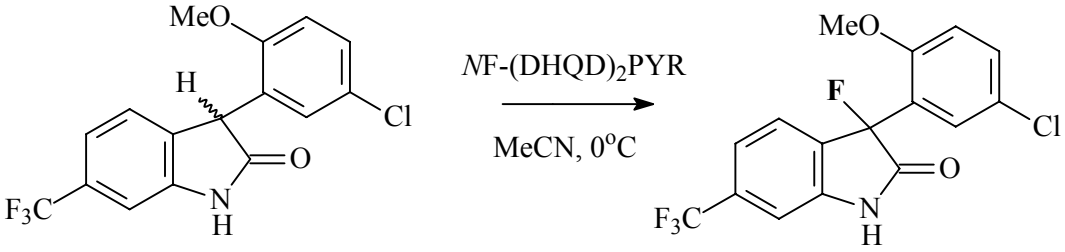

fluorooxindole S-1

Scheme 13

Antonio Togni and his group[54] (the Swiss Federal Institute of Technology, Zurich) achieved the first catalytic enantioselective electrophilic fluorination. They found that Selectfluor in the presence of titanium complexes can fluorinate β-ketoesters in high yield and with high enantiomeric excess. They found that Selectfluor in the presence of titanium complexes can fluorinate β-ketoesters in high yield and with high enantiomeric excess. Solvias now has rights to this technology. Since then, other transition-metal catalyst/fluorinating reagent combinations were used, as palladium, nickel or zinc complexes. Despite these successes, catalytic enantioselective

fluorination has been limited to 1,3-dicarbonyls and β-ketophosphonates; the substrate scope is still quite limited, with carbonyls being needed to coordinate to the metal catalysts. Few synthetic routes have been developed for the preparation of homochiral fluorinated building blocks other than α-fluorinated carbonyl compounds.

V. Gouverneur et al.[55] used fluorodesilylstion with Selectfluor of acyclic homochiral allylsilanes to produce enantiopure β-fluorinated-α-substituted carboxylic acids with an allylic monofluorinated stereogenic center (Scheme 14).

To obtain a chiral center bearing a CF_3 moiety, the nucleophilic addition to a trifluoromethylcarbonyl group was used. Good results have been obtained using chiral substrates and the trifluoromethylating reagent $CF_3Si(CH_3)_3$, or TMS-CF_3. Commonly called Ruppert's reagent, (prepared by Ingo Ruppert and coworkers in 1984 at University of Bonn, Germany, and now call as Ruppert-Prakash reagent, after G. K. Surya Prakash[56] at the (University of Southern California) who found its utility as a stable source of the nucleophilic trifluoromethyl anion. Since 1989, TMS-CF_3, trifluoroacetamides[57] and hypervalent iodine reagents (Fig. 4) have been widely used for the trifluoromethylation of carbonyl compounds and other substrates.

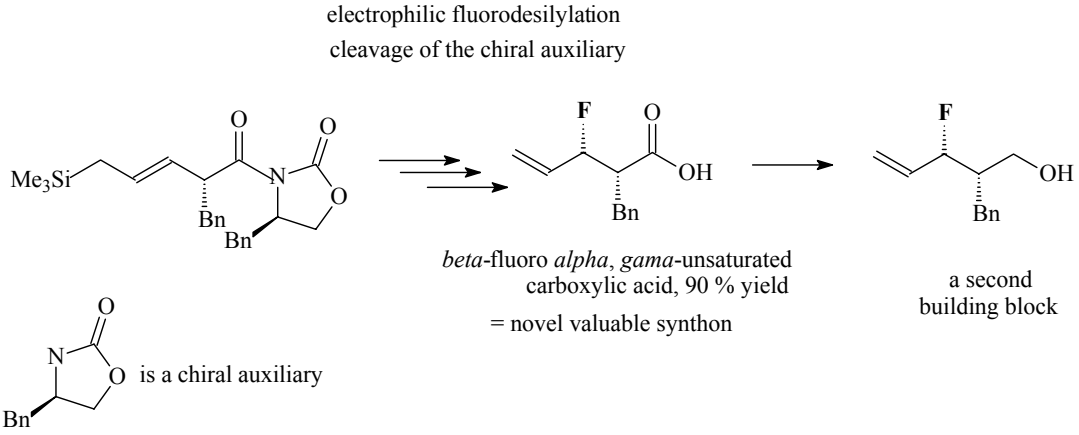

Scheme 14

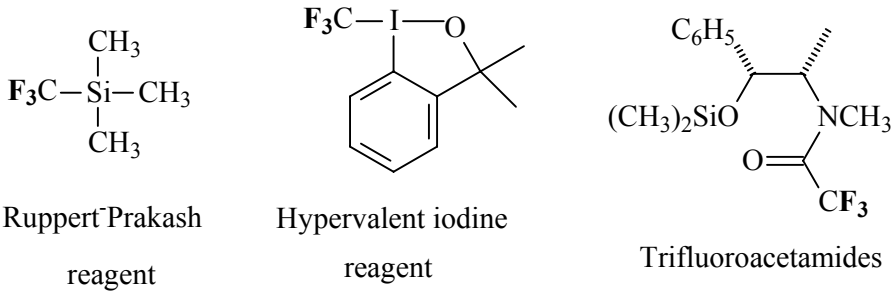

Fig. 4

DIFLUORINATION

Selective introduction of difluoromethyl group (CF_2H) into organic molecules is of great importance due to its ability to contribute special biological properties to those molecules. CF_2H functionality has been known to be isosteric and isopolar to hydroxyl (OH) group and behaves as a hydrogen donor through hydrogen bonding.[58-62] Moreover, CF_2H group has similar high lipophilicity as the trifluoromethyl group, which is useful in applications where a more lipophilic hydrogen bond donor other than OH is required.[60] As a result, CF_2H group has been frequently incorporated into various biologically active compounds (such as enzyme inhibitors,[63] sugars,[64] pesticides,[65] and herbicides[66]) and materials (such as liquid crystals[67] and fluoropolymers[68]). Many CF_2H-containing compounds have also been used as anesthetics, including well-known desflurane and isoflurane.[69]

Several methods have been developed for the preparation of CF_2H-containing compounds, including the deoxofluorination of aldehydes using SF_4, DAST, or SeF_4,[70] nucleophilic fluorination of *gem*-bistriflates using TBAF,[72] fluorination of 1,2- or 1,3-dithianes using BrF_3 and other in situ-generated halogen fluorides,[62,72] adition of CF_2Br_2 into double bonds,[73] $S_{RN}1$ reaction between a nucleophile and CF_2HCl,[74] and hydrogenation of terminal 1,1-difluoroalkenes.[75] Nucleophilic introduction of a CF_2H building block into carbonyl compounds has been reported, using (difluoromethyl)dimethylphenylsilane,[76] (chlorodifluoromethyl)trimethylsilane,[60] or difluoromethyl phenyl sulfone[77] as the CF_2H precursor.

Some recent difluorinations are presented below.

The synthesis of α, α-difluoroamides via direct fluorination was recently reported using DAST as the fluorinating reagent in a one-pot reaction (Scheme 15) to give the corresponding difluoro compound; decreasing the molar ratio of DAST to substrate resulted in the formation of the respective α-ketoamide.[78]

Various fluorinated chiral compounds were synthesized using bis(2-methoxyethyl)aminosulfur trifluoride (Deoxofluor) as a nucleophilic fluorinating reagent; reaction with diols in methylene chloride at room temperature led to the formation of the corresponding fluoro derivatives in good yields (Scheme 16).[79]

Iodotoluene difluoride (tol-IF_2). Treatment of phenylsulfanylated lactams with one equivalent of iodotoluene difluoride (tol-IF_2) results in the unsaturated heterocycle in moderate to good yields. When two equivalents of the reagent were used, the lactams were fluorinated in the α- and β-positions resulting in the diastereomeric difluoride (Scheme 17).[80]

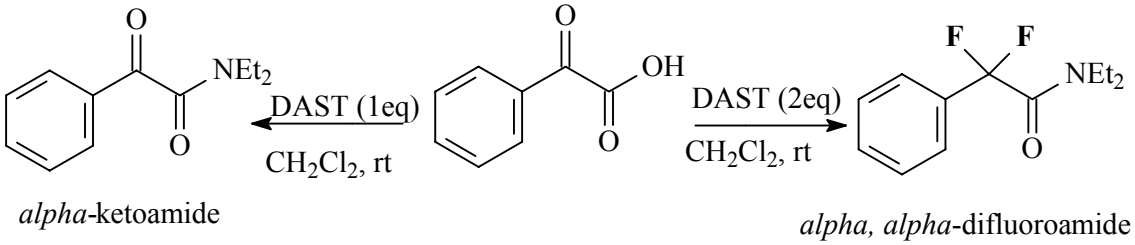

Scheme 15

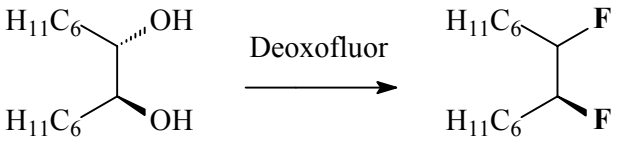

Scheme 16

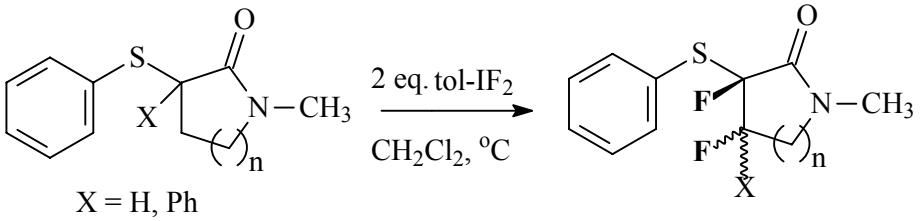

Scheme 17

Difluoromethyl Phenyl Sulfone ($PhSO_2CF_2H$). In 2003, Prakash, Hu and Olah (Loker Hydrocarbon Research Institute and Department of Chemistry, University of Southern California, Los Angeles, USA), reported the preparation of difluoromethylsilanes via the magnesium metal-mediated reductive difluoromethylation of chlorotrialkylsilanes using difluoromethyl phenyl sulfone ($PhSO_2CF_2H$) as difluorinating agent.[81]

In the next two years (2004-2005), Prakash, Olah and Hu[82, 83] reported a facile and efficient nucleophilic difluoromethylation of primary alkyl

halides (Scheme 18)[82] and carbonyl compounds.[83] that has been disclosed through a novel nucleophilic substitution-reductive desulfonylation strategy, using difluoromethyl phenyl sulfone as a difluoromethyl anion ("CF_2H^-") equivalent. This new synthetic methodology possesses many advantages, including convenience, cost, and efficiency, and promises to be a highly useful synthetic tool for many other potential applications.

J. Hu and C. Ni[84] reported the nucleophilic (phenylsulfonyl)difluoromethylation of (R)-(N-tert-butylsulfinyl)aldimines with difluoromethyl phenyl sulfone yielding the corresponding chiral α-difluoromethyl amines in excellent yields and with high diastereoselectivity (dr > 99%).

The two Chinese researchers reported also a new nucleophilic difluoromethylation chemistry using fluoride-induced (phenylsulfonyl) difluoromethylation with $TMSCF_2SO_2Ph$ followed by the magnesium-metal-mediated desulfonylation. This methodology is compatible with both enolizable and non-enolizable aldehydes and ketones and has special advantage in the case of enolizable aldehydes. The new efficient desulfonylation method is considered to be environmentally benign due to the absence of mercury (Scheme 19).[85]

Just recently, the first Lewis acid-catalyzed trifluoromethylation reactions of aldehydes with Me_3SiCF_3 under TiF_4/DMF, $Ti(O^iPr)_4$/DMF and $Cu(OAc)_2$/dppp/toluene conditions are described by Shibata et al.[86] They have successfully applied this methodology to the difluoromethylation of aldehydes using Me_3SiCF_2SePh, $Me_3SiCF_2P(O)OEt_2$ and Me_3SiCF_2SPh (Scheme 20).

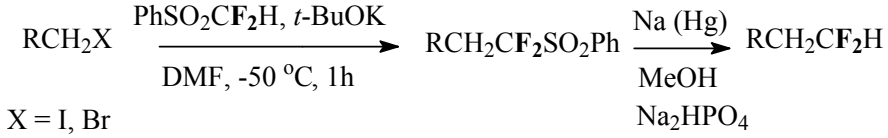

Scheme 18

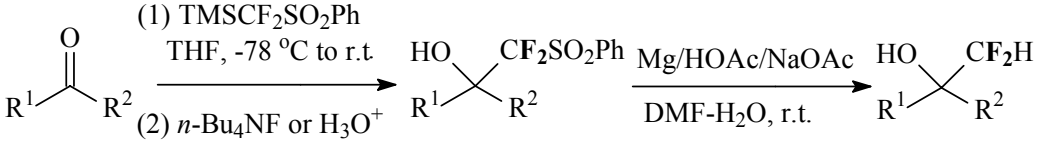

Scheme 19

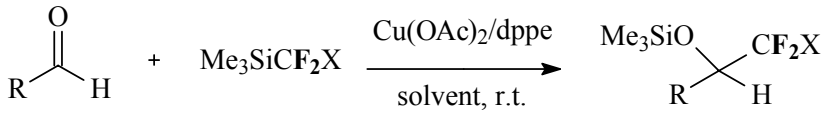

X = **F**, SePh, SPh, $P(O)(OEt)_2$

Scheme 20

NUCLEOPHILIC TRIFLUOROMETHYLATION REACTIONS

In 1989 Prakash and co-workers showed the trifluoromethylating properties of $(TMS)CF_3$ and the utilization of this compound as a nucleophilic trifluoromethylating agent has rapidly become the method of choice.[87-92] $(TMS)CF_3$ was used as a precursor to the trifluoromethide anion, which was liberated by activation with a fluoride source (nucleophilic initiator). Most commonly, tetraalkylammonium fluorides are used as initiators.

In 2001, G. K. Surya Prakash, Mihirbaran Mandal and George A. Olah reported the first examples of chiral trifluoromethylated allylic amines.[93] The trifluoromethide ion generated in situ from $TMSCF_3$ and TBAT (tetrabutylammonium triphenyldifluorosilicate), as well as TMAF (tetramethylammonium fluoride), adds to the *alpha*, *beta*-unsaturated *N*-*tert*-butanesulfinimines exclusively in a 1,2 fashion with high diastereoselectivities (Scheme 21).

Since the late 1990s, a series of nucleophilic trifluoromethylation methods, employing

fluoroform, fluoral, and trifluoroacetic and trifluoromethanesulfinic acid derivatives, as well as CF_3I and tetrakis(dimethylamino)ethylene (TDAE) have been developed. In 2001, Dolbier's group[94] from the University of Florida reported the method of using TDAE and CF_3I in an effort to develop a reagent that would be easy to use (Scheme 22).

In a convenient and efficient procedure, the nucleophilic trifluoromethylation of aldehydes with sodium trifluoroacetate was reported by Ying Chang and Chung Cai, using copper halides as the catalyst (Scheme 23).[95]

In 2006, B. Langlois et al.[96] reported the using of β-fluoroalkylated enones as dienophiles in Diels-Alder cycloadditions (Scheme 24).

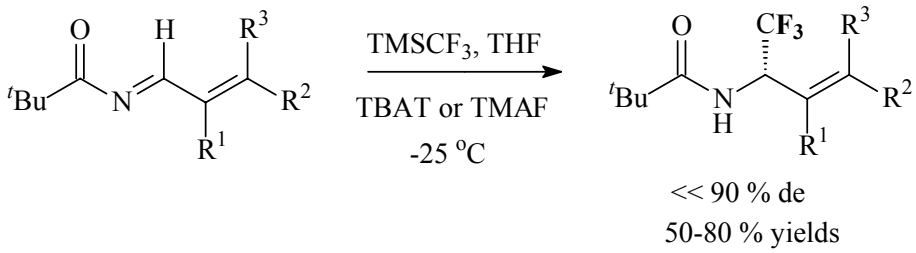

Scheme 21

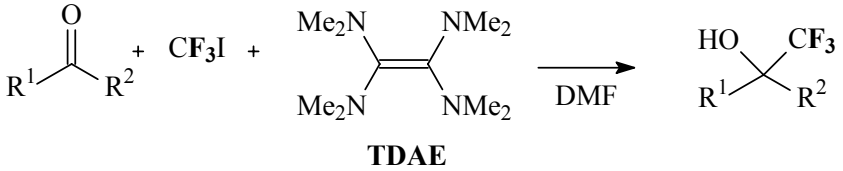

Scheme 22

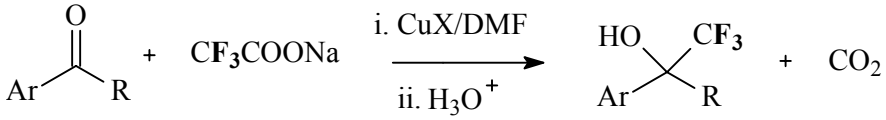

Scheme 23

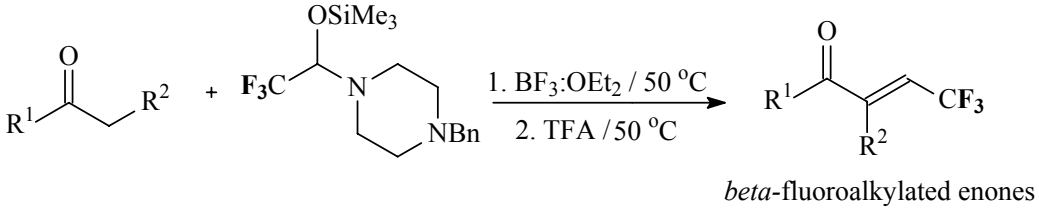

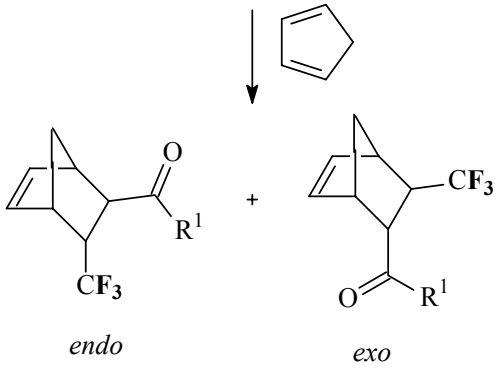

Scheme 24

FLUORINATED HETEROCYCLES

A strategically positioned fluorine in heterocyclic compounds, especially those containing trifluorometyl groups plays an important role in medicines and agrochemicals. Specifically, the fluorinated pyrazoles have been shown to possess high biologicalactivities as herbicides,fungicides, insecticides, analgesics, antipyretics and antiinflammatories.

Krishnaiah and B. Narsaiah reported a new synthetic methodology for the formation of trifluoromethyl substituted pyrazoles.[97] The 3-cyano-4-trifluoromethyl –6-phenyl 2(1H) pyridones (**1**) on reaction with hydrazine hydrate, gave exclusively in 5-trifluoromethyl – 3-substituted pyraxoles (**2**) through a novel method. A possible mechanistic pathway for change in the site of nucleophilic attack due to the CF_3 group in 2(*1H*) pyridones is described (Scheme 25).

V. Dinoiu[98] reported the synthesis of new CF_3–containing pyrazole and pyrazol-5-one derivatives, using the building block method, by reaction of 3,5-Dialkyl-4-hydroxybenzylhydrazine **4** with hexafluoroacetylacetone and trifluoroacetylacetone yielding the pyrazoles **5** bearing trifluoromethyl and/or methyl substituents in positions 3 and 5. The same hydrazine derivatives **4** afforded with trifluoroacetoacetic acid ethyl ester the pyrazol-5-one, which might have the tautomeric structures **6** or **7** (Scheme 26)

The synthesis by Duff formylation of a series of fluorinated benzaldehydes and their use in the Wittig synthesis of fluoro-substituted stilbenes (a series of fluorinated analogues of the anticancer drugs) is described by Lawrence et al.[99] (Scheme 27).

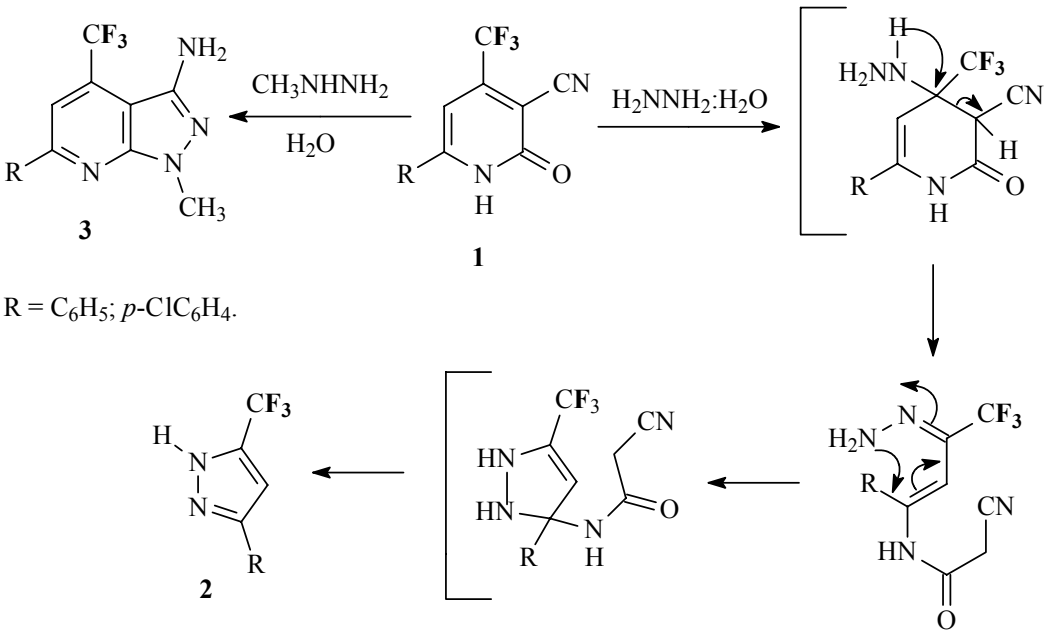

Scheme 25

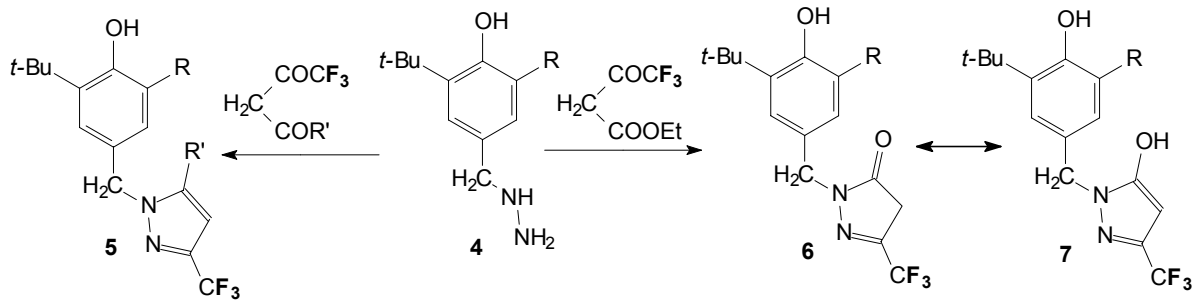

Scheme 26

[4+2]-Cycloadditions of cyclopentadiene with the monofluorinated dienophiles are exo-selective and yield cycloadducts (Scheme 28).[100]

In 2006, V. Dinoiu[101] reported the conversion of the perfluoroester (heptafluorobutanoic acid) into new pyridazin-3-ones and α,β-unsaturated lactams, as mixtures of diastereomers(Scheme 29). The building block method was used to obtain the corresponding CF_3-containing heterocycle derivatives in seven reaction steps, and a possible reaction mechanism was discussed. Starting from perfluoroester, it was synthesized perfluoroketene dithioacetal that is an excellent building block for the synthesis of new fluorinated heterocycles.[102]

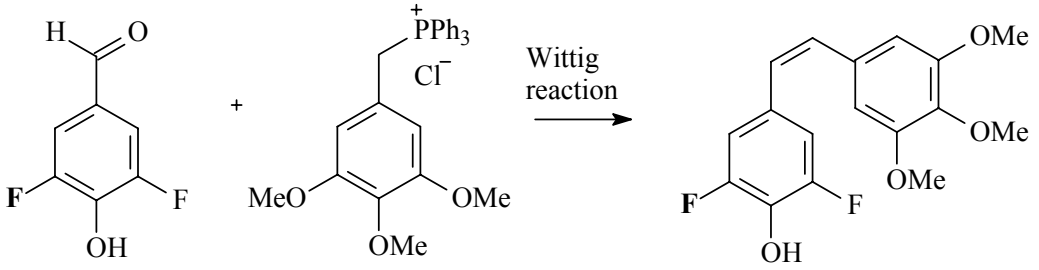

Scheme 27

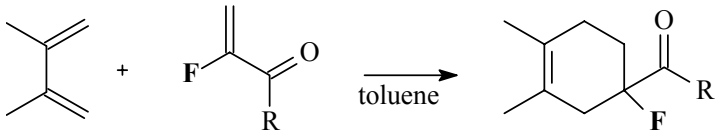

Scheme 28

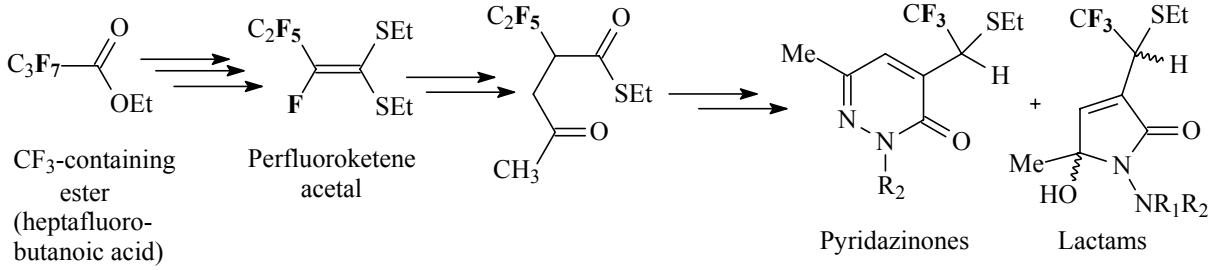

Scheme 29

HIGHER FLUORINATION

A chemoselective bis-trifluoromethylation of acyl chlorides using the CF_3I/TDAE-derived nucleophilic trifluoromethyl anion reagent was reported by Dolbier Jr. et al.[103] An ester product was obtained with very high yields by sequential nucleophilic bis-trifluoromethylation, followed by acylation of the resultant alcoholate (Scheme 30).

N,N-Diethyl-1,1,2,3,3,3-hexafluoropropylamine ($Et_2NCF_2CHFCF_3$), known as Ishikaya's reagent, displayed the ability to insert a fluoro(trifluoromethyl)methylene moiety in unsaturated alcohols (Scheme 31).[104]

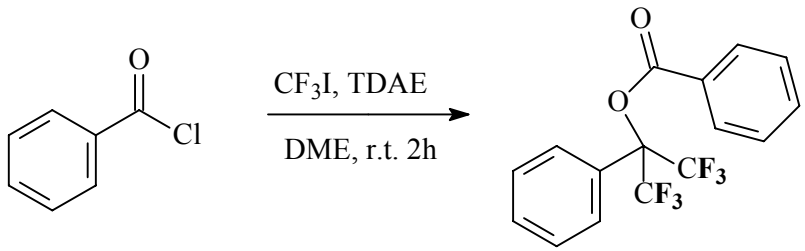

Scheme 30

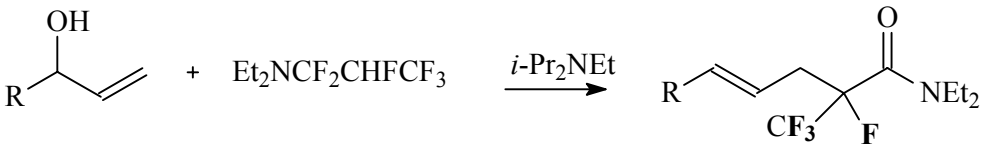

Scheme 31

CONCLUSIONS

The development of new fluorination reactions is expected to increase the availability of fluorine-containing structures and spark the interest of drug and agrochemical producers. As customers find it easier to explore having fluorine in their molecules, fine chemicals manufacturers hope demand for custom syntheses and building blocks will grow.

Fluorine chemistry has an important role to play in clean technology, both in catalyst and solvent replacement technologies. Fluorine is a very light element and provides excellent value in terms of activity-per-gram. It is also recognised that fluorochemicals are frequently more effective and are required in smaller quantities than non-fluorinated compounds-in the case of fluorine, 'less is more'. High effect, low dosage fluorinated formulations allow reductions in the use of materials and energy all along the production chain: less non-renewable feedstocks are consumed, transport and packaging is reduced, and the quantity of post-consumer waste is minimised.

Even though fluorochemicals have also been involved in some of the more negative aspects of the chemical industry, fluorine-containing compounds have a great potential for clean synthesis, and utilisation of the high activity that fluorinated groups can impart molecules may help to reduce the quantities required of certain classes of chemicals that are used in the biosphere, including pesticides and pharmaceuticals.

Acknowledgments: The author is deeply indebted to **JSPS Japan** for granting him a post-doc. fellowship at Hokkaido University, Sapporo, Japan, (1998-2000) and to **EGIDE France** for granting him a NATO post-doc. fellowship, at Rouen University, IRCOF, France, in 2005, in fluorine chemistry.

REFERENCES

1. H. Schofield, *J. Fluorine Chem.*, **1999**, *100*, 7.
2. R. Filler, Y. Kobayashi and Y. L. Yagupolskii, "Organofluorine Compounds in Medicinal Chemistry and Biological Applications", Elsevier, Amsterdam, 1993.
3. R. E. Banks, B. E. Smart and J. C. Tatlow, "Organofluorine Chemistry: Principles and Commercial Applications", Plenum Press, New York, 1994.
4. J. T. Welch, "Selective Fluorination", ACS Symposium Series 456, American Chemical Society, Washington, DC, 1991.
5. M. Hudlicky and A. E. Pavlath, "Chemistry of Organic Fluorine Compounds II. A Critical review", ACS Monograph 187, American Chemical Society, Washington, DC, 1995.
6. J. T. Welch, *Tetrahedron*, **1987**, *43*, 3123.
8. J. A. Wilkinson, *Chem. Rev.*, **1992**, *92*, 505.
9. J. Mann, *Chem. Soc. Rev.*, **1987**, *16*, 381.
10. "Biomedical Fontiers of Fluorine Chemistry", I. Ojima, J. R. McCarthy and J. T. Welch, Eds., American Chemical Society, Washington, DC, 1996.
11. A. Bondi, *J. Phys. Chem.*, **1964**, *68*, 441.
12. R. E Banks, *J. Fluorine Chem.*, **1998**, *87*, 1.
13. B. E. Smart, *J. Fluorine Chem.*, **2001**, *109*, 3
14. J. Parsch and J. W. Engels, *J. Am. Chem. Soc.*, **2002**, *124*, 5664.
15. J. D. Dunitz and R. Taylor, *Chem. Eur. J.*, **1997**, *3*, 89.
16. T. J. Barbarich, C. D. Rithner, S. M. Miller, O. P. Anderson and S. H. Strauss, *J. Am. Chem. Soc.*, **1999**, *121*, 4280.
17. D. D. DesMarteau, Z. Q. Xu and M. *J.* Witz, *Org. Chem.*, **1997**, *57*, 6629.
18. D. Seebach, *Angew. Chem., Int. Ed. Engl.*, **1990**, *29*, 1320.
19. J. E. Huheey, *J. Phys. Chem.*, **1965**, *69*, 3284.
20. M. A. McClinton and D. A. McClinton, *Tetrahedron*, **1992**, *48*, 6555.
21. J. A. Gladysz and D. P. Curran, "Fluorous chemistry", *Tetrahedron*, **2002**, *58*, Elsevier, New York.
22. S. T. Purrington and B. S. Kagan, *Chem. Rev.*, **1986**, *86*, 997.
23. D. Alker, D. H. R. Barton, R. H. Hesse, J. Lister-James, R. E. Markwell, M. M. Pechet, S. Rozen, T. Takeshita and H. T. Toh, *Nouv. J. Chim.*, **1980**, *4*, 239.
24. M. Schlosser and G. Heinz, *Chem. Ber.*, **1969**, *102*, 1944.
25. S. Rozen and O. Lerman, *J. Org. Chem.*, **1980**, *45*, 672.
26. S. Rozen, O. Lerman, M. Kol and D. Hebel, *J. Org. Chem.*, **1985**, *50*, 4753.
27. E. H. Appelman, L. J. Basile and R. C. Thompson, *J. Am. Chem. Soc.*, **1979**, *101*, 3384. 28. R. Filler, *Isr. J. Chem.*, **1978**, *17*, 71.
29. R. P. Singh and J. M. Shreeve, *Synthesis*, **2002**.2561.
30. R. Anilkumar and D. J. Burton, *Tetrahedron Lett*., 2003, 44, 6661.
31. R. P. Singh and J. M. Shreeve, *J. Fluorine Chem.*, **2002**, *116*, 23.
32. R.P. Singh and J. M. Shreeve, *Acc. Chem. Res*., **2004**, 37, 31.
33. A .B. Eldrup, *J. Med. Chem*., **2004**, *47*, 5284.
34. T. Inagaki, *Tetrahedron Lett.*, **2003**, *44*, 4117.
35. M. Yoshida, K. Fujikawa, S. Sato and S. Hara, *ARKIVOC*, **2003**, 36.
36. G. Tomizawa, *Bull. Chem. Soc. Jpn.,* **1986**, *59*, 3625.
37. T. Umemoto, S. Fukami, G. Tomizawa, K. Harasawa, K. Kawada and K. Tomita, *J. Am. Chem. Soc.*, **1990**, *112*, 8563.
38. T. Umemoto, K. Harasawa, G. Tomizawa, K. Kawada and K. Tomita, *Bull. Chem. Soc. Jpn.*, **1991**, *64*, 1081.

39. T. Umemoto, K. Harasawa, G. Tomizawa, K. Kawada and K. Tomita, *J. Fluorine Chem.*, **1991**, *53*, 369.
40. G. Tomizawa and T. Umemoto, *J. Fluorine Chem.*, **1991**, *54*, 205.
41. F. Oberdorfer, E. Hofmann, W. Maier-Borst, *J. Labelled Compd. Raidopharm.*, **1988**, *25*, 999.
42. I. Shimizu and H. Ishii, *Chem. Lett.*, **1989**, 577.
43. P. C. B. Page, F. Hussain, J. L. Maggs, P. Morgan and B. K. Park, *Tetrahedron*, **1990**, *46*, 2059.
44. M. Ihara, T. Kai, N. Taniguchi and K. Fukumoto, *J. Chem. Soc., Perkin Trans.*, **1990**, *1*, 2357.
45. A. J. Poss, M. van Der Puy, D. Nalewajek, G. A. Shia, W. J. Wagner and R. L. Frenette, *J. Org. Chem.*, **1991**, *56*, 5962.
46. T. Umemoto, K. Tomita and K. Kawada, *Organic Syntheses, Coll. Vol. 8,* **1993**, 286.
47. L. Saint-Jalmes, *J. Fluorine Chem*., **2006**, *127*, 85.
48. H. Sun and S. G. DiMagno, *Angew. Chem. Int. Ed*., **2006,** *45*, 2720.
49. S. Takei, "ACS Meeting, San Diedo, California, March 13-17, 2005, Tehnical Reports", Vol. 10, Nr. 15, pag. 6.
50. E. Differding and R. W. Lang, *Tetrahedron Lett*., **1998**, *29*, 6087-6090.
51. Y. Takeuchi, T. Suzuki, A. Satoh, T. Shiragami and N. Shibata, *J. Org. Chem*., **1999,** *64*, 5708.
52. S. Bruns and G.Haufe, *J. Fluorine Chem*., **2000**, *104*, 247.
53. N. Shibata, T. Ishimaru, E. Suzuki, and K. L. Kirk, *J. Org. Chem*., **2003**, *68*, 2494.
54. L. Hintermann and A. Togni, *Angew. Chem. Int. Ed*., **2000,** *39*, 4359.
55. M. Tredwell, K. Tenza, C. Pacheco and V. Gouverneur, *Org. Lett*., **2005**, *7*, 4495.
56. G. K. S. Prakash, J. Hu, and G. A. Olah, *J. Org. Chem*., **2003**, *68*, 4457.
57. J. Joubert, S. Roussel, C. Christophe , T. Billard, B. R. Langlois and T. Vidal, *Angew. Chem. Int. Ed*., **2003**, *42*, 3133.
58. "Fluorine in Bioorganic Chemistry", J. T., Welch and S. Eswarakrishnan, Eds., Wiley, New York, 1991.
59. "Modern Fluoroorganic Chemistry", P. Kirsch, Ed., Wiley-VCH, Weinheim, 2004.
60. A. K. Yudin, G. K. S. Prakash, D. Deffieux, M. Bradley, R. Bau and G. A. Olah, *J. Am. Chem. Soc.*, **1997**, *119*, 1572.
61. J. A. Erickson and J. I. McLoughlin, *J. Org. Chem.*, **1995**, *60*, 1626.
62. R. Sasson, A. Hagooly and S. Rozen, *Org. Lett.*, **2003**, *5*, 3635.
63. M. F. Parker, K. E. McElhone, R. A. Mate, J. J. Bronson, Y. Gai, C. P. Bergstrom, L. R. Marcin and J. E. Macor, WO 2003053912, 2003; *Chem. Abstr.*, **2003**, *139*, 85645.
64. (a) S. Kaneko, T. Yamazaki and T. Kitazume, *J. Org. Chem.*, **1993**, *58*, 2302. (b) S. J. Houlton, W. B. Motherwell, B. C. Ross, M. J. Tozer, D. J. Williams and A. M. Z. Slawin, *Tetrahedron,* **1993**, *49*, 8087.
65. M. Markl, W. Schaper, O. Ort, H. Jakobi, R. Braun, G. Krautstrunk, U. Sanft, W. Bonin, H. Stark, S. Pasenok and I. Cabrera, WO 2000007998, 2000; *Chem. Abstr.,* **2000**, *132*, 166248.
66. W. F. Groure, K. L. Leschinsky, S. J. Wratten and J. P. Chupp, *J. Agric. Food Chem.,* **1991**, *39*, 981.
67. T. Kondou, S. Matsui, K. Miyazawa, H. Takeuchi, Y. Kubo, F. Takeshita and E. Nakagawa, WO 9813324, 1998; *Chem. Abstr.,* **1998**, *128*, 302171.
68. "Fluorine-containing Molecules. Structure, Reactivity, Synthesis and Applications", J. F. Liebman, A. Greenberg and W. R. Dolbier, Jr., Eds., VCH, New York, 1988.
69. L. A. Rozov, C. Huang, D. F. Halpern and G. G. Vernice, U.S. Patent 5,283,372, 1994.
70. (a) W. J. Middleton, *J. Org. Chem.,* **1975**, *40*, 574. (b) G. A. Olah, M. Nojima and I. Kerekes, *J. Am. Chem. Soc.,* **1974**, *96*, 925.
71. G. A. Martinez, O. J. Barcina, A. Z. Rys and L. Subramanian, R. *Tetrahedron Lett.,* **1992**, *33*, 7787.
72. (a) S. C. Sondej and J. Katzenellenbogen, A. *J. Org. Chem.,* **1986**, *51*, 3508. (b) "Synthetic Fluorine Chemistry", G. A. Olah, R. D. Chambers and G. K. S. Prakash, Eds., Wiley, New York, 1992.
73. J. Gonzales, C. J. Foti and S. Elsheimer, *J. Org. Chem.,* **1991**, *56*, 4322.
74. (a) J. Hine and J. J. Porter, *J. Am. Chem. Soc.,* **1960**, *82*, 6178. (b) B. R. Langlois, *J. Fluorine Chem.,* **1988**, *41*, 247.
75. J. S. Houltona, W. B. Motherwell, B. C Ross,. M. J. Tozer, D. J. Williams and A. M. Z. Slawind, *Tetrahedron,* **1993**, *49*, 8087.
76. T. Hagiwara and T. Fuchikami, *Synlett*, **1995**, 717.
77. (a) G. P. Stahly, *J. Fluorine Chem.,* **1989**, *43*, 53. (b) G. K. S. Prakash, J. Hu, T. Mathew and G. A. Olah, *Angew. Chem., Int. Ed.,* **2003**, *42*, 5216.
78. R. P. Singh and J. M. Shreeve, *J. Org. Chem.*, **2003**, *68*, 6063.
79. R. P. Singh and J. M. Shreeve, *J. Fluorine Chem*., **2002**, *116*, 23.
80. M. F. Greaney, W. B. Motherwell and D. A Tocher, *Tetrahedron Lett.*, **2001**, *42*, 8523.
81. G. K. S Prakash,. J. Hu and G. A. Olah, *J. Org. Chem.*, **2003**, *68*, 4457.
82. G. K. S. Prakash, J. Hu, Y. Wang, and G. A. Olah, *Org. Lett*., **2004**, *6*, 4315.
83. G. K. S. Prakash, J. Hu, Y. Wang, and G. A. Olah, *Eur. J. Org. Chem*., **2005,** 2218.
84. J. Hu and C. Ni, *Angew. Chem. Int. Ed*., **2005,** *44*, 5882.
85. J. Hu and C. Ni, *Tetrahedron Lett*., **2005**, *46*, 8273.
86. S. Mizuta, N. Shibata, S. Ogawa, H. Fujimoto, S. Nakamura and T. Toru, *Chem. Commun.,* **2006**, 2575.
87. R. P. Singh and J. M. Shreeve, *Tetrahedron,* **2000**, *56*, 7613.
88. G. K. S. Prakash and M. Mandal, *J. Fluorine Chem.,* **2001**, *112*, 123.
89. J.-A. Ma and D. Cahard, *J. Org. Chem.,* **2003**, *68*, 8726.
90. G. P. Stahly and D. R. Bell, *J. Org. Chem.,* **1989**, *54*, 2873.
91. G. K. S. Prakash, R. Krishnamurti and G. A. Olah, *J. Am. Chem. Soc.,* **1989**, *111*, 393.
92. G. K. S. Prakash and A. K. Yudin, *Chem. Rev.,* **1997**, *97*, 757.
93. G. K. S. Prakash, M. Mandal and G. A. Olah, *Org. Lett.,* **2001**, *3*, 2847.
94. S. Ait-Mohand, N. Takechi, M. Médebielle and W. R. Dolbier, Jr., *Org. Lett*., **2001**, *3*, 4271.
95. Y. Chang and C. Cai, *Tetrahedron Lett*., **2005**, *46*, 3161.
96. J. Leuger, G. Blond, R. Fröhlich, T. Billard, G. Haufe and B. R. Langlois, *J. Org. Chem*., **2006**, *71*, 2735.
97. A. Krishnaiah and B. Narsaiah, *J. Fluorine Chem*., **2002**, *115*, 9-11.
98. V. Dinoiu, *Rev.Chim. (Bucharest),* 2005, *56*, 649.
99. N. J. Lawrence, L. A. Hepworth, D. Rennison, A. T. McGown and J. A. Hadfield, *J. Fluorine Chem.*, **2003**, *123*, 101.
100. M. Essers, T. Ernet and G. Haufe, *J. Fluorine Chem.*, **2003**, *121*, 163.
101. V. Dinoiu, *Rev. Roum. Chim*., **2006**, *in press*.
102. B. Hénin, J-F. Huot and C. Portella, *J. Fluorine Chem.,* **2001**, *107*, 281.
103. N. Takechi, S. Ait-Mohand, M. Medebielle and W. R. Dolbier, Jr., *Tetrahedron Lett.*, **2002**, *43*, 4317.
104. K-i. Ogu, *Tetrahedrom Lett*., **1998**, *39*, 305.

Revue Roumaine de Chimie, **2007**, *52*(3), 235–241

SYNTHESIS AND OPTICAL PROPERTIES OF TiS_2 NANOCLUSTERS

Alexandru L. LET,* David MAINWAING, Colin RIX and Pandiyan MURUGARAJ

School of Applied Science, Science, Engineering and Technology Portfolio, Royal Melbourne Institute of Technology, GPO Box 2476V, Melbourne, Vic-3001, Australia

Received May 22, 2006

High-quality, nano-sized clusters of TiS_2 have been successfully grown inside inverse micellar cages and their optical properties studied. The clusters exhibit large blueshifts in the optical-absorption features with decreasing cluster size due to quantum confinement, affording control of the absorption thresholds and a demonstration of the crossover from band-like to molecule-like spectra as the size of the clusters becomes smaller than that of the exciton in the bulk.

INTRODUCTION

In its most common form, bulk titanium disulphide (TiS_2) crystallizes in a hexagonal layered structure ($P3\bar{m}1$) consisting of one hexagonally packed sheet of metal atoms contained between two hexagonal sheets of chalcogens for each layer, where atoms within a layer are bound by strong covalent forces.

This structural arrangement leads to metal atoms surrounded by six chalcogen atoms in an octahedral environment (Fig. 1), resulting in weak chalcogen-chalcogen van der Waals interactions between adjacent layers with S-Ti-S sandwiches stacked along the c axis. (c=5.6912 Å).[1]

Titanium disulfide possesses one of the highest intercalation energies when lithium diffuses into the van der Waal's gap between sulfur layers and most research has focused on its use as the cathode material in lithium rechargeable batteries. This has arisen from the need to produce portable power supplies; as the computer, medical and other devices become smaller, there is a need to produce smaller storage batteries to power them. Other applications include its use as a solid state lubricant in space-borne vehicles, as a hydrogenation catalyst [2], and as a possible hydrogen storage material.[3]

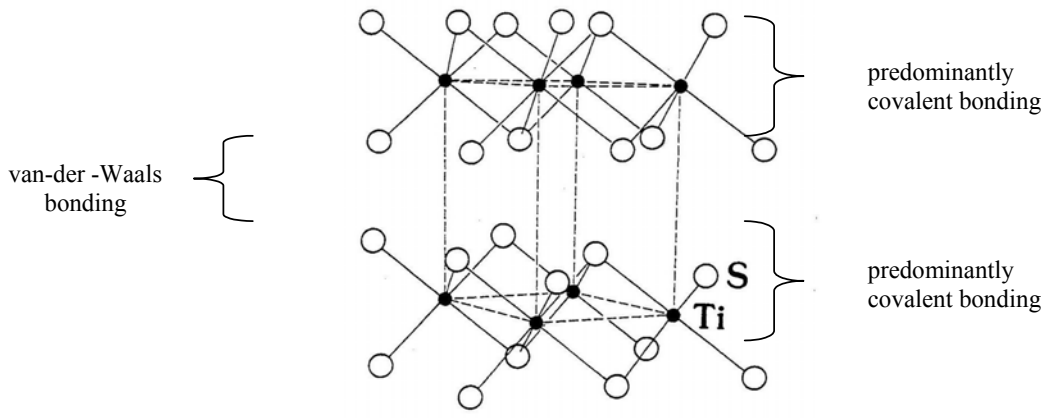

Fig. 1 – Structure of TiS_2.

* Corresponding author: alexandu.let@cap-xx.com

The bulk form of TiS_2 is optically opaque. Myron and Freeman[4] determined the electronic energy band structure of layered TiS_2 using the Korringa-Kohn-Rostoker (KKR) method and found it to behave as a semiconductor with a fundamental gap of 2.0 eV and a smaller indirect gap of 1.4 eV. The electronic spectrum of bulk TiS_2 has been studied extensively and consists of two main absorption bands between 0 and 3.5 eV.[5,6] The low energy band is centered around 2.3 eV with a width of 1.5 eV (as shown in Fig. 5, dotted line) and can be ascribed to electronic transitions from the upper p-bands into the lower triplet of non-bonding d-bands, followed by a window due to the separation between the lower non-bonding and the upper non-bonding d bands.

The optical and electronic properties of semiconductor nanoclusters have recently been studied experimentally and theoretically, especially in group II-VI semiconductors (CdS, CdSe, ZnS, ZnSe).[7] Much of this interest results from the potential application of nanoscale electronic and optical devices. Many of these applications exploit the fact that the properties of these materials can be quite different from those of bulk semiconductors.

Nano-size clusters are a special class of material which possess a variety of unique electronic and chemical properties as a consequence of quantum confinement, and their very large surface-to-volume ratios, and they are often referred to as "quantum dots" (QDs). The evolution of cluster properties with size is an important phenomenon, since the manifestation of electron and hole confinement gives way to discrete molecule-like electronic states as the cluster size decreases below the excitonic Bohr radius.

Quantum confinement results in the dense continua of valence and conduction band electronic states becoming discrete, well separated states and causes an increase in the band gap energy.[8-10] Thus, in nanometer sized semiconductor particles, the valence and conduction bands are replaced by manifolds of individual, delocalized electronic states. The energy shift of the band edge, as well as the separations between conduction and valence band states, can be larger than 1eV. In addition to these delocalized electronic states, semiconductor nanoclusters can also have localized electron and hole traps which often accumulate at the nanocluster surface, and the large surface to volume ratio can result in a high density of trap states. The presence of a high density of localized states along with finite relaxation rates between localized and delocalized states can affect the observed nanocluster optical properties.[11]

The preparation of such nanoparticles requires an appropriate "nanochemical reactor" in which to perform synthesis reactions, and this can be achieved using micelle structures, which are able to create a reaction template in the appropriate size range. It is well known that size control during colloidal growth requires the distinct separation of nucleation from growth. If nucleation occurs continuously, in either space or time, a wide range of cluster sizes will inevitably occur. However, if confinement of the reactant precursors can be achieved to limit growth to a restricted region of space, a narrow size distribution of clusters will occur.

Surfactant molecules can form segregated droplet-like aggregates called inverse micelles whose dimensions are typically 1-10 nm. The modifier "inverse" refers to the negative curvature between the surfactant-oil interface (the oil is the continuous medium). Nucleation only occurs in the micelle interior because of the total lack of solubility of charged species in the low dielectric constant inert oils used as the continuous medium.[12-13]

In this paper we report the synthesis of novel nano-sized clusters of titanium disulfide (TiS_2) using a synthetic strategy similar to that described previously for MoS_2 and WS_2 nanoclusters.[14-18] This represents the first reported room temperature synthesis of TiS_2 nanoparticles having a unimodal distribution of particle diameters in the range 3-5nm.

RESULTS

The nanoclusters were characterized by high resolution transmission electron microscopy (HRTEM) and optical spectroscopy. Figure 2 shows a HRTEM micrograph of TiS_2 clusters deposited on a carbon grid. The nanocluster images indicate they are very thin with irregular shapes and dimensions of about 3 to 6 nm. The darker images indicate that these particles are thicker and are believed to be aggregates. Some degree of aggregation is very difficult to avoid under the conditions of sample preparation.

It is difficult to obtain x-ray diffraction from such small clusters, but the electron diffraction patterns in the Fig.3 (a,b) shows that the clusters retain the bulk structure.

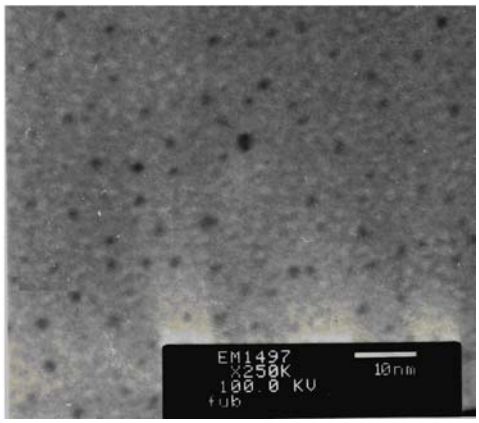

Fig. 2 – TEM image of TiS_2 nanoclusters having dimensions of approximately 2-5 nm.

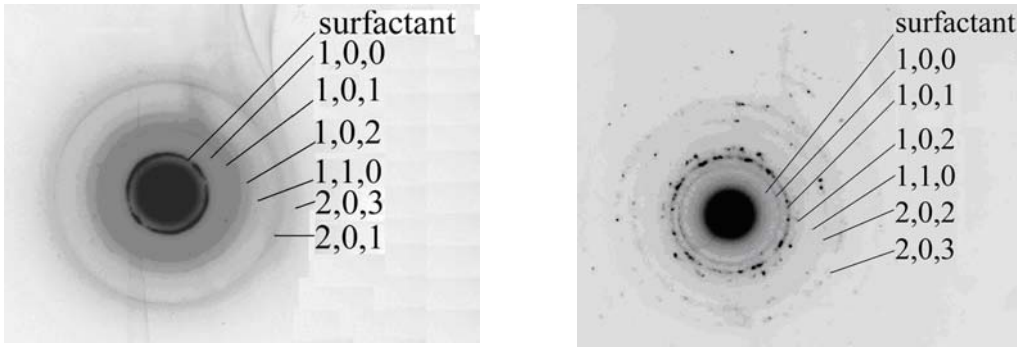

a b

Fig. 3 – Electron diffraction results taken from TiS_2 nanoclusters. a and b correspond to shorter and longer exposures respectively of the same sample.

The diffraction pattern shows continuous rings containing some discrete spots for short exposures and more discrete spots, rather than continuous rings, for longer exposures. This results from there being a finite number of nanoclusters or nanocluster aggregates on the irradiated surface. The electron diffraction results yield information regarding the nanocluster morphology. The reflections associated with only the c-axis, specifically the (0,0,1), (0,0,2), (0,0,3), (0,0,4) and (0,0,5) are absent in the observed electron diffraction pattern, which indicates that there is no long-range periodicity along the c-axis. The crystallographic c-axis is perpendicular to the planes associated with the S-Ti-S trilayers in bulk TiS_2, and so the electron diffraction pattern is consistent with the nanoclusters being two-dimensional, specifically consisting of a single, or only a few trilayers. The nanoclusters are expected to grow by the addition of Ti and S at the reactive trilayer edges. Growth along the c-axis corresponds to further nucleation and should therefore be relatively slow. This single trilayer morphology has been observed in images of MoS_2[17] and PtS_2[19] nanoclusters which also possess a layered crystal structure.

Table 1 also indicates that particle sizes calculated from the Debye-Scherrer expression change with the h,k,l refection used, indicating the lamella morphology of the TiS_2 nanoclusters. Generally, the lattice parameters showed a gradual increase with decreasing particle size as may be expected from lattice relaxation in nanosized crystallites, with the c_o parameter showing significant size dependence consistent with weak van der Waals forces along the c-axis.

Titanium sulfide nanoclusters in both octane and acetonitrile/TDAI/hexanol phases show nearly identical absorption spectra, with the lowest energy maxima at 359 nm. For comparison, the absorption spectrum of TiS_2 (bulk) and TiS_2 (nanoclusters) synthesized in ternary micelles and extracted into octane and acetonitrile are presented in Fig. 4, which illustrates the blue shift with decreasing size, and a cross-over from solid-like to molecular spectra of the small TiS_2 nanoclusters in acetonitrile.

Table 1

Calculated lattice parameters and particle sizes from the XRD, electron diffraction and HRTEM data on TiS_2 nanoparticles

XRD Reflections	FWHM	Particle Size (nm)	Lattice parameters (nm)	
			a_o	c_o
(1,0,1)	0.253	38.00	0.3405[a]	0.5612
(0,0,1)	0.163	40.57		
(1,0,1)	0.804	11.96	0.3405[a]	0.5692
(0,0,1)	0.471	15.21		
		3-5 (HRTEM)	0.3408*	0.5701*

* indicates the parameters are obtained from electron diffraction
[a] the parameters of the TiS_2 obtained by sol-gel[20]

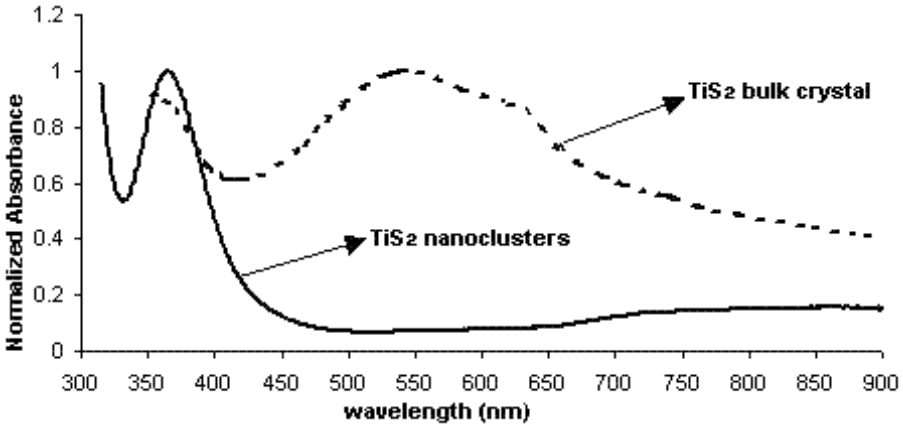

Fig. 4 – Absorption spectrum of small TiS_2 nanoclusters in octane compared with TiS_2 bulk[5].

DISCUSSION

Comparison of the spectrum of the clusters to that of the bulk crystal reveals a large blueshift for the clusters, and preservation of the excitonic features in the spectrum of the clusters. The TiS_2 nanoclusters studied should also have an indirect transition at lower energy but this transition is forbidden, and sufficiently weak that it is not observed in the absorption spectra. The first direct transition in the clusters spectrum occurs at λ = 359 nm (3.46 eV) which is associated with the excitonic peak of the bulk material at λ = 542 nm (2.29 eV), corresponding to a blueshift of 1.17 eV for the 3.0 nm clusters. This blue shift is a consequence of the quantum confinement of the electronic charge carriers in small clusters. The spacing between energy levels increases by decreasing the cluster size, and leads to an increase in the bandgap and shifts in the band edges.[21]

Because of the presence of I^- (from TDAI) during the synthesis, it was possible that the UV-visible peak was due to molecular species rather than nanoclusters, specifically I_3^- / I_5^-. Two results indicate that the peak is due to TiS_2 nanoclusters rather than I_3^- / I_5^-. First, the blank spectrum (synthesis, except without the $TiCl_4$) shows no absorbance at wavelengths > 290 nm in either the acetonitrile or octane phases. Secondly, I_3^- / I_5^- is insoluble in the octane phase. These results indicate that while it is possible to get spectral contamination in the acetonitrile phase, this does not occur in the octane phase and the absorption is due exclusively to TiS_2 nanoclusters. The introduction of a small amount of I_2 into the blank followed by extraction gives the I_3^- absorption peaks only in the acetonitrile phase since it is insoluble in the octane phase.

The blueshift of the first absorption peak in the nanocluster spectra may be qualitatively understood in terms of simple quantum confinement theory.[21-23] In this effective mass approximation theory, the energy shift of the first absorption peak in a quantum confined semiconductor is given by :

$$\Delta E = \frac{\hbar^2 \pi^2}{2R^2}\left[\frac{1}{m_e^*} + \frac{1}{m_h^*}\right] - \frac{1.8e^2}{\varepsilon R} + \textit{polarization terms} \quad (1)$$

where m_e^* and m_h^* are the electron and hole effective masses, respectively, ε is the dielectric constant, and R is the radius of the particle. This treatment assumes the particle to be spherical, and assumes that the motions of electron and hole may be described in terms of their effective masses. It also ignores the effect of surface atoms. The first and second terms on the right of Eq.1 are kinetic energy and electrostatic (Coulombic) attraction terms, respectively. The basic relationship between size and optical spectra was first developed and confirmed for ZnS and CdS nanoparticles. It is generally found that the kinetic energy term dominates, resulting in a blueshift in the absorption spectrum as the size of a nanocluster is decreased. In this simple treatment, as the cluster gets smaller, the band gap gets larger because the conduction band moves to more negative potentials, and the valence band moves to more positive potentials. The extent to which each band moves depends on the relative values of m_e^* and m_h^*. In most semiconductors, m_e^* is much less than m_h^*, so that most of the increase in the band gap is due to the conduction band moving to more negative potentials, the valence band moves very little.[22-25] If the bulk TiS_2 dielectric constant (13.7)[26] and typical electron (0.23 m_e)[27] and hole ($\sim m_e$) effective masses are used, then the Bohr radius may be estimated as being 2.5 nm.

Equation (1) may not be rigorously and quantitatively applied to the TiS_2 nanoclusters studied because the assumptions underlying the equation are rather poor approximations in this case, since the nanoparticles are certainly not spherical, as is assumed by Eq.1. Furthemore, the effective mass approximation, which is implicit in Eq.1 is derived from the periodic nature of the lattice. Nevertheless, Eq.1 can be used to provide qualitative insights into the size dependent properties of TiS_2 nanoclusters.

While the absorption spectra of these nanoclusters are the same in the octane and acetonitrile environments, the emission studies reveal some differences. The emission spectra of the TiS_2 nanoclusters in octane and acetonitrile, when λ_{exc}=312 nm, are compared in Fig. 5. The octane emission spectrum has a broad shoulder at around 430 nm and a peak centered at 450 nm, whereas the acetonitrile emission spectrum has a shoulder at 400 nm and a broad peak at 415 nm.

When excited at 360 nm, the spectrum of the TiS_2 clusters in octane exhibits an emission peak centered at 450 nm and the acetonitrile spectrum has a stronger peak at 400 nm accompanied by a broad and weaker peak at 415 nm.

In nanoclusters, a large number of the atoms are at or near the surface, leading to a preponderance of dangling bonds and defects, which result in surface states. Adsorbed impurities can also produce additional surface states and all these states can act as traps or recombination sites. The fate of photogenerated electron-hole pairs in a semiconductor is determined by traps and recombination processes.

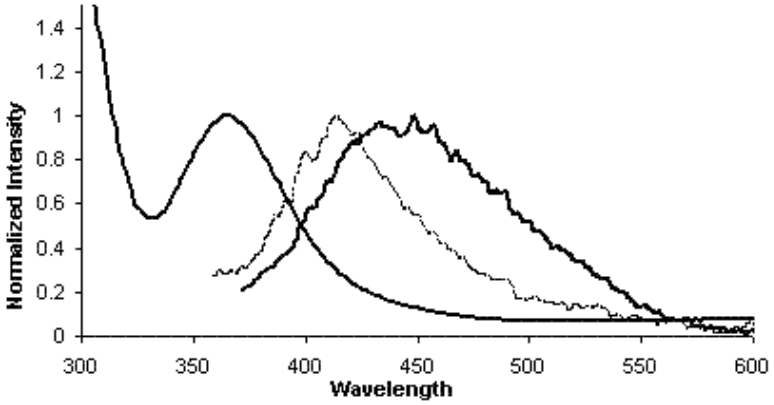

Fig. 5 – Absorption and emission spectra of TiS_2 nanoclusters. The absorption spectrum in octane (solid curve on left), emission spectrum in octane (solid curve on right) and the emission spectrum in acetonitrile (dotted curve) are shown for comparison. The emission spectra were excited at 312 nm.

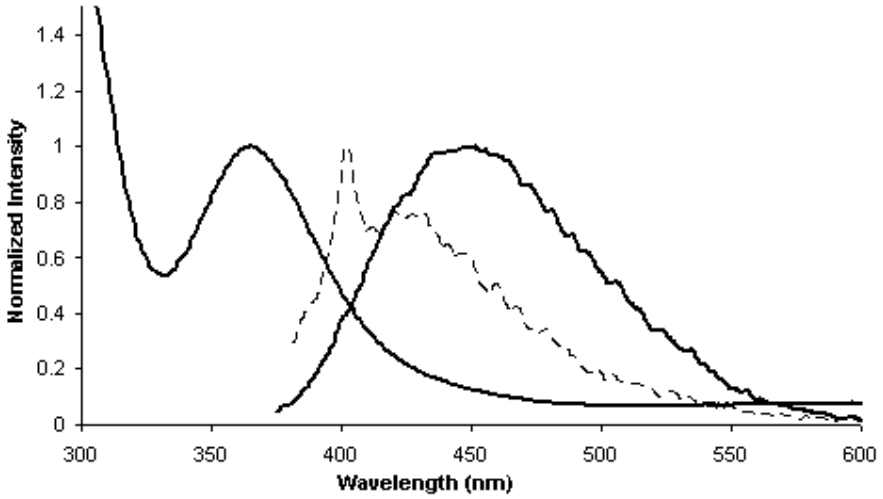

Fig. 6 – Absorption and emission spectra of TiS_2 nanoclusters, showing the absorption spectrum in octane (solid curve on left), emission spectrum in octane (solid curve on right) and the emission spectrum in acetonitrile (dotted curve) after excitation at 360 nm.

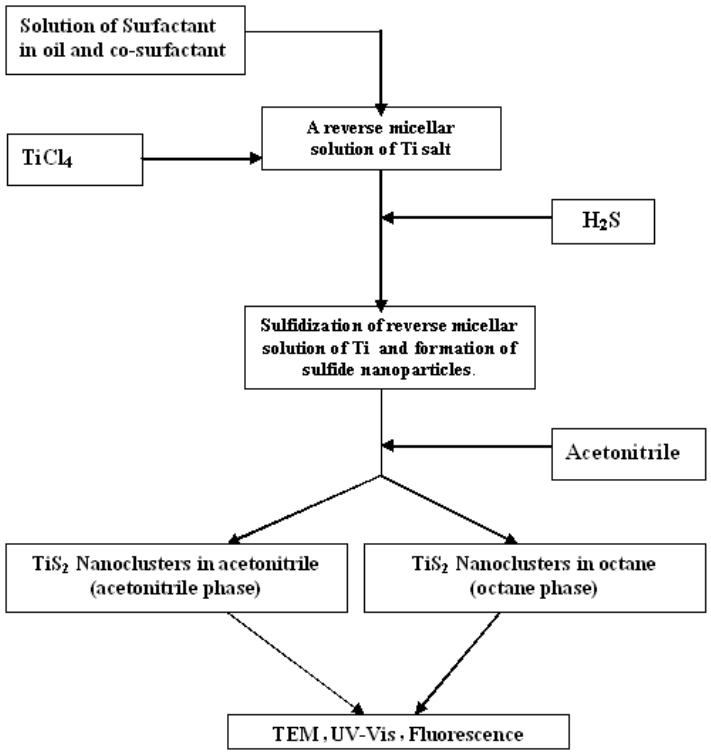

Fig. 7 – Scheme for TiS_2 nanoparticle synthesis using reverse micelles at room temperature.

In summary, we have successfully synthesized nano-size clusters of the layered semiconductor, TiS_2, at room temperature, and report their structural and optical characteristics. The large blue shift in the optical absorption spectrum with decreasing cluster size affords the potential to tailor band gaps. Significant photoluminescence is observed at room temperature, which is absent in the bulk material, demonstrating the crossover from solid-like to molecule-like optical absorption spectra as the size of the clusters becomes smaller than that of the exciton in the bulk. Nanocluster systems, such as the TiS_2 synthesized here, offer the possibility of optimizing solar absorbance by using systems with mixed size band-gaps and potentials.

EXPERIMENTAL

The flow scheme presented in Figure 7 outlines the experimental procedure adopted for the synthesis of titanium disulphide nanoparticles in reverse micelles. Titanium tetrachloride was dissolved in a degassed ternary mixture containing a surfactant (tridodecylmethyl ammonium iodide (TDAI)), hexanol and octane in a weight ratio of 8/8/84, to give an inverse micelle solution (typical sample volumes were 6 mL) at a concentration of 8×10^{-4} M $TiCl_4$. A steady stream of hydrogen sulfide (H_2S) gas was then bubbled through the solution at room temperature for 5 minutes, during which time the clear solution turned dark yellow but no solid was observed to form. Following H_2S addition, the mixture was allowed to stir for 2 hours to ensure complete reaction, then the TiS_2 nanoclusters were extracted with an equal volume of acetonitrile. This dissolved the inverse micelles, with the hexanol and TDAI entering the acetonitrile phase, whilst the nanoclusters distributed between both the nonpolar octane phase and the polar acetonitrile/TDAI/hexanol phase.

High-resolution transmission electron microscopy (HRTEM) using Philips CM 200 FEG microscope has been used to study the microstructure of particles. Fluorescence measurements were carried out on a Perkin-Elmer LS-50B.

Acknowledgements: The CRC for Microtechnology is acknowledged for financial support of the project, together with Ju Lin Peng for assistance with the HRTEM.

REFERENCES

1. Y.-S. Kim, M. Masataka, T. Isao and A. Hirohiko, *Material Transaction, JIM*, **1988**, *39*, 709 - 713.
2. R.C. Bill, *Wear,* **1985**, *106*, 283 – 289.
3. J. Chen, S.Li, Z.L. Tao, Y.T. Shen and C.X. Cui, *J.Am.Chem. Soc*., **2003**, *125*, 5284 – 5286.
4. H.W. Myron and A.J. Freeman, *Phys. Rev. B,* **1974**, *9*, 481.
5. T.J. Wieting and M. Schlűter, "Electrons and Phonons in Layered Crystal Structures", Reidel, Holland, 1979, p. 190-223.
6. A.R. Beal, J.C. Knights and W.Y.Liang, *J.Phys. C: Solid State Phys.,* **1972**, *5*, 3540 - 3547.
7. A.D. Yoffe, *Adv. Phys.,* **1993**, *42*, 173 – 209.
8. L.E. Brus, *J. Phys. Chem.,* **1986**, *90*, 2555 – 2563.
9. M.V. Rama and R.A. Friesner, *J. Chem. Phys.,* **1991**, 95, 8309 - 8315
10. P.E. Lippens and M. Lannoo, *Phys. Rev. B,* **1989**, *39*, 10935 – 10943.
11. J.M. Huang and D.F. Kelley, *J. Chem. Phys.,* **2000**,*113*, 793 – 797.
12. J.P. Wilcoxon, G. Samara, P. Newcomer, *Materials Research Society Symposium Proceedings*, **1995**, *358*, 277 - 283.
13. J.S. Huang, *J. Phys. Chem. B.*, **1985**, *82*, 480 - 487.
14. R. Doolen, R. Laitinen, F. Parsapour and D.F. Kelley, *J. Phys. Chem. B,* **1998,** 102, 3906 - 3913.
15. J.M. Huang, R.A. Laitinen and D.F. Kelley, *Phys. Rev. B*, **2000,** 62, 10995 - 11003.
16. J.M. Huang and D.F. Kelley, *J. Chem. Phys*, **2000,** 113, 793 - 799
17. J.P. Wilcoxon and G.A. Samara, *Phys. Rev. B*, **1995,** 51, 7299 – 7305.
18. F. Parsapour, D.F. Kelley, S. Craft and J. P. Wilcoxon, *J. Chem. Phys*. **1996,** 104, 4978 - 4983.
19. F. Parsapour, D.F. Kelley and R.S. Williams, *J. Phys. Chem. B*, **1998,** 102, 7971 - 7975.
20. A. Let PhD thesis, Royal Melbourne Institute of Technology, Melbourne.
21. J.P. Wilcoxon, G.A. Samara, D. Bliss and P. Newcomer, *Proceedings Electrochemical Society,* **1996,** *95-25*, 432 – 443.
22. L.E. Brus, *J. Chem. Phys,* **1983**, 79, 5566 - 5572.
23. L.E. Brus, *J. Chem. Phys*, **1984,** 80, 4403 - 4412.
24. L.E. Brus *J. Phys. Chem,* **1986,** 90 2555 - 2563
25. R. Rosetti, J.E. Ellison, J.M. Gibson and L.E. Brus, *J.Chem. Phys,* **1984**, 80, 4464 - 4472.
26. L.E. Oliveira, *Phys. Stat. Sol. B: Basic Research,* **1988,**147, 223 - 231.
27. H. Isomaki, J von Boehm and P. Krusius, *J. Phys.C: Solid State Physics,* **1979,** 12, 3239 - 3245.

Revue Roumaine de Chimie, **2007**, *52*(3), 243–252

IMPLICATIONS OF THE ACID-BASE CHARACTER FOR SOME FIXED VISCOSITY POINTS, FOR OXIDE VITREOUS SYSTEMS

Dorel RADU[a] and Claudiu MAZILU[b*]

[a]Politehnica University of Bucharest, Faculty of Applied Chemistry and Materials Science, Department Science & Engineering of Oxide Materials and Nanomaterials, Str.Polizu, No.1-3, P.O. Box 12-134, E-mail: d.radu@oxy.pub.ro, Roumania
[b]National Glass Institute, Theodor Pallady Blv., no.47, zip code 032266, tel. 3452510/214, Bucharest, Roumania

Received October 13, 2005

Considering the oxide glasses as chemical systems, the acid-basic character of the glasses has known in time, different theoretical approaches. One of the theories proposed the basicity percentage (pB) notion as a measure of the acid-base character for oxide glasses. This work shows that, by its defining mode, the basicity percentage is a complex parameter which considers a series of structural characteristics such as bond's ionicity percentage, coordination number, pB correlating in fact with all the other structural characteristics at an atomic level (the electrostatic field's strength, the electronegativity, the oxygen's electronic ability to polarize, the oxidation number, bonding energies, etc.).
Taking into account that the basicity percentage is an indicator which "senses" the modification of the structural characteristics of oxide glasses, it is to be expected that the properties which present interest (temperatures corresponding to the structural transformation, the thermal expansion coefficient, the refraction index, etc.) to have an important correlation with the basicity percentage. In the present work, a series of correlations between the values of some fixed viscosity points of practical interest and the basicity percentage for the studied glasses have been presented. These correlations are seen for some simpler glasses as well as for some complex oxide compositions of industrial type.

INTRODUCTION

The vitreous systems are solids that from the point of view of the degree of order are placed between the ideal crystals (perfectly ordered) and the amorphous systems (perfectly disordered).

Goldschmidt (1927), Zachariasen (1932), Dietzel (1942), Huggins and Sun (1947), Muller (1967), Goodman (1976) have proposed a series of theories which correlated the oxides capacity of forming vitreous systems with a series of atomic characteristics such as: ionic radii, coordination number, ionization potential, oxidation state, electronegativity, etc. A synthesis of these theories is presented. [1,2] At the same time, especially for the simple vitreous systems, a series of properties were correlated qualitatively and, sometimes, quantitatively with different structural characteristics at atomic level. Since now, with all recorded success this kind of approach for the simple vitreous systems' structure and characteristics, a major impediment could not be surpassed: the impossibility of using the quantitative analysis on complex glasses. This was the case for one fundamental property of the oxide glasses: their acid-base character.

1. The evolution of the acid-basis theories

In time numerous acid-base theories have been developed, having more or less limited application domains. Latest researches in the field of glass have led to new and interesting ideas concerning the acid-base concept for glasses. A synthesis of these theories (Paul and Douglas, Lux and Flood, Weyl and Marboe, Lewis, etc.) is presented in.[3, 4] The most of the elaborated theories concerning the acid-base character of glasses have in common the qualitative aspects of this characteristic. At the same time, a series of experimental methods to determine this property have been developed. Far less are the essays of theoretical calculus.

In this way, Duffy and Ingram,[5] have established that the optical basicity of a glass can be calculated from the parameters attributed to the constitutive oxides of glass. Such calculus, when applied to a series of compositions in a system,

* Corresponding author: claudiumazilu@yahoo.com

indicates the tendency of the basicity and usually approaches what is experimentally obtained.

2. Establishing the glass basicity (pB)

In order to evaluate the basicity of the oxide vitreous systems, Balta and co-workers [2, 6] have proposed the notion of basicity percentage (pB), taking into account the ionic degree of the chemical bonds. Considering that O^{2-} has, in principle, the highest electron donor power, also proven by the extremely low ionization potential (–6.5eV), it was assigned with the maximal value, pB=100%, respectively.

This oxygen species constitutes an end of the oxide basicity scale, thus showing its natural character. In these conditions, the calculation of the basicity (pB), in %, for an oxide can be done with the Balta and Radu relation: [2]

$$\lg pB_i = 1{,}9(NC)^{0{,}02} - 0{,}023P_i/NC \quad (1)$$

where: NC is the coordination number of the cation related to the oxygen;
P_i the ionization potential of the cation in the given valence state.

In the case of oxide glasses, the basicity (pB) is calculated with the relation:

$$pB = \sum_{i=1}^{n} c_i \cdot pB_i \quad (2)$$

where: c_i is the gravimetric fraction of oxide i;
pB_i the basicity of oxide i.

As the basicity percentage is a "sensitive" indicator of the characteristics and structural changes of the oxide glasses [6-8] it would be most probable that their properties, in a great proportion, present an important correlation with this parameter. In this direction, correlations have been reported in literature [2, 6-9] between pB and:

The vitreous transition temperature for binary and ternary silicate systems;

The refraction index for binary and industrial silicate glasses;

The biocompatibility of vitreous bio-materials;

The chemical stability of glasses, including the reinforcement fibers;

The interaction between glass melting – refracting bricks;

The reactivity of the raw materials batch, etc.

In present work, there are presented new results, for different types of industrial glasses, concerning the correlation of certain fixed points of viscosity with the pB.

THE THEORETICAL BASIS

As it can be seen from relations (1) and (2), the basicity percentage, besides the fact that it represents a natural scale for the oxide systems, also has the advantage that it is defined in comparison with a series of characteristics that mirror the structural characteristics of the vitreous system: coordination number, oxidation number, ionization potential. Besides these dependencies, a series of correlations were shown between the basicity percentage and other structural characteristics such as: the intensity of the electrostatic field, Z/a^2, electronic polarization capability of the oxygen ion, $\alpha_{O^{2-}}$, Sanderson's electronegativity, x(S), and Gordy's electronegativity, x(G). [10] Additionally, although they have different starting bases, between the optical basicity and the basicity percentage a strong interdependency was discovered [8] for the most often found oxides in the glass composition.

Generally, the established correlations have the form:

$$y = a - b \cdot pB\ ; \quad (3)$$

in which y is the considered structural parameter and a and b – coefficients.

In Table 1 the values of these coefficients are given taking into account the nature of the y parameter.

Table 1

The values of the statistic coefficients from relation (3)

Nr.	Nature of y parameter	a	b	Correlation coefficient, R
1	Z/a^2	3.1452	0.0330	0.980
2	$1/\alpha_{O^{2-}}$	1.1560	0.0090	0.950
3		4.2538	0.0394	0.974
4	x(S)	2.9636	0.0232	0.993
5	x(G)	3.7282	0.0326	0.995
	$1/\Lambda$			

There is also to be taken into account that a high value of the correlation coefficient is recorded in the case when the analysis extends to a greater number of oxides. In this way, by processing the primary data obtained for a number of 32 oxides, [11] the function that correlates the ability of polarization of oxygen ion with the pB is plotted in Fig. 1.

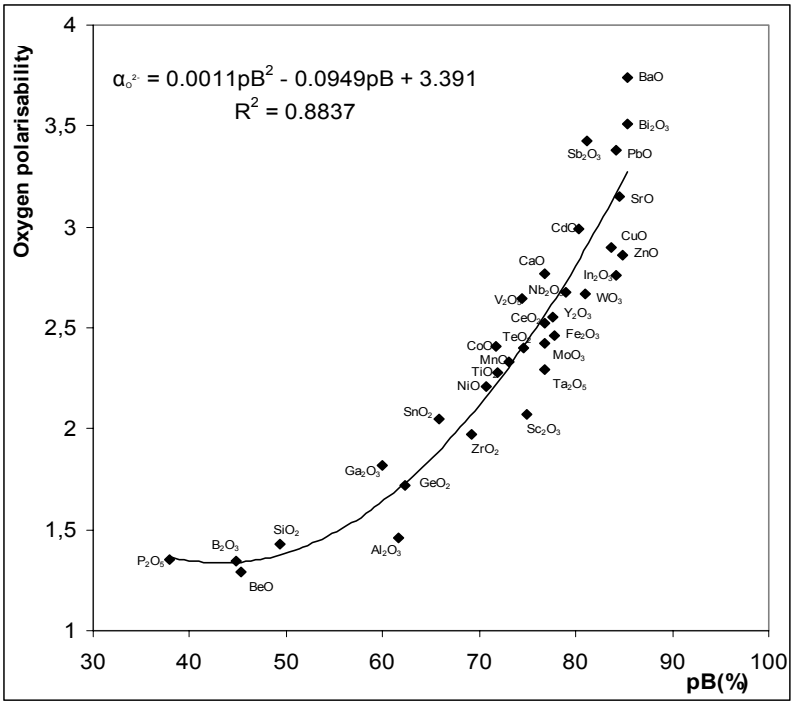

Fig. 1 – The dependence between the electronic ability to polarize of oxygen and the basicity percentage, for crystalline oxides.

More over, for the considered oxides, the dependencies of the form (3) were obtained between the bonding energy (O1s) E_b,[11] the bonding energy of the cation from the oxide, E_c,[11] and pB. These results are presented in Figs. 2 and 3, respectively.

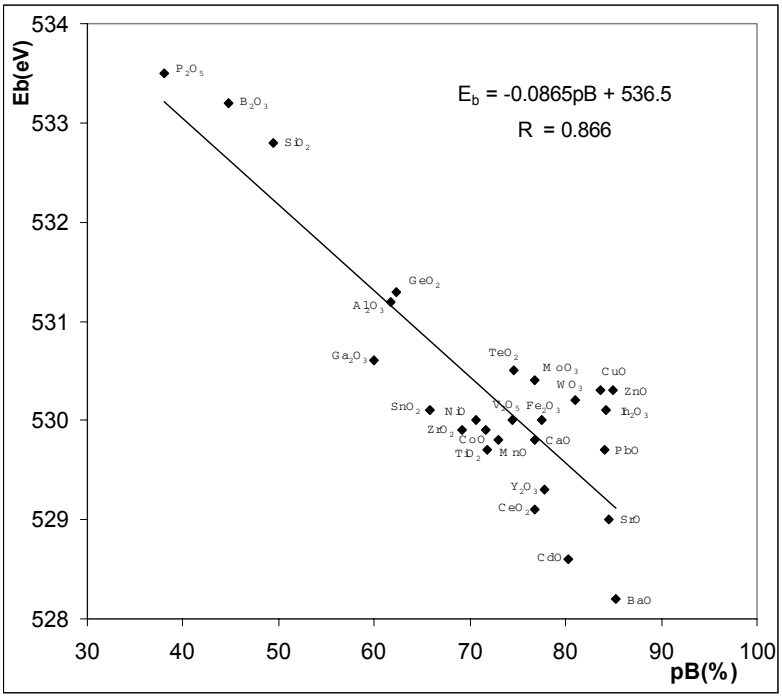

Fig. 2 – The dependence between the bonding energy (O1s) E_b and the basicity percentage, for crystalline oxides.

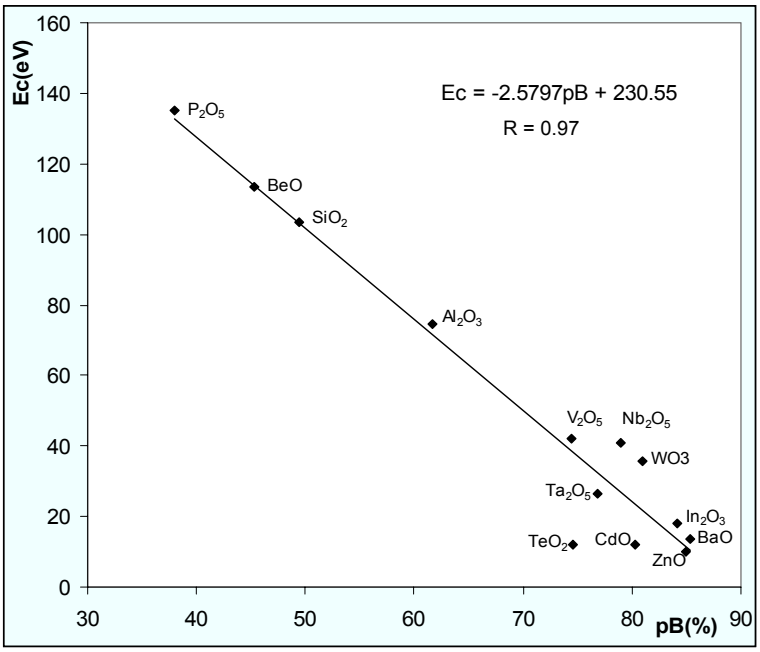

Fig. 3 – The dependence between the bonding energy of the cation in oxides E_B^c and the basicity percentage, for crystalline oxides.

The high values of the correlation coefficients associated to the Figs.1-3 seem to bring sufficient arguments to consider the pB a complex structural parameter which includes implicitely, as well as explicitely the majority of the structural characteristics of the atoms present within the crystalline oxides. From this point of view it is expected that a series of properties, such as thermal expansion coefficient and viscosity, to be correlated with the pB. This is because that effective values of some « fixed viscosity points » are influenced by the nature and the weight of oxides in the chemical composition, as well as by a series of structural particularities (the type and the way of interconnection of the coordination polyhedra, the energy of the cation-oxygen bonds, etc.), and the majority of the structural parameters are closely correlated with pB.

The dependence of the temperature on the viscosity of the silicate melts can be represented in the under cooled liquids domain (between $T_{liq.}$- T_g) by the Vogel-Fulcher-Tammann relation: [1,2]

$$\lg \eta = A + B/(T-T_0) \tag{4}$$

where A, B and T_0 – constants that depend on the oxide composition of glasses.

Yan, Wood and Mills [12] have used the optical basicity to develope a model to estimate the viscosity of glasses, at temperatures between $T_{liq.}$ and $T_{g.}$. This way, for the silicate glasses, the relations [12] between the optical basicity and coefficients A, B, T_0 associated to the equation (4), were obtained by the analysis of the multiple regression from the viscosity-oxide composition data presented by Lakatos in. [13]

Taking into account the relation between the optical basicity and the basicity percentage, the A,B and T_0 coefficients can be written in relation with pB :

$$A = \frac{474.78 - pB}{571.8 - 5 \cdot pB} \tag{5}$$

$$B = \frac{82.6 - pB}{0.011 - 0.98 \cdot 10^{-4} \cdot pB} \tag{6}$$

$$T_o = \frac{99.45 - pB}{0.15 - 0.0013 \cdot pB} \quad (7)$$

It can be seen that in such an approach, the viscosity of the glasses is put in dependency with the temperature, the chemical composition and a series of structural characteristics, correlated with the pB parameter which can be easily calculated.

RESULTS AND DISCUSSION

For the oxide vitreous systems (in particular), the viscosity represents one of the most important properties, for the melted glass, when lgη = 1- 4, as well as for the solid state glass, when lgη = 15- 16. This is motivated by the fact that viscosity is a property highly influenced by the structure of the glass. On the other hand, this property has an important role in different technological stages that are passed through until obtaining a finite product from the mix of raw materials (melting, homogenization, annealing).

Taking this into account, a series of viscosity "fixed points" were defined, such as: the vitreous transition temperature T_g, when lgη = 13.3, the processing interval, "the glass length" ΔT respectively, for which lgη ranges between 4 and 7.6, "the melting temperature", T_f, when lgη ≈ 2, etc. [1, 2]

1. The correlation between the vitreous transition temperature (T_g) and basicity (pB)

For a series of binary and ternary silicate glasses, the experimental data have shown a decrease of the T_g values with the increase of the pB. [8, 9] By processing some primary literature data, the verification of this type of dependency is also thought for glasses with complex oxide compositions.

Some inorganic glasses are also used as materials for waveguides in hi-tech domains such as: optical communication systems, optical integrated circuits, etc.

A series of compositions of oxide silicate glasses used as waveguide and lain down through the serigraphy process, are presented in.[14] They are framed in the base system SiO_2 –B_2O_3 – PbO(ZrO_2)- Na_2O- K_2O to which small quantities of Al_2O_3, BaO, La_2O_3, Bi_2O_3 can be added.

Knowing the oxide composition for a number of 16 glasses,[14] the basicity percentage was calculated with relations (1) and (2). In Fig. 4 the correlation between the measured values for T_g and pB is shown.

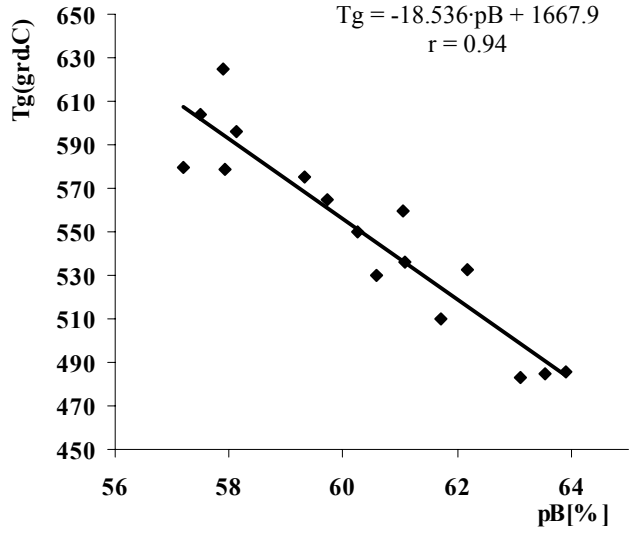

Fig. 4 – The correlation between T_g – pB.

A linear decrease of the vitreous transition temperature with an increase of basicity (pB) can be observed, with an increase of alkaline oxides quantity, respectively. The explanation consists in the decrease of the viscosity of glasses at the same temperature for the presented compositions, with the introduction of new quantities of network-modifying oxides. At the same time, it is known that alkaline oxides have higher basicities (pB) than the glass forming oxides that they replace in the structure of

the glass. As a consequence, a diminishing of the degree of polymerization of the vitreous structure is recorded, which leads in the end, to smaller values for the vitreous transition temperature.

An interdependency of the same nature was found for another category of glasses of great practical interest: bio-glasses. The bioactive glasses are defined as glasses that form chemical bonds with the bone cells and are used in prosthetics, in modern reparatory medicine.

For a series of 15 compositions of bioactive glasses, presented in [15], their basicity (pB) have been calculated and correlated with their Tg. The results are presented in Fig. 5.

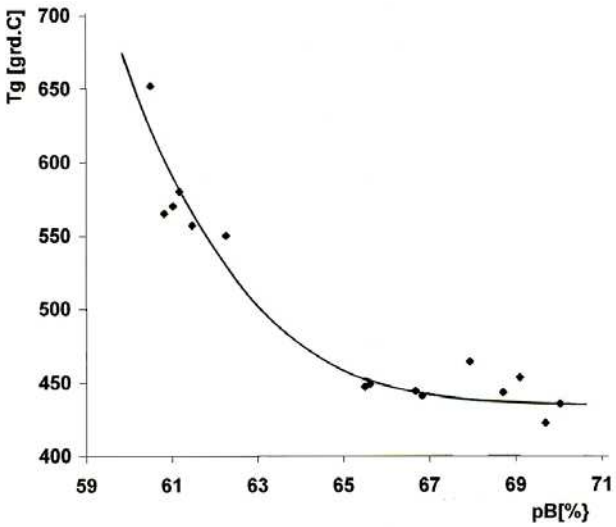

Fig. 5 – The T_g - pB correlation, for a series of bioactive glasses.

A linear correlation of pB with Tg can be observed until approximately 65% pB, due to depolimerization of the vitreous structure, with the increasing of the alkalis percentage and basicity percentage. In basic medium (>65% pB) it is expected that the basicity (pB) is less influenced by the decreasing of Tg, as a consequence of the fact that the depolimerization is less obvious like in the first step.

These results also show that for silicate glasses, an increase of basicity determines the decrease of the vitreous transition temperature. Some experimental data for glasses of certain composition show an inverse dependency. Thus, for glasses within the binary system $SiO_2 – P_2O_5$ [16], for a percentage of SiO_2 between 56 and 100% is presented in Fig. 6 the variation of T_g with pB.

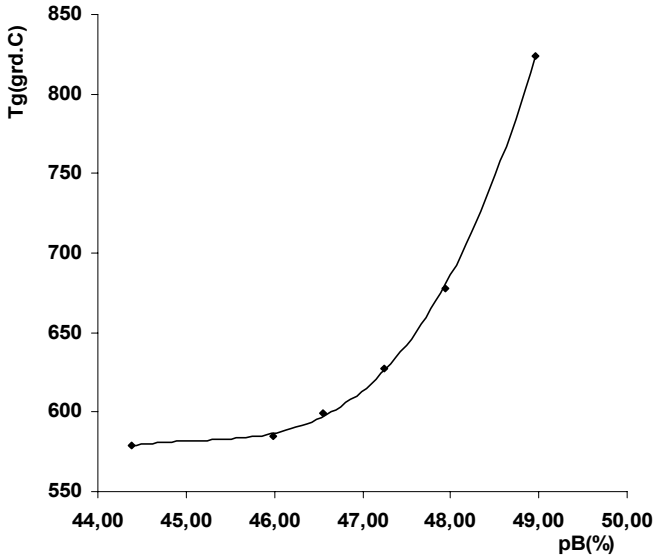

Fig. 6 – The correlation T_g - pB for glasses from the binary system $SiO_2 – P_2O_5$.

It is shown that an increase of the pB determines an increase for T_g. This result is explained by the fact that the basicity percentage for SiO_2 is higher than that of P_2O_5. By increasing the SiO_2 percentage pB increases, but simultaneously the refractoryness of the system increases, too (the melting temperature of SiO_2 is several time higher than that of P_2O_5). The consequence is an increase of Tg.

2. The correlation between the temperature corresponding to some fixed viscosity values and basicity (pB)

Being a transport property, and therefore depending on the characteristics of the ions present in the glass, viscosity can be correlated with basicity (pB). To verify this hypothesis, a first analysis was done on a number of 20 glasses using their oxide compositions given in literature. [13] For these glasses, the values of the temperatures at which lgη = 2, 4 and 6 were determined experimentally. The first investigated set was formed of glasses 1-11 having the compositions within the oxide system SiO_2 - Al_2O_3 - CaO - Na_2O, considered as referential.

The second considered set represents glasses with complex chemical composition, resulted by adding to the basic system different oxides (Li_2O, K_2O, BaO, ZnO, PbO); they are numbered 12-20 in Tab. 2.

Table 2
The oxide composition of glasses and the temperature of the melts at 3 viscosity values

		%weight												
		SiO_2	Al_2O_3	Na_2O	CaO	Li_2O	BaO	ZnO	PbO	K_2O	MgO	T(°C)		
No. Gl	pBox / pBgl.	49.42	72.49	89.05	86.38	88.85	87.61	79.52	84.11	91.44	78.17	lgη=2	lgη=4	lgη=6
1	59.71	72.69	1.23	13.87	12.21	0	0	0	0	0	0	1433.9	1016.8	822.9
2	59.49	73.23	1.24	13.22	12.30	0	0	0	0	0	0	1446.7	1026.2	830.2
3	59.16	74.07	1.26	12.23	12.44	0	0	0	0	0	0	1465.5	1040.1	841.1
4	58.89	74.95	1.27	14.69	9.09	0	0	0	0	0	0	1484.2	1031.9	824.1
5	57.90	77.66	1.32	15.22	5.80	0	0	0	0	0	0	1544.1	1053.0	829.5
6	59.28	73.91	1.25	14.49	10.35	0	0	0	0	0	0	1461.0	1023.8	822.0
7	58.31	76.55	1.30	15.00	7.15	0	0	0	0	0	0	1519.7	1044.4	827.3
8	59.83	72.41	1.23	14.19	12.17	0	0	0	0	0	0	1427.5	1012.1	819.3
9	59.38	73.66	1.25	14.44	10.66	0	0	0	0	0	0	1455.3	1021.8	821.6
10	60.09	71.37	1.21	13.99	11.99	0	0	0	0	0	1.44	1417.0	1013.2	821.3
11	60.22	70.86	1.20	13.89	11.91	0	0	0	0	0	2.14	1411.7	1013.5	822.1
12	61.86	66.89	0.57	2.86	6.91	0.64	2.90	3.83	4.97	10.43	0	1484.0	1048.2	833.7
13	62.33	65.87	0.56	2.47	6.81	0	2.86	3.77	4.89	12.77	0	1502.8	1072.6	860.9
14	61.97	66.71	0.57	1.74	6.90	0.77	2.89	3.82	4.96	11.65	0	1491.4	1064.2	838.8
15	61.43	67.76	0.57	4.21	7.00	0.93	2.94	3.88	5.03	7.67	0	1467.8	1027.4	811.5
16	61.84	66.90	0.57	3.77	6.91	0.42	2.90	3.83	4.97	9.73	0	1483.2	1047.6	834.0
17	62.17	66.19	0.56	3.41	6.84	0	2.87	3.79	4.92	11.42	0	1495.4	1064.1	852.2
18	61.71	67.12	0.57	6.16	6.94	0	2.91	3.85	4.99	7.48	0	1474.4	1040.0	828.8
19	61.56	67.48	0.57	4.60	6.97	0.64	2.93	3.87	5.01	7.93	0	1472.3	1033.6	819.0
20	61.83	66.89	0.57	4.22	6.91	0.31	2.90	3.83	4.97	9.40	0	1481.3	1046.7	833.8

In Tab. 2 there are also given the pB values of the component oxides ($pB_{ox.}$) calculated with relation (1), as well as the pB value of the glass ($pB_{st.}$), established with relation (2). The coordination number for the cations was considered as the most probable for these type of glasses. For the glasses 1-11, in Fig.7-9 are presented the correlations temperature - pB for lgη=2 case (a); lgη= 4 case (b); lgη=6 case (c). It can be seen that, for a constant value of viscosity, the temperature of the glass decreases with the increase of the basicity. This result is understood because, for the first 11 analyzed glasses, an increase of the percentage of (Na_2O+CaO) is realized in the detriment of SiO_2 percentage, which leads to a more and more depolimerization degree of the structure. This favors the flowing process of glass at lower temperatures of treatment (for η = constant).

The correlation coefficient r drops from the value 0.998 (case a), to under 0.9 (case c). This observation confirms that pB has a more important

influence in the case of molten glass (case a), than in the case of more viscous glasses corresponding to lower temperatures. At higher viscosities (cases b and c), apart from the influence of basicity, it is expected to be sensed the action of the glass, which becomes more and more rigid. Moreover, the variation with ± 1% of the value for pB, implies the modification with approximately ±60°C of the temperature of the glasses for lgη=2 and with aprox. 20°C and 4°C, in cases b and c respectively.

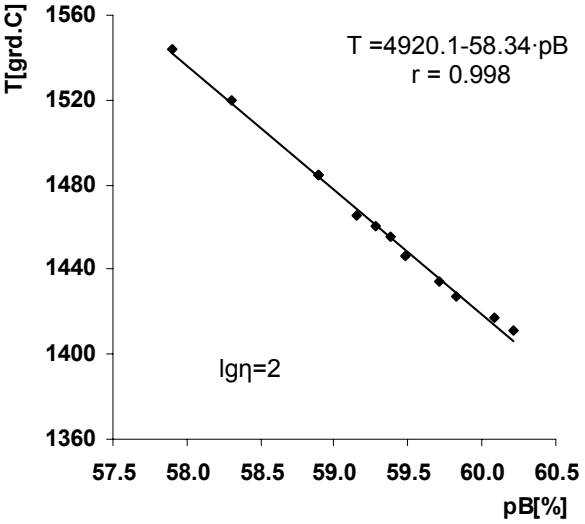

Fig. 7 – Correlation T(°C) - pB la lg η = 2 for the 1-11 compositions.

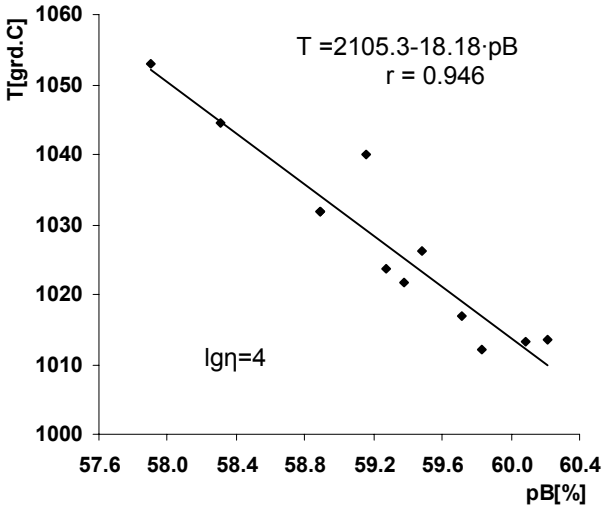

Fig. 8 – Correlation T(°C) - pB at lg η = 4 for the 1-11 compositions.

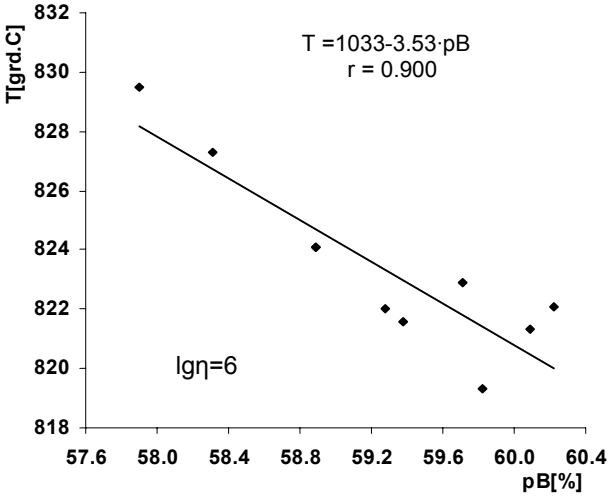

Fig. 9 – Correlation T(°C) - pB at lg η = 6 for the 1-11compositions.

In Figs.10-12 is presented the variation of the temperature of the glasses 12-20 with pB, for the same constant value of viscosity. In this case, somewhat surprisingly, the increase of the values for pB determines the increasing of temperature values for η=const; the modification of the basic oxide composition (glasses 1-11) by introducing some new oxides implies contrary effects over the viscosity. In this way, the decrease of $\%Na_2O$ and increase of K_2O determines an increase of the viscosity of glasses. In exchange, the decrease of %CaO and increase of ZnO, BaO and PbO implies the decrease of the viscosity (at T=const.), the decrease of the temperature (at η=const.), respectively. Practically, in case c), for lgη=6, the effect of the increase of the glasses' temperature is quite strongly correlated with the presence, in an always increasing manner, of K_2O, as it can be

seen in Fig.13. As K_2O has the highest basicity value compared with any other oxide component, then the glass pB increases with the increase of the temperature (for η=const.).

It must be also remarked that, for this set of glasses, the effect of the basicity is not so different for different values of viscosity.

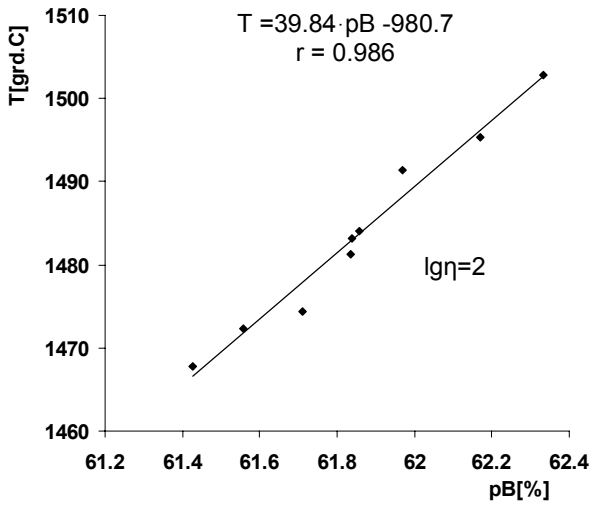

Fig. 10 – Correlation T(°C) - pB at lg η = 2 for the 12-20 composition.

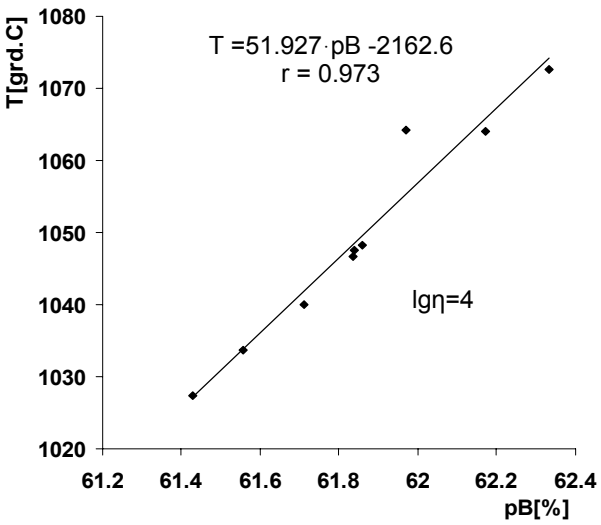

Fig. 11 – Correlation T(°C) - pB at lg η = 4 for the 12-20 compositions.

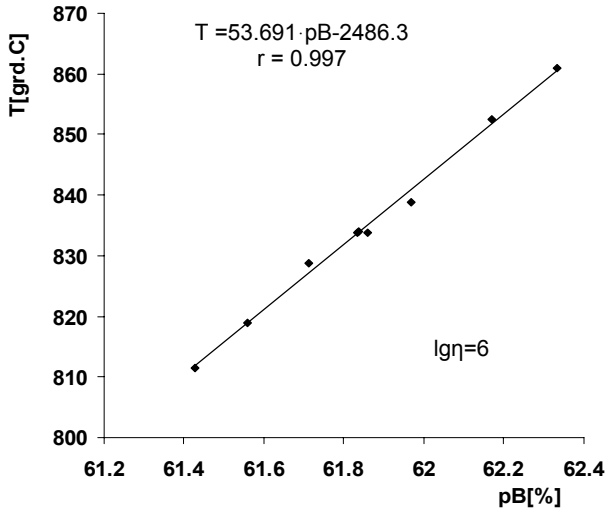

Fig. 12 – Correlation T(°C) - pB at lg η = 6 for the 12-20 compositions.

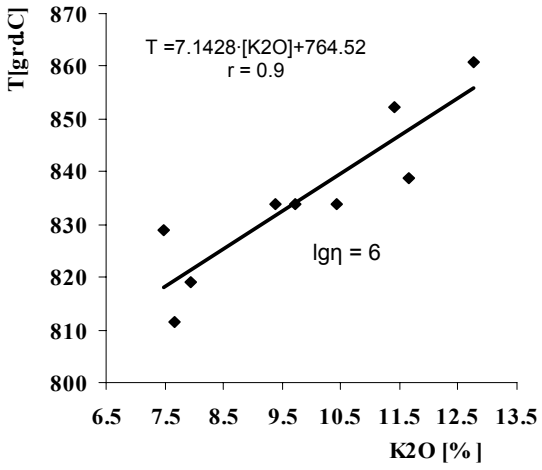

Fig. 13 – Correlation T(°C) – %(grav.)K_2O at lg η =6.

As it is shown in the plottings presented in Figs. 7-9, and 10-12, respectively, the two glass groups present a dependency between the temperature corresponding to some fixed viscosity points and their basicity percentage (pB). These results also lead to the conclusion that it can not be always said that there is a direct or inverse proportionality between temperature (for η = ct.) and pB. The interdependency type is established for each case in particular taking into account the particularities of the each studied oxide system. Of practical interest is also the establishing of the glass "length", which is a measure of its processing ability. "Long" glasses have greater values for ΔT than the "short" glasses, harder to process, where:

$$\Delta T = T_{(\lg\eta=4)} - T_{(\lg\eta=7.6)} \; ; \qquad (8)$$

In the vitreous system SiO_2 - Na_2O, for 8 compositions between SiO_2 and $Na_2O{\cdot}SiO_2$ the ΔT intervals and the corresponding pB values were calculated. In Fig.14 is presented the interdependence of these 2 quantities that can be described by the regression equation:

$$\ln\Delta T = 10.35 - 0.078 \cdot pB; \qquad r = 0.93 \qquad (9)$$

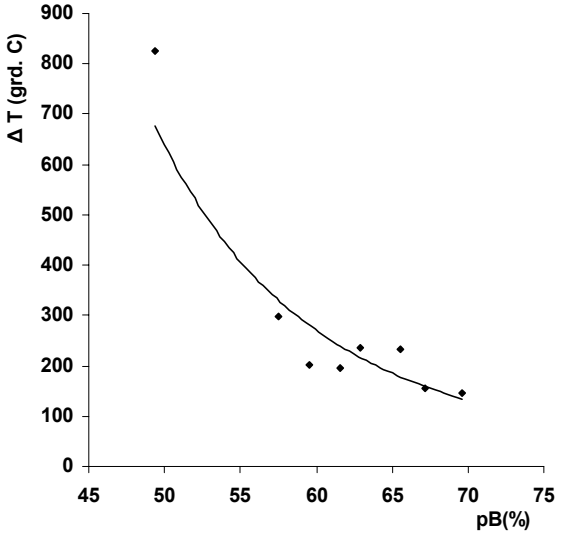

Fig. 14 – Correlation ΔT – pB, for glasses of the SiO_2 - Na_2O oxide system.

The result as shown in Fig. 14 is that the basicity percentage strongly influences the length of the glass processing interval. The increase of pB determines an increase of the tendency of glass crystallization, a decrease of their stability and, as a consequence, the glass is characterized by smaller ΔT values (the glass becomes "shorter").

CONCLUSIONS

The basicity percentage represents a complex structural parameter for the oxide glasses. It strongly correlates with, practically, any other structural characteristic at atomic level (the strength of the electrostatic field, the electronegativity, the electronic polarizability of the oxygen, the coordination number, the oxidation number, the bonding energies, etc.). Because of this, pB can be considered a "globalizing structural indicator" for oxide glasses.

In the present work, the concept through which the properties of the glasses are determined by their structural particularities has been tested. The applications have shown strong inter-correlations between the values of some fixed viscosity points of practical interest, and the basicity percentage for the studied glasses. These correlations are seen for some simpler glasses as well as for some complex oxide compositions of industrial type.

REFERENCES

1. H. Scholze, "Le verre", Ed. Dunod, Paris, 1990.
2. P. Baltă, "Tehnologia sticlei", Editia a-II-a, Editura Didactică si Pedagogică, Bucureşti, 1984.
3. I. Burnea and L. Burnea, "Teoria energo-structurala", Scrisul Românesc, Craiova, 1988.
4. P. Baltă and O. Dumitrescu, *Roum. J. Mat.*, **1991**, *XXI*, 130-132.
5. A. I. Duffy and M. D. Ingram, *J.Non-Cryst.Solids*, **1976**, *21*, 373-411.
6. P. Baltă, C. Spurcaciu, D. Radu and O. Dumitrescu, *J.Non-Cryst.Solids*, **1985**, *71*, 69-75.
7. P. Baltă, *Proc. 15th.* International Congress on Glass, Leningrad, **1989**, 211-214.
8. D. Radu, A. Volceanov and M. Lupescu, *Proc.10th Chech Conference on Glass*, Podebrady, **1997**, 120-129.
9. P. Baltă and D. Radu, *Rev.Roum.Chim*., **1995**, *40*, 10, 977- 982.
10. D. Radu, C. Mazilu and M. Eftimie, *Roum. J. Mat.*, **2003**, *33*, 278-283.
11. V. Dimitrov and S. Sakka, *J. Appl. Phys.,* **1996**, *79*, 1736.
12. F. Y. Yan, F. J. Wood and K. C. Wills, *Proc. 17th. International Congress on Glass,* Beijing, **1995**, 177-182.
13. T. Lakatos, L. G. Johansson and B. Simmingskold, *Glass Technol.*, **1972**, *13*, 88-95.
14. E. M. Rabinovich, A. J. Brue and N. A. Kopylov, "Glasses for Electronic Applications", Florida, 1990.
15. K. H. Karlsson and M. Ronulof, *Glastech.Ber. Glass Sci.Technol.*, **1998**, *71*, 141-145.
16. V. Dimitrov and T. Komatsu, *J. Non-Crystalline Solids*, **1999**, *249*, 160-179.

Revue Roumaine de Chimie, **2007**, *52*(3), 253–259

SYNTHÈSE DE NOUVEAUX DÉRIVÉS *N*-ACYLPHÉNOTHIAZINIQUES POTENTIELLEMENT ACTIFS EN CHIMIOTHÉRAPIE

SYNTHESIS OF NEW *N*-ACYLPHENOTHIAZINIC DERIVATIVES WITH POTENTIAL ACTIVITY IN CHEMOTHERAPY

Elena BÂCU,[a*] Dalila BELEI,[a] Axel COUTURE[b] et Pierre GRANDCLAUDON[b]

[a]Département de Chimie Organique et Biochimie, Faculté de Chimie,
Université "Al. I. Cuza" Iaşi, 11 Bd Carol I, Iaşi-700506, Roumanie
[b]UMR 8009 "COM", Laboratoire de Chimie Organique Physique, Bâtiment C3 (2),
Université des Sciences et Technologies de Lille 1 F-59655 Villeneuve d'Ascq Cedex, France

Reçu le 25 novembre, 2005

Divers sels de cycloimonium **3-6** ont été préparés par alkylation d'hétérocycles azotés (3-methylisoquinoléine, pyrrolopyridine et triazole) par la *N*-(chloroacétyl)phénothiazine. Les composés azapolycycliques **7-9** ont été obtenus par cycloaddition [1,3] sur l'ylure dérivé du sel de 3-methylisoquinolinium **3** avec des dipolarophiles acétyléniques et oléfiniques. Tous les composés synthétisés ont été caractérisés par spectroscopie IR et RMN (^{1}H et ^{13}C).

An array of cycloimonium derivatives **3-6** has been synthesized by alkylation of a variety of azaheterocycles (3-methylisoquinoline, pyrrolopyridine and triazole) with *N*-(chloroacetyl)-phenothiazine. The azamethine ylide derived from 3-methylisoquinolinium salt **3** has been involved in [1,3] cycloaddition reactions with acetylenic or olefinic dipolarophiles to provide the adducts **7-9**. All the synthesized compounds were identified by IR, ^{1}H and ^{13}C NMR spectroscopy.

INTRODUCTION

Il est connu qu'un grand nombre de dérivés phénothiaziniques, obtenus par diverses modifications chimiques effectuées sur la phénothiazine, présentent diverses propriétés pharmacologiques, telles que: tranquillisantes et spasmolytiques,[1-4] antihistaminiques, anticonvulsivantes,[5] antibactériennes[6-8] et antiinflamatoires.[9,10] Plus récemment des études *in vitro* ont révélé que certains dérivés de la phénothiazine étaient dotés de propriétés antitumorales.[4,11-13] Des développements sont encore en cours pour trancher entre des effets cytostatiques et cytotoxiques.[14]

En règle générale, les dérivés phénothiaziniques qui jouent un rôle important en chimiothérapie présentent une chaîne latérale intégrant un deuxième atome d'azote.[15-19]

Dans le cadre de nos recherches engagées sur la synthèse de nouveaux dérivés de la phénothiazine[20-24] et sur l'étude de leurs propriétés,[25-27] notre intérêt s'est porté récemment sur la création de différents modèles structuraux **3-9** construits sur la base de la phénothiazine liée à une variété d'aza-hétérocycles par le biais d'une chaîne carbonée de deux atomes. Un examen de la littérature révèle que quelques dérivés de ce type incluant une *N*-acylphénothiazine présentent des activités physiologiques.[28-30]

RESULTATS

A partir des divers éléments rapportés ci-dessus, nous avons choisi de préparer un certain nombre de sels de cycloimonium **3**, **4**, **6** (3-méthylisoquinolinium, pyrrolopyridinium et triazolium) greffés sur la *N*-acylphénothiazine et de

* Auteur pour correspondance. Tel: 0040 232 201347; Fax: 0040 232 201313; E-mail: elena@uaic.ro

convertir le sel de 3-méthylisoquinolinium en assemblages *N*-acylphénothiazine-benzoindolizine diversement substitués **7**-**9**.

L'introduction de la chaîne de deux atomes de carbone et sa fonctionnalisation terminale ont été directement réalisées par condensation entre la phénothiazine **1** et le chlorure de chloroacétyle pour fournir la *N*-(chloroacétyl)phénothiazine **(2)**.[24,31] Ce dérivé de la phénothiazine constitue une base de départ idéale pour le greffage de divers hétérocycles azotés. En effet le traitement du composé **2** par la 3-méthylisoquinoléine ou par la 4-chloro-1-methyl-1*H*-pyrrolo[3,2-*c*]pyridine dans le dichlorométhane à reflux conduit aux sels quaternaires correspondants **3** et **4** par alkylation de l'azote hétérocyclique (Schéma 1).

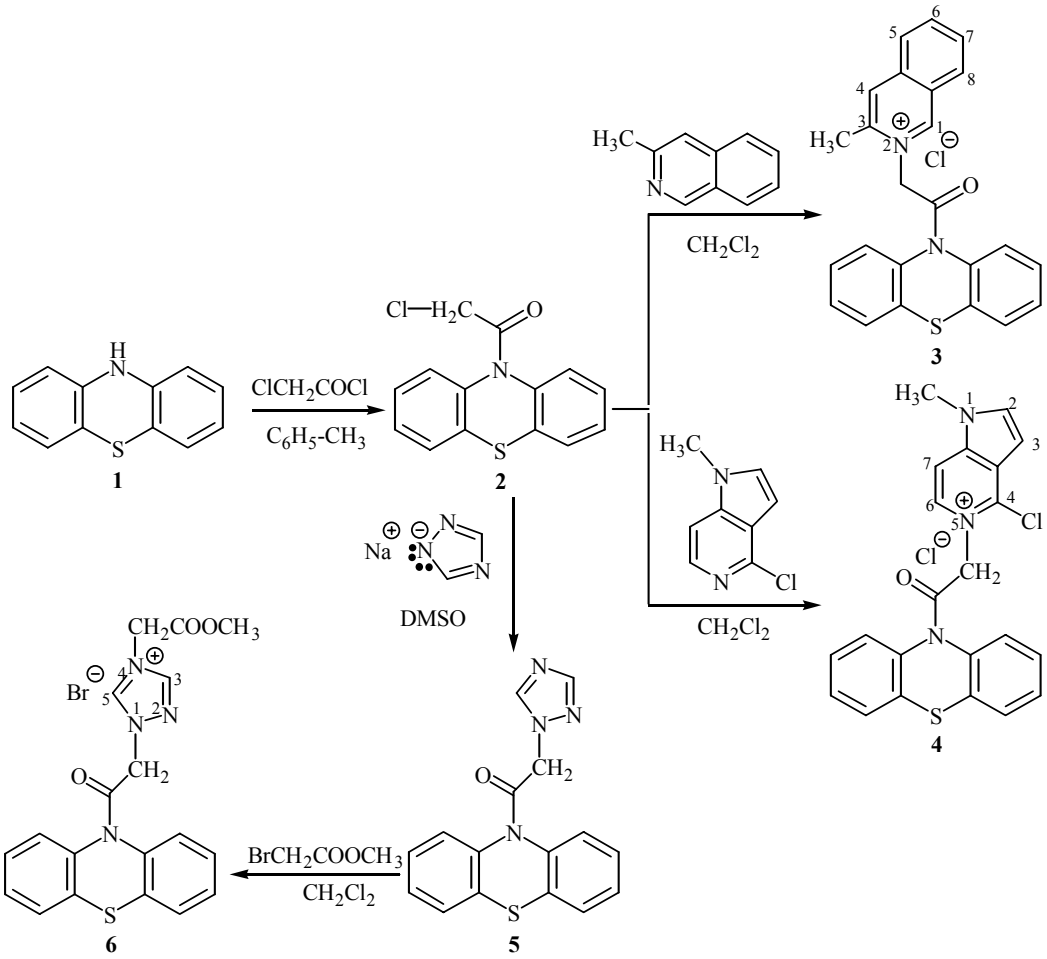

Schéma 1

La condensation de la *N*-(chloroacétyl) phénothiazine (**2)** avec le sel de sodium du 1,2,4-triazole donne accès à un assemblage triazole-phénothiazine **5**. La conversion du composé **5** en sel **6** est réalisée par alkylation sélective de l'un des atomes d'azote du cycle triazolique avec du 2-bromoacétate d'méthyle.

L'une des méthodes les plus efficaces pour bâtir de nouvelles structures polycycliques azotées, souvent difficiles à obtenir par d'autres techniques de synthèse, est la cycloaddition [1,3] d'ylures de cycloimonium avec des dipolarophiles acétyléniques ou oléfiniques. De plus il a été largement démontré que les additions dipolaires d'ylures sont hautement régio- et stéréosélectives.[32-37]

En application de ces principes, le traitement par la triéthylamine du sel quaternaire **3**, dérivé de la 3-méthylisoquinoléine, délivre l'ylure correspondant. La mise en réaction directe de ce *N*-ylure intermédiaire, obtenu *in situ* à partir du sel **3**, avec un dipolarophile acétylénique monosubstitué (propiolate de méthyle ou d'éthyle) dans CH_2Cl_2 à reflux conduit à la formation d'une unité benzoindolizine. Les produits partiellement insaturés, initialement formés au cours de la réaction, ne sont pas isolés car ils sont convertis

spontanément en dérivés aromatiques **7** et **8** (Schéma 2) par isomérisation et ré-aromatisation probablement liées au haut degré de conjugaison des produits finaux.

En revanche, le traitement de l'ylure intermédiaire avec un dipolarophile éthylénique cyclique tel que le *N*-phénylmaléimide, dans CH_2Cl_2 à reflux, permet d'isoler l'adduit primaire **9** qui présente une structure *endo*, thermodynamiquement la plus stable.[36] (Schéma 2).

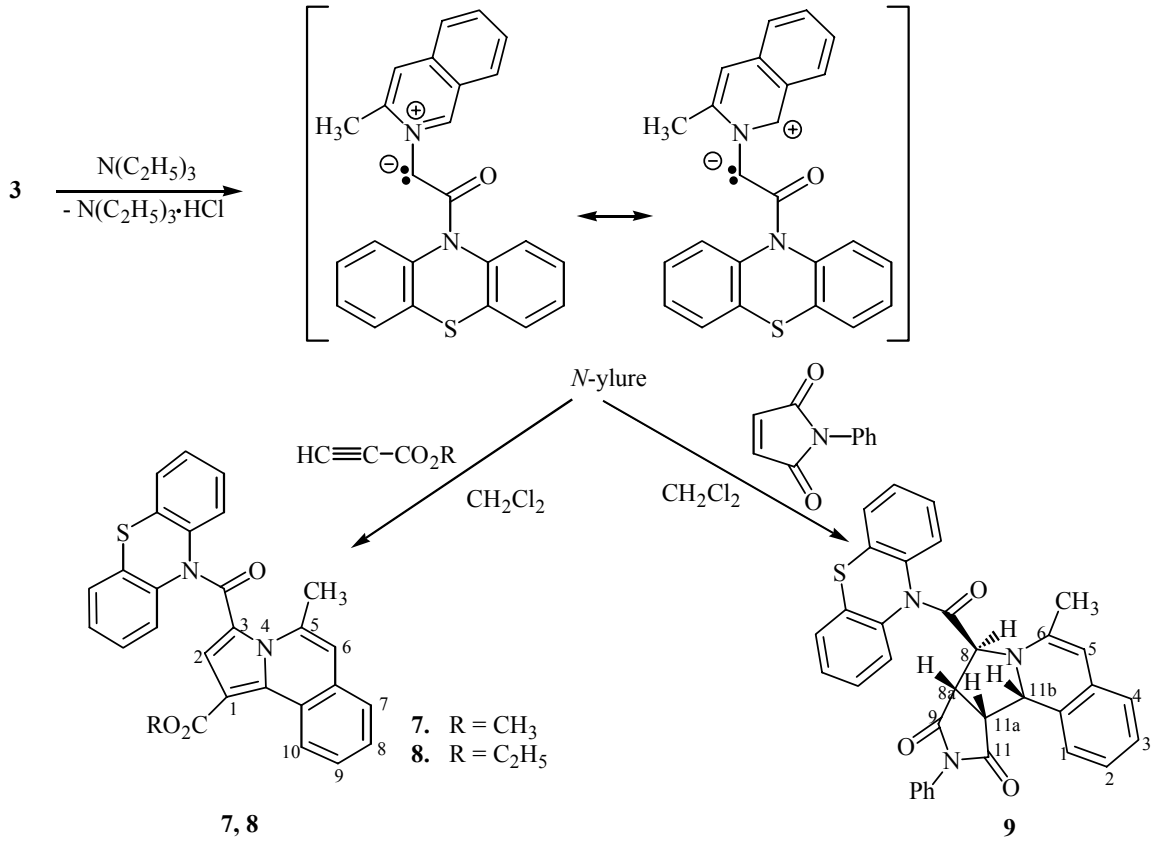

Schéma 2

Tous les composés isolés **3**-**9** ont été caractérisés à l'aide des données spectrales obtenues en IR et en RMN (H^1 et C^{13}).

Les diverses synthèses réalisées ont permis le greffage de différents hétérocycles azotés (pyrrolopyridine, isoquinoléine, pyrroloisoquinoléine et triazole) sur l'atome d'azote de la phénothiazine dans le but d'accéder à des molécules susceptibles de présenter des potentialités thérapeutiques vis-à-vis de différentes pathologies.

DISCUSSION

La structure des nouveaux composés synthétisés **3**-**9** a été établie sur la base des données spectrales suivantes:

Tous les spectres IR présentent, à côté des absorptions spécifiques du cycle phénothiazinique, des absorptions très intenses dues à la vibration du groupement C=O de la fonction amide à ν = 1677-1688 cm^{-1}. Dans le spectre du cycloadduit **9** coexistent deux bandes d'absorptions pour les C=O d'amide et d'imide à ν = 1670 et 1701 cm^{-1}. En outre, pour le sel **6**, le signal le plus important (à ν = 1736 cm^{-1}) peut être attribué au groupement C=O de la fonction ester. Il en va de même pour les spectres des composés **7** et **8**, obtenus par réaction de cycloaddition 1,3 dipolaire, qui présentent également des absorptions de grande intensité pour le groupement C=O de la partie amide à ν = 1661 cm^{-1} ainsi que pour le groupement C=O de la partie ester à ν = 1706 cm^{-1}.

Les spectres RMN (^1H et ^{13}C) fournissent les informations essentielles concernant les structures proposées (Tableau 1).

Tableau 1

Quelques caractéristiques des spectres RMN (^{1}H et ^{13}C) enregistrés pour les composés **3-9**

Produit	Solvant	RMN ^{1}H (δ, ppm)			RMN ^{13}C (δ, ppm)						
		CH_3	**N-CR^1R^2-CO**	**H^{α}**	**CH_3**	**N-CR^1R^2-CO**	**C^{α}**	**$C^{\alpha'}$**	**N-C=O**	**COOR**	**O-R**
3	DMSO-d_6 / D_2O, (2:5)	2,56 ($_3C$-CH_3)	4,80 ($R^1R^2 = H_2$)	9,62	19,0 ($_3C$-CH_3)	masqué (Csec.)	151,5	143,1	164,2	-	-
4	DMSO-d_6	4,00 (N-CH_3)	3,96 ($R^1R^2 = H_2$)	9,02	34,5 (N-CH_3)	59,5 (Csec.)	167,1	142,3	164,4	-	-
5	DMSO-d_6	-	5,34 ($R^1R^2 = H_2$)	8,42	-	50,8 (Csec.)	151,3	-	165,0	-	-
6	DMSO-d_6 / D_2O, (1:1)	5,48 (O-CH_3)	5,16 ($R^1R^2 = H_2$)	8,91	-	49,4 (Csec.)	146,1	145,6	164,2	167,5	54,3 (R=CH_3)
7	DMSO-d_6	2,94 ($_5C$-CH_3) 3,75 (O-CH_3)	-	-	21,2 ($_5C$-CH_3)	121,1 (Cq)	129,5	131,7	164,3	160,3	51,7 (R = CH_3)
8	DMSO-d_6	2,97 ($_5C$-CH_3)	-	-	21,5 ($_5C$-CH_3)	120,9 (Cq)	134,6	138,4	163,8	160,3	14,0 et 60,0 (R = CH_2CH_3)
9	DMSO-d_6	1,13 ($_6C$-CH_3)	5,67 (R^1 = H)	5,08	18,0 ($_6C$-CH_3)	63,3 (Ct)	100,4	138,1	167,8 et 173,9	-	-

Une augmentation du déplacement chimique ($\Delta\delta$ = 0,49 ppm) pour les deux atomes H^{α} (C_3-H et C_5-H) situés à proximité de l'azote cationique du sel de cycloimonium **6** (δ = 8,91 ppm) par comparaison avec les mêmes atomes dans le produit non ionique **5** (δ = 8,42 ppm) est en faveur de la structure de sel. Les atomes H^{α} dans la partie pyridinium des composés **3** (C_1-H) et **4** (C_6-H) apparaissent dans la même zone de glissement chimique: δ = 9,62 et δ = 9,02 ppm, respectivement.

Des résultats similaires sont obtenus en RMN ^{13}C pour les atomes de carbone situés près de l'azote quaternaire. Ainsi dans le sel **3**, les déplacements chimiques correspondant aux atomes de carbone C_1 (δ = 151,5 ppm) et C_3 (δ = 143,1 ppm) situés en α de l'azote de l'entité pyridinium sont plus élevés que les déplacement chimiques de ces mêmes carbones dans les structures de type azacyclique **7-9** (δ voisin de 135 ppm; Tableau 1).

Dans le cas des cycloadduits **7** et **8** les spectres RMN (^1H et ^{13}C) confirment le caractère insaturé (aromatique) des structures par l'absence de signaux correspondants à la résonance de protons cyclaniques (δ situé entre 3,5-6,0 ppm) et de carbones tertiaires (δ situé entre 52-100 ppm).

Au contraire, l'adduit **9** présente en RMN ^1H quatre signaux à δ = 3,63 ppm (1H, t, CH_{11a}, J = 7,9 Hz), δ = 3,9-4,3 ppm (1H, s bande large, $_{8a}CH$), δ = 5,08 ppm (1H, m, $_{11b}CH$), δ = 5,67 ppm (1H, s, $_{8}CH$) ainsi que les signaux des carbones tertiaires (CH) correspondants à δ = 47,8; 51,5; 63,3; et 100,4 ppm, qui permettent de valider la structure saturée de ce cycloadduit.

Tous les autres signaux des spectres RMN (^1H et ^{13}C) des produits **3-9** sont en concordance avec les structures proposées.

PARTIE EXPERIMENTALE

Les spectres RMN (^1H et ^{13}C) ont été enregistrés sur un spectromètre Bruker-AM 300 ou Bruker DRX 400, en utilisant comme solvants deutérés le diméthylsulfoxyde (DMSO-*d6*) ou des mélanges DMSO-d_6/D_2O; déplacements chimiques en ppm par rapport au TMS. Les spectres IR ont été enregistrés sur un appareil IR-TF JASCO 660+ ou sur un spectromètre Perkin-Elmer 880. Les analyses élémentaires C, H, N ont été réalisées sur un appareil Carlo-Erba CHNS-11110. Les points de fusion, en tube capillaire, ont été déterminés avec un appareil MEL-TEMP II et ne sont pas corrigés.

La *N*-(chloroacétyl)phénothiazine (**2**) a été préparée selon un protocole décrit précédemment.[24,31]

Chlorure de 3-méthyl -2-[2-oxo-2-(10*H*-phénothiazin-10-yl)-éthyl]-isoquinolinium (3)

Une solution de *N*-(chloroacétyl)phénothiazine (**2**, 2,75 g, 10 mmol) et de 3-méthyl-isoquinoléine (1,57 g, 11 mmol) dans CH_2Cl_2 (15 mL) est portée à reflux pendant une période de 5 h. Après refroidissement, le produit **3** qui se sépare est filtré, lavé avec CH_2Cl_2, séché puis recristallisé dans un mélange éthanol/acétone; Cristaux blancs, F = 278-280 °C. Analyse: $C_{24}H_{19}ClN_2OS$ (418,5), calc.%: C, 68,81; H, 4,57; N, 6,69; tr.% : C, 68,73; H, 4,61; N, 7,03; Spectre IR (KBr) ν_{max}, cm^{-1}: 1678 (CO_{amide}); RMN ^1H (300 MHz, DMSO-d_6/D_2O, 2:5), δ_H, ppm: 2,56 (s, 3H, CH_3); 5,5 et 6,4 (s, large, 2H, ^+N-CH_2CO); 7,2-7,87 (m, 8H, H_{phen}); 7,95-8,4 (m, 5H, H_{iso}); 9,63 (s, 1H, H_1); RMN ^{13}C (DMSO-d_6-D_2O, 2:5), δ_C, ppm: 19,0 (CH_3); CH_2 masqué; 127,5 126,0 126,1 129,5 130,5 137,5 138,2 143,1 (C et CH); 151,5 ($_1CH$); 164,2 (NC=O).

Chlorure de 4-chloro-1-méthyl-5-[2-oxo-2-(10*H*-phénothiazin-10-yl)-éthyl]-1*H*-pyrrolo[3,2-*c*]pyridin-5-ium (4)

A une solution de 2,75 g (10 mmol) de *N*-(chloroacetyl) phénothiazine dans CH_2Cl_2 (15 mL) sont ajoutés sous agitation 2 g (12 mmol) de 4-chloro-1-methyl-pyrrolo[3,2-*c*]pyridine. La solution est portée à reflux pendant une période de 4 h. Après refroidissement, le produit 4 qui se sépare est filtré, séché, puis recristallisé dans l'éthanol; Rdt = 78%. Produit blanc, F = 218-219 °C. Analyse: $C_{22}H_{17}Cl_2N_3OS$ (442), calc.% : C, 59,73; H, 3,87; N, 9,5; tr.% : C, 59,57; H, 3,74; N, 9,61; Spectre IR (KBr) ν_{max}, cm^{-1}: 1681 (CO_{amide}); RMN ^1H (300 MHz, DMSO-d_6), δ_H, ppm, J Hz: 3,96 (s large, 2H, ^+N-CH_2CO); 4,0 (s, 3H, N-CH_3); 7,03 (d, 1H, J = 3,3, H_3); 7,25-7,85 (m, 8H, H_{phen}); 8,05 (d, 1H, J = 3,3, H_2); 8,31-8,33 (d, 1H, J =7,2, H_7); 9,02 (d, 1H, J = 7,2, H_6); RMN ^{13}C (DMSO-d_6), δ_C, ppm: 34,5 (CH_3-N); 59,5 (CH_2); 103,8; 108,1; 124,4; 127,0-128,5; 132,7-138.1; 138,4; 138,9; 139,3; 140,0 (C et CH); 142,3 ($_6C$); 164,4 (NC=O); 167,1($_4C$).

1-(10*H*-Phénothiazin-10-yl)-2-[1,2,4] triazol-1-yl-éthanone (5)

Un mélange de 2,75 g (10 mmol) de *N*-(chloroacétyl) phénothiazine et de 1 g (10 mmol) de sel de sodium du 1,2,4-triazole dans 15 mL de DMSO est porté à reflux pendant 5h. Après refroidissement, NaCl formé qui se sépare est éliminé par filtration. Le filtrat est alors ajoute dans l'eau pour précipiter un solide qui est filtré et recristallisé dans l'éthanol; Rdt = 75%. Produit blanc, F = 167-169 °C. Analyse: $C_{16}H_{12}N_4OS$ (308), calc. %: C, 62,32; H, 3,92; N, 18,17; tr. % : C, 62,58; H, 3,89; N, 18,43; Spectre IR (KBr) ν_{max}, cm^{-1}: 1682 (CO_{amide}); RMN ^1H (400 MHz, DMSO-d_6), δ_H, ppm: 5,25-5,55 (s, large, 2H, CH_2); 7,28-7,80 (m, 8H, H_{phen}), 7,96 (s, 1H, H_3); 8,42 (s, 1H, H_5); RMN ^{13}C (DMSO-d_6), δ_C, ppm: 50,8 (CH_2); 127,0; 127,6; 128,1; 132,2; 137,2 (CH et C_{pheno}); 145,6 ($_3CH$); 145,6 ($_5CH$); 165,0 (NC=O).

Bromure de 4-méthoxycarbonylmethyl-1-[2-oxo-2-(10*H*-phénothiazin-10-yl)-ethyl]-1*H*-1,2,4-triazol-4-ium (6)

Une solution de 1 g (3,2 mmol) de 1-(10*H*-phénothiazin-10-yl)-2-[1,2,4] triazol-1-yl-éthanone (**5**) et 1 mL (9 mmol) de bromoacétate d'éthyle dans CH_2Cl_2 (15 mL) est maintenu à température ambiante pendant deux jours. Le sel qui se sépare est filtré et recristallisé dans l'éthanol; Rdt = 70%. Produit blanc; F = 225-227 °C.

Analyse: $C_{19}H_{17}BrN_4O_3S$ (461), calc.%: C, 49,47; H, 3,71; N, 12,14; tr.%: C, 49,24; H, 3,63; N, 12,26; Spectre IR (KBr) ν_{max}, cm^{-1}: 1688 (CO_{amide}); 1736 (CO_{ester}); RMN ^1H (400 MHz, DMSO-d_6), δ_H, ppm: 5,16 (s, 4H, $2CH_2$); 5,48 (s, 3H, OCH_3);

7,24-7,60 (m, 8H, H_{pheno}); 8,91 (s, 2H, $H_{3,5}$); RMN ^{13}C (DMSO-d_6), δ_C, ppm: 49,4 (CH_2); 54,3 (OCH_3); 127.2-137.3 (CH et C_{pheno}); 145,6($_3$CH); 146,1($_5$CH); 164,2 (NC=O); 167,5 (OC=O).

Méthode générale pour la synthèse des adduits 7 et 8

De la triéthylamine (TEA, 0,83 mL, 6 mmol) est additionnée goutte à goutte à une suspension agitée de 2 g (5 mmol) de chlorure de 2-[2-oxo-2-(10*H*-phénothiazin-10-yl)-ethyl]-3-methyl-isoquinolein-2-ium (**3**) dans CH_2Cl_2 (10 mL). Le méthyl ou l'éthyl propiolate (6 mmol) est ensuite ajouté. Le mélange est porté à reflux pendant 3 h. Après refroidissement, le chlorhydrate de triéthylamine est filtré, la solution est concentrée et le produit brut est précipité par addition d'éthanol. Le solide obtenu est filtré puis recristallisé dans l'acétone.

5-Méthyl-3-(10*H*-phénothiazin-10-carbonyl)-pyrrolo[2,1-*a*]isoquinoléine-1-carboxylate de méthyle (7)

Produit blanc: Rdt = 73%; F = 237-238 °C. Analyse: $C_{28}H_{20}N_2O_3S$ (464), calc.%: C, 72,39; H, 4,34; N, 6,03; tr.%: C, 72,24; H, 4,27; N, 6,21; Spectre IR (KBr) ν_{max}, cm^{-1}: 1661 (CO_{amide}); 1706 (CO_{ester}); RMN ^1H (300 MHz, DMSO-d_6), δ_H, ppm, *J* Hz: 2,94 (s, 1H, CH_3); 3,75 (s, 3H, OCH_3); 6,85 (s, 1H, H_{2pyr}); 7,25-7,68 (11H, m, $8H_{phen}$+$3H_{iso}$); 7,85 (d, 1H, *J* = 7,2 H_7); 9,52 (dd, 1H, *J* = 7,5 et 1,3, H_{10}); RMN ^{13}C (DMSO-d_6), δ_C, ppm: 21,2 ($_5$C-CH_3); 51,7 (OCH_3); 107,8; 115,6; 119.9; 121,1; 121,6; 123,0; 126,1; 126,9; 127,3; 127,4; 128,0; 128,7;129,5; 131,7; 134,1; 135,0; 137,3 (C et CH); 160,3 (COOMe); 164,3 (CON).

5-Méthyl-3-(10*H*-phénothiazin-10-carbonyl)-pyrrolo[2,1-*a*]isoquinoléine-1-carboxylate d'éthyle (8)

Produit blanc: Rdt = 75%; F = 231-232°C. Analyse: $C_{29}H_{22}N_2O_3S$ (478), calc.%: C, 72,78; H, 4,63; N, 5,85; tr.%: C, 72,56; H, 4,57; N, 5,95; Spectre IR (KBr) ν_{max}, cm^{-1}: 1661 (CO_{amide}); 1706 (CO_{ester}); RMN-^1H (300 MHz, DMSO-d_6), δ_H, ppm, *J* Hz: 1,23 (t, 3H, *J* = 7,2, CH_3); 2,97 (s, 3H, CH_3); 4,21 (q, 2H, *J* = 7,2, OCH_2); 6,91 (s, 1H, H_2); 7,25-7,33 (m, $4H_{phen}$); 7,35 (s, 1H, H_6); 7,53-7,62 (m, 6H, $4H_{phen}$+ H_8+H_9); 7,80 (dd, 1H, *J* = 7,2 et 1,4, H_7); 9,53 (dd, 1H, *J* =8,0 et 1,7, H_{10}); RMN-^{13}C (DMSO-d_6), δ_C, ppm: 14,0 (CH_3); 21,5 (CH_3); 60,0 (OCH_2); 108,3 ($_1$C); 115,5 ($_2$CH); 121,0 ($_3$C); 121,6 ($_6$CH); 123,0 ($_{10a}$C); 126,2; 126,8; 127,2; 127,4; 127,8; 128,6 (CH_{phen} + CH_{izo}); 129,5 ($2C_{phen}$); 131,8 ($_{6a}$C); 134,0 ($2C_{phen}$); 134,6 ($_5$C); 138,4 ($_{10b}$C) ; 160,3 (COOEt); 163,8 (CON).

6-Méthyl-8-(10*H*-phenothiazin-10-carbonyl)-10-phényl-8,8a,9,11,11a,11b-hexahydro-7*H*-pyrrolo[3',4':3,4]pyrrolo[2,1-*a*]isoquinoléine-9,11-dione (9)

Une solution de TEA (0,52 mL) dans CH_2Cl_2 (5 mL) est ajoutée goutte à goutte à une suspension de 1,3 g (3,1 mmol) de 2-[2-oxo-2-(10*H*-phénothiazin-10-yl)-éthyl]-3-methyl-isoquinolein-2-ium chlorure (**3**) dans CH_2Cl_2 (5 mL). Ensuite 0,6g (3,4 mmol) de *N*-phénylmaléimide sont ajoutés et le mélange est agité à température ambiante pendant 48 h. L'évolution de la réaction est suivie par chromatographie sur couche mince. Le chlorhydrate de triéthylamine est lavé à l'eau et le solvant est évaporé. Le solide brut obtenu est recristallisé dans un mélange éthanol/acétone/acétate d'éthyle (7:3:4); Rdt = 83%; Produit blanc; F = 217-219 °C. Analyse: $C_{34}H_{25}N_3O_3S$ (555), calc.%: C, 73,49; H, 4,53; N, 7,56; tr.%: C, 73,23; H, 4,49; N, 7,73; Spectre IR (KBr) ν_{max}, cm^{-1}: 1670 et 1701 (CO_{amide}); RMN ^1H (300 MHz, DMSO-d_6), δ_H, ppm, *J* Hz: 1,13 (s, large, 3H, CH_3); 3,63 (t, 1H, *J* =7,95, H_{11a}); 4,20 (m, 1H, H_{8a}); 5,08 (m, 1H, H_{11b}); 5,67 (s, 1H, H_8); 6,73-7,98 (m, 18H, $H_{aromatiq}$); RMN ^{13}C (DMSO-d_6), δ_C, ppm: 18,0 (CH_3); 47,8,($_{11a}$CH); 51,5 ($_{8a}$CH); 63,3 ($_8$CH); 100,4 ($_{11b}$CH); 123,4-141,0 (CH et $C_{aromatiq}$); 167,8 (CON); 173,9 (2CO).

RÉFÉRENCES

1. A. S. Horn, "Comprehensive Medicinal Chemistry. The Rational Design, Mechanistic Study, and Therapeutic Application of Chemical Compounds: Membranes and Receptors", vol 3, Pergamon Press, Oxford, 1990, 321.
2. E. Usdin, H. Eckert, I. S. Forrest (Eds.), "Developments in Neuroscience. Phenothiazines and structurally Related Drugs: Basic and Clinical Studies", vol. 7, Elsevier, New York, 1980.
3. A. Lespagnol, *Bull. Soc. Chim. Fr.*, **1960**, 1291-1299.
4. R. R. Gupta (Ed.), "Bioactive Molecules. Phenothiazines and 1,4-Benzothiazines: Chemical and Biomedical Aspects", vol.4, Elsevier, Amsterdam, 1988.
5. M. L. Laws, R. R. Roberts, J. M. Nicholson, R. Butcher, J. P. Stables, A. M. Goodwin, C. A. Smith et K. R. Scott, *Bioorg. Med. Chem.*, **1998,** *6*, 2289-2299.
6. J. E. Kristiansen, *Dan. Med. Bull.,* **1989**, *36*, 178-185.
7. L. Amaral, J. E. Kristiansen, M. Viveiros et J. Atouguia, *J. Antimicrob. Chemother.*, **2001**, *47*, 505-511.
8. L. Amaral, M. Viveiros et J. Molnar, *In Vivo*, **2004**, *18*, 725-731.
9. S. Sharma, S. Lata, A. Kumar et V. K. Srivastava, *Indian J. Physiol. Pharmacol*., **2002**, *46*, 235-240.
10. S. Sharma, V. K. Srivastava et A. Kumar, *Pharmazie*, **2005**, *60*, 18-22.
11. N. Motohashi, S. R. Gollapudi, J. Emrani et K. R. Bhattiprolu, *Cancer Investigation*, **1991**, *9*, 305-319.
12. L. R. Morgan, A. H. Rodgers, B. W. Leblanc, S. M. Boué, Y. Yang, B. S. Jursic et R. B. Cole, *Bioorg. Med. Chem. Lett*., **2001**, *11*, 2193-2195.
13. F. Barbieri, A. Alama, B. Tasso, V. Boido, C. Bruzzo et F. Sparatore, *Invest. New Drugs*, **2003**, *21*, 413-420.
14. Z. Zhelev, H. Ohba, R. Bakalova, V. Hadjimitova, M. Ishikawa, Y. Shinohava et Y. Baba, *Cancer Chemother. Pharmacol*., **2004**, *53*, 267-275.
15. S. P. Massie, *Chem. Rev.,* **1954**, *54*, 797-833.
16. C. Bodea et I. Silberg, *Adv. Heterocycl. Chem*., **1968**, *9*, 321-460.
17. S. Saraf, F. Al-Omran et B. Al-Saleh, *Heterocycles*, **1987**, *26*, 239-273.
18. M. Sainsbury (Ed), "1,4-Thiazines, 1,4-Benzothiazines, Phenothiazines and Related Compounds, in Rodd's Chemistry of Carbon Compounds" (2nd Edition), vol 4, Elsevier, Amsterdam, 1998, p. 575-608.
19. D. Lednicer et L. A. Mitscher, "The Organic Chemistry of Drug Synthesis", vol 1, Wiley, New York, 1976, p. 372-392.
20. M. Petrovanu, E. Bâcu, P. Grandclaudon et A. Couture, *Phosphorus, Sulfur, Silicon,* **1996**, *108*, 231-237.
21. E. Bâcu, M. Petrovanu, P. Grandclaudon et A. Couture, *Roum. Biotech. Lett*., **1997**, *2*, 383-389.
22. E. Bâcu, M. Petrovanu, A. Couture et P. Grandclaudon, *Phosphorus, Sulfur, Silicon*, **1999**, *149*, 207-220.
23. E. Bâcu, A. Couture et P. Grandclaudon, *Synth. Commun.,* **2003,** *33*, 143-151.

24. E. Bâcu, D. Belei, G. Nowogrocki, A. Couture et P. Grandclaudon, *Org. Biomol. Chem.,* **2003**, *1*, 2377-2382.
25. E. Bâcu, M. Petrovanu, C. Antohie, I. Ciocoiu et O. C. Mungiu, *Ann. Pharm. Fr*., **1997**, *55*, 268-271.
26. D. Belei, C. E. Lupuşoru, C. M. Ghiciuc, E. Bâcu, I. Antonesei, L. Tartau, A. Couture et P. Grandclaudon, *Terapeutica, Toxicologie, Farmacologie clinica*, **2004**, *VIII*, 97-101.
27. C. M. Ghiciuc, D. Belei, C. E. Lupuşoru, E. Bâcu, I. M. Antonesi, O. Jerca, R. Lupuşoru, A. Couture et P. Grandclaudon, *Ann. Pharm. Fr.,* **2004**, *62*, 43-48.
28. E. Lukevics, M. Trushule, S. Germane et I. Turovskii, *Chem. Heterocycl. Compd.*, **1997**, *33*, 229-233.
29. V. Singh, R. Khanna, V. K. Srivastara, G. Palit et K. Shanker, *Arzneim-Forsch*, **1992,** *42*, 277-280.
30. A. Sparatore et F. Sparatore, *Farmaco*, **1994**, *49*, 5-17.
31. Y. Imakura, T. Konishi, K. Uchida, H. Sakurai, S. Kobayashi, A. Haruno, K. Tajima et S. Yamashita, *Chem. Pharm. Bull.*, **1994**, *42*, 500-511.
32. A. W. Johnson, "Ylide Chemistry", Academic Press, New York, 1966.
33. I. Zugrăvescu et M. Petrovanu, "N-Ylide Chemistry", McGraw Hill, New York, 1976.
34. G. Surpăţeanu, J. P. Catteau, P. Karafiloglou et A. Lablache-Combier, *Tetrahedron*, **1976**, *32*, 2647-2663.
35. G. Surpăţeanu et A. Lablache-Combier, *Heterocycles*, **1984**, *22*, 2079-2128**.**
36. O. Tsuge, S. Kanemasa et S. Takenaka, *Bull. Chem. Soc. Jpn*, **1985**, *58*, 3137-3157.
37. O. Tsuge et S. Kanemasa, *Adv. Heterocycl. Chem.*, **1989,** *45*, 231-349.

Revue Roumaine de Chimie, **2007**, *52*(3), 261–266

HPLC METHOD FOR QUANTIFICATION OF NIZATIDINE AND ITS N-DESMETHYLMETABOLITE IN HUMAN PLASMA

Silvia IMRE[a*], Laurian VLASE[b] and Sorin E. LEUCUȚA[b]

[a]Faculty of Pharmacy, University of Medicine and Pharmacy, Gheorghe Marinescu 38, Targu-Mures, RO-540139, Roumania, E-mail: silsta@yahoo.com
[b]Faculty of Pharmacy, University of Medicine and Pharmacy "Iuliu Hatieganu", Emil Isac 13, Cluj-Napoca, RO-400023, Roumania

Received August 3, 2006

A simple and fast HPLC method for quantification of nizatidine and N-desmethylnizatidine in human plasma has been developed and validated. After protein precipitation from plasma sample with perchloric acid, clear supernatant was injected at 42 ºC into a C18 column. The elution was made in 4 minutes at 1 ml min^{-1} in gradient mode, with an UV detection at 314 nm, using a mixture of aqueous potassium dihydrogenophosphate 40 mM pH 2.3, methanol and acetonitrile. The linearity domains were established between 80 to 3200 ng ml^{-1} for nizatidine and between 12 and 484 ng ml^{-1} for N-desmethylnizatidine, respectively. Accuracy (bias%) and precision (CV%) were less than 5.3% for intra-day assay and 8.1%, for inter-day assay, and less than 11.4% and 17.2%, respectively, at the limits of quantification. The recovery ranged between 93.9 and 104.2%. The analytes were proved to be stable in plasma over a period of 6 months below -20 ºC.

INTRODUCTION

Nizatidine, N-[2-[[[2-[(dimethylamino)methyl]-4-thiazolyl]methyl]thio]ethyl]-N'-methyl-2-nitro-1,1-ethenediamine, is a competitive reversible H_2-receptor antagonist approved in adults for the treatment of acid-related gastrointestinal disorders, including duodenal and gastric ulcers, erosive and ulcerative esophagitis, and gastroesophageal reflux disease.[1,2]

The literature of the analytical chemistry of nizatidine in human plasma is extensive, with methods based on HPLC with ultraviolet[3-5], MS[6-8] or electrochemical detection.[9,10] The sample preparation approach was mainly liquid-liquid extraction[11,13], but solid-phase extraction was also used.[6,7,12]

In a single-dose pharmacokinetic/ bioequivalence (PK/BE) study of a medicinal product, the extrapolated area of the curve which describes plasma concentration of the drug and metabolites versus time after administration must not be greater than 20% of total calculated area. To achieve this requirement a quantifiable concentration must be obtained after five half-life times and the sensitivity of the applied analytical method plays an important role. In the mean time, a bioequivalence study involves analysis of hundred of samples and the development of a suitable chromatographic method must take into account not only a sensitive procedure, but also a fast one.

Taking into account these facts, the primary aim of the study was to develop a fast HPLC method with enough sensitivity to quantify simultaneously nizatidine and N-desmethylnizatidine in human plasma by applying protein precipitation after oral administration of 300 mg nizatidine. None of the studied articles applied protein precipitation, a simple and low cost plasma sample preparation. The developed and validated method was successfully applied for bioequivalence investigation of two medicinal products containing nizatidine by monitoring the signal of both parent drug and its N-desmethylmetabolite.

RESULTS AND DISCUSSION

The endogenous compounds or the used anticoagulant did not interfere at the retention

* Corresponding author.

times of nizatidine and N-desmethylnizatidine (figure 1). The short gradient with high concentration of acetonitrile was introduced just before analytes elution only for within-run column recondition and to have a run-time as short as possible; in fact the elution of the analytes is on the isocratic condition.

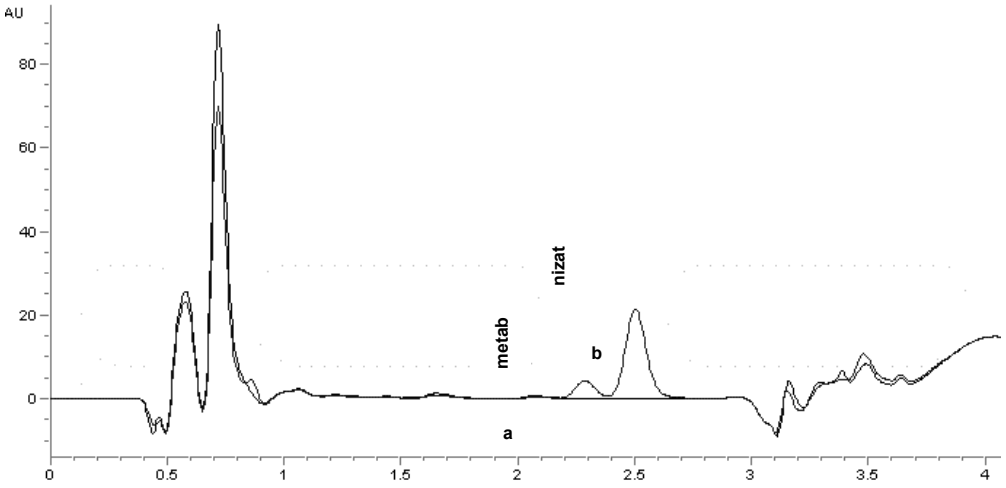

Fig. 1 – Chromatogram of a. blank plasma and b. plasma sample of a healthy volunteer at 1.5 hours after oral administration of 300 mg nizatidine (retention times: 2.5 minutes nizat – nizatidine; 2.3 minutes metab – N-desmethylnizatidine).

The calibration curves showed linear response over the range of concentration used in the assay procedure. The mean calibration curves were: for nizatidine in the concentration range 80 - 3200 ng/ml, Area = 0.1117 c (±0.0002) – 2.088(±0.240), N = 7 calibration points, n = 3 days, weigth factor 1/c, coefficient of correlation greater than 0.999, with the residuals distribution within ±16%; for N-desmethylnizatidine in the concentration range 12 - 484 ng/ml Area = 0.1106 c (±0.0002) – 0.3854(±0.0334), N = 7 calibration points, n = 3 days, weigth factor 1/c, coefficient of correlation greater than 0.999, with the residuals distribution within ±18%.

The inter- and intra-day precision and accuracy results are showed in Table 1 for nizatidine and in Table 2 for desmethylmetabolite and were less than 5.3 % for intra-day assay and 8.1 %, for inter-day assay. The lower limits of quantification were established at 80 ng/ml nizatidine and 12 ng/ml N-desmethylnizatidine, with intra- and inter-day accuracy and precision less than 15.7% and 17.2%, respectively, and were sensitive enough to monitor concentrations of analytes over 12 hours after oral administration of 300 mg nizatidine.

The recovery was consistent and ranged between 93.9 and 102.5% for nizatidine and between 93.5 and 104.2%, for N-desmethylnizatidine (Tables 1 and 2), with a standard deviation which allowed the quantitative determination of the analytes without using internal standard.

The stability study demonstrated that nizatidine and N-desmethylnizatidine could be stored below -20 ºC at least six months. The back calculated concentrations ranged between -0.7 to 3.8 % for nizatidine and between 4.6 to 8.9%, for metabolite (Table 3), respectively. The values were between ±15%, the acceptable limits for bioequivalence methods accuracy.

The validated method was applied for bioequivalence investigation of two medicinal products containing nizatidine. The concentration profiles of nizatidine and its desmethylmetabolite after oral administration of 300 mg nizatidine are given in Figure 2. In six assay runs 576 unknown plasma samples were analyzed, each analytical run consisting of seven calibration standards, six quality control samples (QC) and 96 unknown samples of four volunteers in the study. The calibration curve slopes had a normal variation domain (slope ± 2s) of 0.1119 ± 0.0028 for nizatidine and 0.1109 ± 0.0012 for metabolite

(n = 6). The results of the quality control QC samples analysis provided the basis of accepting or rejecting the runs during clinical samples analysis. At least four out of six QC samples were within ±15% of their respective nominal value in each analytical run and no tendency of concentration variation was observed (Figure 3). All the runs were validated.

Table 1

Intra- and inter-day precision and accuracy (n = 3) for nizatidine

$c_{nominal}$, ng ml^{-1}	Intra-day				Inter-day		
	Mean c_{found}, ng ml^{-1} (±SD)	CV%	Bias, %	Recovery % (±SD)	Mean c_{found}, ng ml^{-1} (±SD)	CV%	Bias, %
80.06	88.6(3.7)	4.2	10.7	102.5(5.5)	92.6(2.1)	2.3	15.7
160.1	166.6(8.9)	5.3	4.1	93.9(5.6)	172.8(3.6)	2.1	7.9
1601	1559(38.5)	2.5	-2.6	100.3(2.5)	1564(33.2)	2.1	-2.3
2402	2363(42)	1.8	-1.6	100.8(1.8)	2365(47.8)	2.0	-1.5

Table 2

Intra- and inter-day precision and accuracy (n = 3) for N-desmethylnizatidine

$c_{nominal}$, ng ml^{-1}	Intra-day				Inter-day		
	Mean c_{found}, ng ml^{-1} (±SD)	CV%	Bias, %	Recovery % (±SD)	Mean c_{found}, ng ml^{-1} (±SD)	CV%	Bias, %
12.12	13.5(0.7)	5.2	11.4	104.2(7.5)	14.2(0.4)	2.8	17.2
24.24	25.5(0.4)	1.6	5.2	93.5(1.9)	26.2(0.7)	2.7	8.1
242.4	237.2(6.3)	2.7	-2.2	104.2(2.8)	238.3(4.0)	1.7	-1.7
363.6	361.1(6.8)	1.9	-0.7	104.1(2.0)	358.0(7.1)	2.0	-1.5

Table 3

Results of the stability study below -20 ºC (n = 3)

Tested sample / Time, months		0	2	4	6
347.0 ng ml^{-1} nizatidine	CV%	1.0	3.2	3.5	1.0
	Bias%	-0.7	3.8	3.3	0.5
67.2 ng ml^{-1} N-desmethylnizatidine	CV%	2.0	1.2	4.2	1.6
	Bias%	5.6	8.9	8.2	4.6

In conclusion, the proposed method proved to be accurate and precise and, in less than four minutes, both analyte and its N-desmethylmetabolite are well separated from endogenous compounds. Without using internal standard and applying a single and simple extraction step, a specific and efficient analysis of a large number of plasma samples could be performed. The successfully transfer of the method between two laboratories proved the reproducibility of the method.

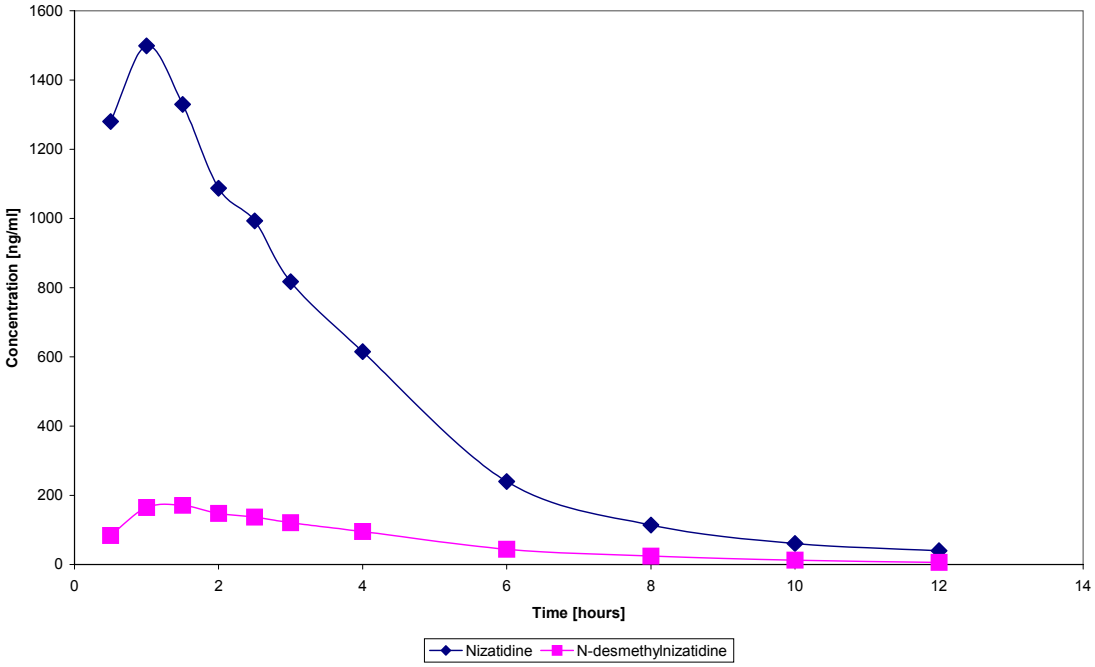

Fig. 2 – Concentration profiles of nizatidine and N-desmethylnizatidine in plasma of a healthy volunteer after receiving 300 mg nizatidine.

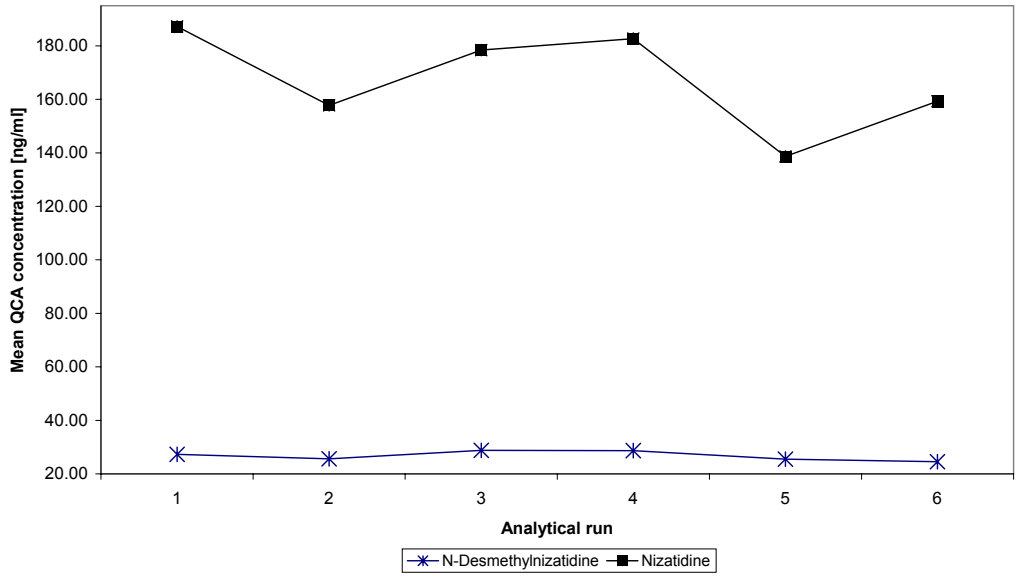

Fig. 3 – Mean QCA values of the analytical runs during clinical samples analysis.

EXPERIMENTAL

Materials

Nizatidine and N-desmethylnizatidine were working standards provided by Utraco Holland B.V. (Netherland). Acetonitrile, methanol, potassium dihydrogenophosphate and perchloric acid 85% were Merck products (Merck KgaA, Darmstadt, Germany). Distilled, deionised water was produced by a Direct Q-5 Millipore (Millipore SA, Molsheim, France) water system. The human blank plasma was supplied by the Local Bleeding Centre Cluj-Napoca, Romania.

Preparation of plasma calibrator and control samples

Stock solutions of 1000 µg ml^{-1} nizatidine and desmethylnizatidine, respectively, were prepared by dissolving an appropriate quantity of standard substance (weighted on a

Mettler Toledo AB 54-S balance from Mettler Toledo, Greifenseee, Switzerland) in 10 ml methanol. Working solutions were then obtained by diluting specific volumes of stock solutions with water and used to spike 0.5 ml of plasma blank, providing finally seven plasma standards with the concentrations ranged between 80 and 3200 ng ml^{-1} nizatidine and 12-484 ng ml^{-1} N-desmethylnizatidine. Accuracy and precision were verified at four levels of concentration, including lower limits of quantification: 80, 160, 1600 and 2400 ng ml^{-1} for nizatidine, and 12, 24, 242 and 363 ng ml^{-1} for metabolite. Duplicated quality control samples, namely QCA, QCB and QCC, of 160, 800 and 2400 ng ml^{-1} nizatidine and 24, 121 and 363 ng ml^{-1} N-desmethylnizatidine, were used during clinical samples analysis, in order to ensure that the method continues to perform adequately.

Sample preparation

At 0.5 ml plasma sample, 0.08 ml water (or total working solutions of analytes) were added and mixed with 0.12 ml perchloric acid 14% for five seconds via a vortex mixer (Genie 2, Scientific Industries Inc., USA). After 15 minutes of rest, a centrifugation for eight minutes at 5000 rpm was made, using a Sigma 204 centrifuge (Germany). The supernatant was transferred in an autosampler vial and 75 µl were injected into the HPLC system.

Chromatographic system and conditions

The HPLC system was an 1100 series model (Agilent Technologies) consisted of a binary pump, an in line degasser, an autosampler, a column thermostat and an UV detector. Data were collected and computed by ChemStation software (ver. A.09.03). The detector was operated at 314 nm. Chromatographic separation was performed in 4.1 minutes at 42 °C with a Zorbax SB-C18 100 x 3 mm, 3.5 µm (Agilent Technologies) column, protected by an on-line filter (2 µm). The elution was made in gradient mode at 1 ml min^{-1}, with a pre-run equilibrating time of 1 minute: 0-2 minutes 100% A (4% methanol and 96% KH_2PO_4 40 mM pH 2.3 with H_3PO_4 85%); between 2-2.01 minutes solvent A decreases from 100% to 35% and B (acetonitrile) increases from 0% to 65%; 2.01-2.4 minutes 35% A and 65% B; 2.4-2.41 minutes A increases from 35% to 100%; 2.41-4.1 minutes 100% A. The mobile phase was degassed, before elution, for 10 minutes in an Elma Transsonic 700/H (Singen, Germany) ultrasonic bath.

Method validation

As a first step of method validation[14,15], specificity was verified using six different plasma blanks obtained from healthy human volunteers who did not take before nizatidine and any other medication. The anticoagulant (Li-heparin) interference was also verified during this stage.

The linearity of the peak area against standard concentration was verified between 80-3200 ng ml^{-1} nizatidine and 12-484 ng ml^{-1} N-desmethylnizatidine in three different days, by applying least-squares linear regression. Distribution of the residuals (% difference of the back-calculated concentration from the nominal concentration) was investigated. The calibration model was accepted, if the residuals were within ±20% at the lower limit of quantification and within ±15% at all other calibration levels and at least 2/3 of the standards meet this criterion.

The limits of quantification were established as the lowest calibration standard with an accuracy and precision less than 20%.

The intra- and inter-day precision (expressed as coefficient of variation %, CV%) and accuracy (relative difference % between found and theoretical concentration, bias%) of the assay procedure were determined by the analysis in the same day of three samples at each of three levels of concentration in the considered concentration range and one sample of each in three different days, respectively. The recoveries at each of previously levels of concentration were measured by comparing the response of the treated plasma standards with the response of standards in water with the same concentration in nizatidine and N-desmethylnizatidine as the final extract from plasma standards.

Aliquots of plasma samples containing 347 ng ml^{-1} nizatidine and 67.2 ng ml^{-1} N-desmethylnizatidine were frozen for six months below -20 ºC and with four occasions during this period, each of three samples were analyzed.

Clinical application and in-study validation

The validated method was applied in a bioequivalence study of two dosage forms containing 300 mg nizatidine. The collecting times were 0, 0.5, 1, 1.5, 2, 2.5, 3, 4, 6, 8, 10, 12 hours after oral administration of 300 mg nizatidine. The accuracy and precision of the validated method was monitored to ensure that it continued to perform satisfactorily during analysis of volunteer samples. To achieve this objective, a number of QC samples prepared in duplicate at three levels of concentration were analyzed in each assay run and reported at the calibration curve of the run. The runs were validated if four out of six QC samples were within ±15% of their nominal concentration. Two but not all QC samples at the same concentration could be outside this range.

REFERENCES

1. A. Thompson, P. Kirdeikis, F. Jamali, M. Tavernini, L. Zuk, B. Marriage, I. Simpson and V. Mahachai, *J. Gastroenterol. Hepatol.*, **1995**, *10*, 546-554.
2. S. Xue, P.O. Katz, P. Banerjee, R. Tutuian and D. O. Castell, *Aliment. Pharmacol. Ther.*, **2001**, *15*, 1351-1356.
3. M. P. Knadler, R.F. Bergstrom, J. T. Callaghan and A. Rubin, *Drug Metab. Dispos.*, **1986**, *14*, 175-182.
4. A. Tracqui, P. Kintz and P. Mangin, *J. Chromatogr. B: Biomed. Sci. Appl.*, **1990**, *529*, 369-376.
5. Y. Gaillard and G. Pépin, *J. Chromatogr. A*, **1997**, *763*, 149-163.
6. R. A. Blum, A. J. Braverman, P. Rice and F. K. Johnson, *J. Clin. Pharmacol.*, **2003**, *43*, 74-83.
7. S. M. Abdel-Rahman, F. K. Johnson, G. Gautheir-Dubois, I. E. Weston and G. L. Kearns, *J. Clin. Pharmacol.*, **2003**, *43*, 148-153.
8. S. M. Abdel-Rahman, F. K. Johnson, J. D. Connor, A. Staiano, C. Dupont, V. Tolia, H. Winter, G. Gauthier-Dubois and G. L. Kearns, *J. Pediatr. Gastroenterol. Nutr.*, **2004**, *38*, 442-451.

9. K. Nikolic, M. Bogavac and B. Stankovic, *J. Pharm. Biomed. Anal*., **1995**, *13*, 683-685.
10. A. A. Al-Majed, F. Belal, A. M. Al-Obaid and A. H. Dawoud, *J. Pharm. Biomed. Anal.*, **1999**, *21*, 319-326.
11. A. Tracqui, P. Kintz and P. Mangin, *J. Forensic Sci.*, **1995**, *40*, 254-262.
12. G. Carlucci, *J. Chromatogr. B Biomed. Sci. Appl*., **1990**, *525*, 490-494.
13. S. Takedomi, H. Matsuo, K. Yamano, T. Iga and Y. Sawada, *Drug Metab. Dispos.*, **1998**, *26*, 318-323.
14. U.S. Department of Health and Human Services, Food and Drug Administration, Guidance for Industry – Bioanalytical Method Validation, **2001**, http://www.fda.gov/cvm.
15. The European Agency for the Evaluation of Medicinal Products, Note for Guidance on the Investigation of Bioavailability and Bioequivalence, **2001**, http://www.eudra.org/emea.html.

Revue Roumaine de Chimie, **2007**, *52*(3), 267–273

FORMATION AND COLLOIDAL STABILITY OF SOME POLYELECTROLYTE COMPLEX DISPERSIONS BASED ON RANDOM COPOLYMERS OF AMPS

Marcela MIHAI and Ecaterina Stela DRĂGAN*

"Petru Poni" Institute of Macromolecular Chemistry, Aleea Grigore Ghica Voda 41 A, 700487 Iasi, Roumania

Received April 4, 2006

The formation of some interpolyelectrolyte complexes between two random copolymers of sodium 2-acrylamido-2-methylpropanesulfonate (AMPS) and *t*-butyl acrylamide (TBA) and two strong polycations of integral type as a function of the ratio between opposite charges and the concentration of polyion pairs was followed in this work. Formation of the complex colloidal dispersion was followed via the optical density at 500 nm (OD_{500}) and the viscometric titration in salt-free aqueous solutions. Colloidal stability of the complex dispersions up to a ratio between charges of 1.8 was emphasized comparing the OD_{500} values measured after 24 h from the preparation with values found after one week of storage. The storage stability of the nonstoichiometric interpolyelectrolyte complexes as colloidal dispersions, with a ratio between charges of 0.6, as a function of polyion concentration (between 0.15 and 7.5 mmol/L), was followed by turbidimetric measurements after 24h and one week from preparation.

INTRODUCTION

The interaction between synthetic complementary polyelectrolytes is frequently involved either in the preparation of new materials, or in many solid-liquid separation processes. Numerous interpolyelectrolyte complexes (IPECs) have been reported, their structures and properties being controlled by some main parameters such as: polyion structure and charge density, polyion molar mass, polyion concentration, ionic strength and salt nature, polyions mixing ratio, and many other parameters that can be varied.[1-28] The known IPECs can be divided in three main types, according to their physical properties: insoluble and amorphous precipitates (polysalts),[1-9] soluble IPECs,[10-17] and IPECs as stable colloidal dispersions.[18-28] Nonstoichiometric IPECs (NIPECs) as colloidal dispersions, bearing positive or negative charges in excess, have already attracted the interest for different practical applications, such as: flocculants for cellulose, clay dispersions and low molecular organic compounds from the waste waters,[18,24] surface modification of different substrates,[22,23] etc. The most important characteristics of NIPECs as colloidal dispersions are their concentration in macromolecular components (as high as possible) as well as the storage colloidal stability of the complex aggregates. In salt-free aqueous solutions, these characteristics can be monitored by the polyion structure, the mixing molar ratio and the addition rate of the titrant.[26-28] In our previous investigations, NIPECs with positive charges in excess corresponding to a molar ratio between charges, n^-/n^+, of 0.7 have been prepared with NaPAMPS as added polyion,[26] and their flocculation efficiency in the removal of monodisperse silica nanoparticles, comparative with the starting polycations, has been demonstrated.[28]

The aim of this paper was first to follow the formation of IPECs as colloidal dispersions, when the anionic components were two ionic/nonionic random copolymers of sodium 2-acrylamido-2-methylpropanesulfonate (AMPS) with *t*-butyl acrylamide (TBA), P($AMPS_{37}$-co-TBA_{63}) and P($AMPS_{54}$-co-TBA_{46}), the complementary polymers being poly(diallyldimethylammonium chloride) (PDADMAC) and an ionene type polycation, containing 95 mol % N,N-dimethyl-2-hydroxypropyleneammonium chloride repeat units (PCA_5), and second to investigate the storage colloidal stability of IPECs as a function of the polyion structure, and polyions addition order, at a

* Corresponding author: e-mail: sdragan@icmpp.ro

constant titrant addition rate. The storage stability of NIPECs as colloidal dispersions with positive charges in excess, obtained from P($AMPS_{54}$-co-TBA_{46}) and PCA_5, at a constant ratio between charges, n-/n+ of 0.6, as a function of total polyions concentration was also investigated. The complex formation and the colloidal stability of the complex dispersions were followed by turbidimetric and viscometric titrations.

RESULTS AND DISCUSSION

The influence of the concentration of complementary polyelectrolytes on the formation of the IPECs as colloidal dispersions between P($AMPS_{54}$-co-TBA_{46}) and PCA_5 was followed by turbidimetric titration. Figure 1 shows the OD_{500} curves obtained when P($AMPS_{54}$-co-TBA_{46}) aqueous solutions with concentration of 10^{-3}, $5x10^{-3}$ and 10^{-2} mol/L were added to PCA_5 aqueous solution, with a concentration ten times lower, as a function of the molar ratio between charges, n^-/n^+, at a constant addition rate of 3.75 mL polyanion/mL polycation x h.

OD_{500} values were used as a measure of the dispersion turbidity. A very strong maximum, followed by the decrease and level off of the OD_{500} values, were observed irrespective of the polyions concentration. As can be seen, OD_{500} values, both before and after the complex stoichiometry (the mixing ratio corresponding to the abrupt increase of the turbidity), were strongly influenced by the concentrations of the complementary polyions. Thus, OD_{500} values increased with increasing polyion concentration, both before and after the complex stoichiometry, the lowest values being found for the lowest concentration. This behavior can be assigned to the increase of the concentration in complex particles and also to the increase of the collision number with the increase of concentration, the aggregation level being thus enhanced. It is known that turbidity values reflect the influence of some parameters that characterize the IPECs dispersions such as concentration, size, shape and polydispersity.[20-26] Therefore, the results presented in Figure 1 could be assigned also to the increase of the sizes and polydispersities of the complex nanoparticles, as it was demonstrated for other systems.[26] The complex stoichiometry was observed at a ratio n^-/n^+ of about 0.9, irrespective of the polyions concentration. The strong maximum characteristic for P($AMPS_{54}$-co-TBA_{46}) as added polyion suggests a lower colloidal stability for the corresponding IPECs dispersions, such maximum being also observed for other ionic/nonionic copolymers used as added polyions.[21]

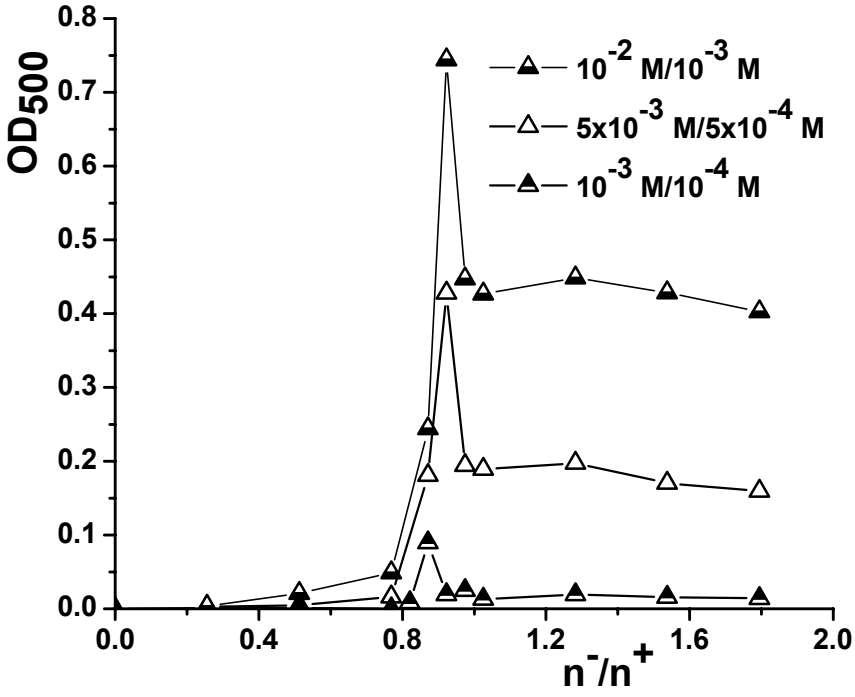

Fig. 1 – OD_{500} values of the IPECs as colloidal dispersions based on P($AMPS_{54}$-co-TBA_{46}) and PCA_5, as a function of polyion concentration.

The formation of IPECs colloidal dispersion between P($AMPS_{37}$-co-TBA_{63}) and P($AMPS_{54}$-co-TBA_{46}), on the one hand, and PDADMAC and PCA_5, on the other hand, as a function of polyions structure and mixing order was viscometrically followed. The variation of the specific viscosity (η_{sp}) values as a function of the molar ratio between charges and the mixing order of the oppositely charged polyions was plotted in Fig. 2. The concentration of the titrant was $5x10^{-3}$ M and that of the staring solution $5x10^{-4}$ M, in these experiments.

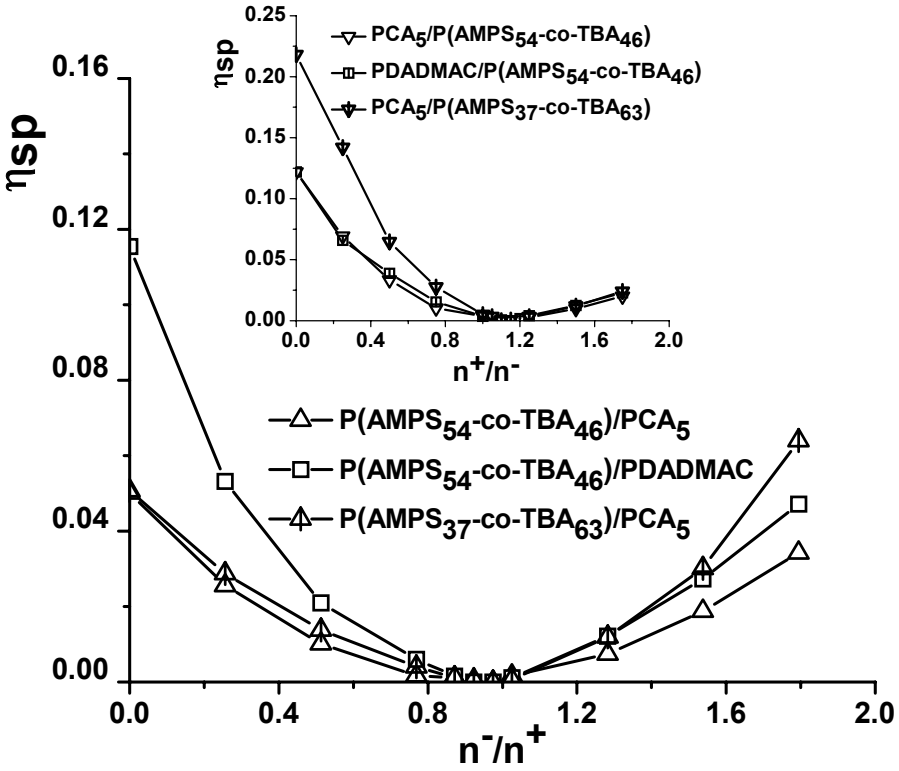

Fig. 2 – Specific viscosity values of IPECs as colloidal dispersions based on P($AMPS_{37}$-co-TBA_{63}) and P($AMPS_{54}$-co-TBA_{46}) as polyanions, and PDADMAC and PCA_5, as polycations; the concentration of the titrant was $5x10^{-3}$ mol/L and that of the starting solution $5x10^{-4}$ mol/L; the inset: the same polyion pairs with a reversed addition order.

The continuous decrease of the η_{sp} values before the stoichiometric point is correlated with the decrease of concentration of the component in excess from the starting solution, and also with the increase of NaCl concentration. As can be seen, before the stoichiometric point higher values of the η_{sp} were obtained when PDADMAC was the starting solution comparative with PCA_5. Comparing the systems P($AMPS_{37}$-co-TBA_{63})/PCA_5 and P($AMPS_{54}$-co-TBA_{46})/PCA_5, one can observe that η_{sp} values were almost identical before the stoichiometric point, irrespective of the polyanion structure, because PCA_5 was the polyion in excess in both cases. After the stoichiometric point, η_{sp} values reflect the polyanion in excess, the higher η_{sp} values being obtained when the titrant was P($AMPS_{37}$-co-TBA_{63}), comparative with P($AMPS_{54}$-co-TBA_{46}). When P($AMPS_{54}$-co-TBA_{46}) was used as titrant, the starting solution being either PDADMAC or PCA_5, the differences between η_{sp} values could be ascribed to the specific interactions between this polyanion and the complementary polycation, the lower values being obtained for the system P($AMPS_{54}$-co-TBA_{46})/PCA_5. This suggests that in this case a higher amount of polyanion has been incorporated in the complex particles. When the polyanion was the starting solution (the inset, Fig. 2), the higher values of η_{sp} before the stoichiometry were found for P($AMPS_{37}$-co-TBA_{63}), comparative with P($AMPS_{54}$-co-TBA_{46}), in agreement with η_{sp} values obtained in the previous case. After the stoichiometric point, η_{sp}

values were close each other, irrespective of the polycation structure. The complex stoichiometry was influenced by the mixing order of polyions, the molar ratio between charges corresponding to the stoichiometry being pushed to higher values when the polycation was the titrant, comparative with curves obtained when the titrant was the polyanion, for the same pair of polyelectrolytes.

Figures 3a and 3b illustrate the colloidal stability of two types of IPECs dispersions based on P($AMPS_{54}$-co-TBA_{46}) and PDADMAC (Fig. 3a) and P($AMPS_{37}$-co-TBA_{63}) and PCA_5 (Fig. 3b) as complementary polyions, comparing the OD_{500} values measured after 24 h from the preparation with values obtained after one week of storage. In all these experiments both possibilities of mixing were taken into account, that is, polyanion as titrant/polycation as starting solution and polycation as titrant/polyanion as starting solution, the concentration of the starting solution being $5x10^{-4}$ M and that of the titrant $5x10^{-3}$ M.

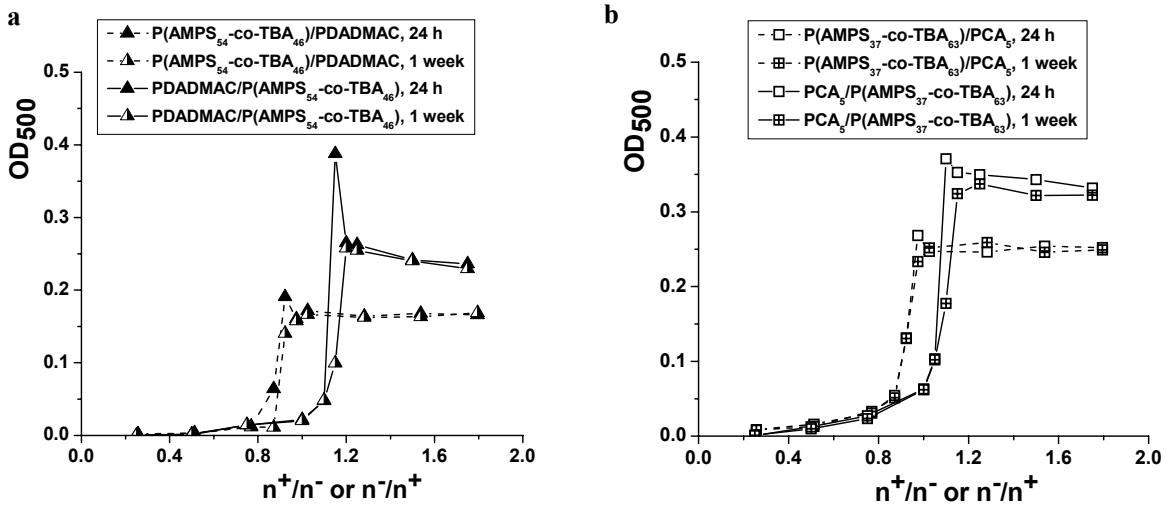

Fig. 3 – Colloidal stability of IPECs colloidal dispersions based on: (a) P($AMPS_{54}$-co-TBA_{46}) and PDADMAC; (b) P($AMPS_{37}$-co-TBA_{63}) and PCA_5; the concentration of the starting solution was $5x10^{-4}$ mol/L and that of the titrant $5x10^{-3}$ mol/L.

A strong maximum was observed when P($AMPS_{54}$-co-TBA_{46}) was used as added polyanion (Fig. 3a), and these results confirm the results already presented in Figure 1 for polyion pair P($AMPS_{54}$-co-TBA_{46})/PCA_5 at the same concentrations. The presence of a maximum at the complex stoichiometry was also observed when P($AMPS_{37}$-co-TBA_{63}) was used as polyanion, but the maximum was much lower than in the first case (Fig. 3b). On the other hand, the OD_{500} values were much higher when the polyanion with a lower charge density was used as added polyion, because a higher amount of polyanion was necessary for the compensation of positive charges up to the complex stoichiometry. The higher values of OD_{500} when either PDADMAC or PCA_5 were used as added polyions show that the polycations under study are less efficient in the stabilization of IPECs particles against collision, bigger aggregates being formed in this case. Except the disappearance of the maximum corresponding to the stoichiometry, very small differences or no differences were observed, both before and after the stoichiometry, after one week of storage, for all systems under study, irrespective of the addition order. This shows a high colloidal stability during the storage time at the polyions concentration selected for this investigation, even if both polyanions contain a nonionic comonomer (TBA).

The system P($AMPS_{54}$-co-TBA_{46})/PCA_5 was selected for the study of the colloidal stability of NIPECs dispersions with positive charges in excess, prepared at a constant ratio between charges, n^-/n^+ of 0.6, and increasing concentrations of the polyions. The OD_{500} values found after 24 h and one week from the NIPECs preparation were plotted in Fig. 4 versus the total polyion concentration (the sum of the concentrations of both polymeric components), c_p. Two consecutive measurements were performed after one week of storage: one without shaking and another one after shaking, both values being included in Fig. 4.

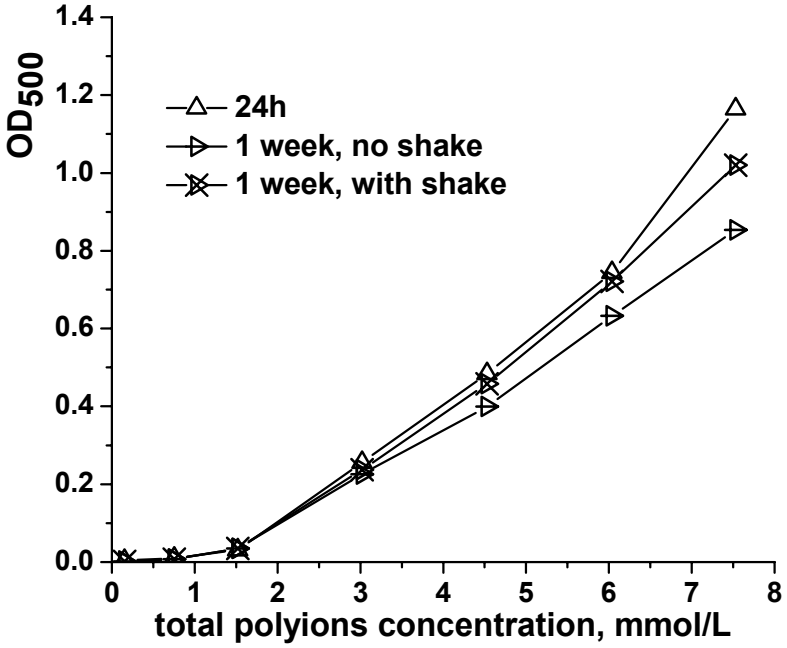

Fig. 4 – OD_{500} values of NIPECs with positive charges in excess prepared from $P(AMPS_{54}$-co-$TBA_{46})$/ PCA_5, at a constant ratio between charges of 0.6, after 24 h and one week from preparation, plotted versus the total polyion concentration.

One can observe three regions concerning the storage stability of these dispersions: first region, $c_p < 3$ mmol/L, is characterized by a very high storage stability, OD_{500} values being approximately the same after 24 h and one week of storage; in the second region, $3 < c_p < 6$ mmol/L, OD_{500} values were lower after one week of storage, when the measurements were performed without shaking the samples comparative with the values found after 24 h; OD_{500} values found for the same samples after shaking became almost similar with those measured after 24 h; for $c_p > 6$ mmol/L, the NIPECs storage stability was poor. The presence of the nonionic comonomer led to the decrease of the storage colloidal stability of the complex aggregates, at high concentrations, comparative with the NIPECs dispersions with positive charges in excess prepared with NaPAMPS as polyanion.[26]

EXPERIMENTAL

Materials

Poly(diallyldimethylammonium chloride) (PDADMAC) purchased from Aldrich was used as received. The polycation PCA_5 was synthesized and purified according to the methods previously described.[29] Copolymers of AMPS were synthesized and purified according to ref. 30. Polyions characteristics were summarized in Tab. 1.

Methods

IPEC Preparation

Aqueous solutions of the complementary polyelectrolytes with different concentrations were prepared by adequate dilution of the stock solutions (10^{-1} mol/L for the added polyion, and 10^{-2} mol/L for the starting polyion), taking into account the molar mass of the repeat unit in g/charge, see Tab. 1) with distilled water. Variable volumes of the aqueous solution of polyanion, or polycation were continuously added to the aqueous solution of the starting polyion, with a constant titrant addition rate of 3.75 mL/mL starting polyion x h, under magnetic stirring, at room temperature (about 25 ^oC), until a certain ratio between opposite charges was achieved. The concentration of the added polyelectrolyte was always 10 times higher than that of the starting polyion. The IPECs dispersions were still stirred for 60 min., and were characterized after 24 h if other duration was not specified.

Complex characterization

The complex dispersion was characterized first by the optical density of NIPECs as colloidal dispersions at λ = 500 nm (OD_{500}), as a function of the polyions concentration and polyion addition order. OD_{500} measurements were carried out with a SPECORD M42 spectrophotometer (standard 1cm quartz cell). Viscosities were measured with an Ubbelohde viscometer with internal dilution, at 25 ^oC.

Table 1

Characteristics of oppositely charged polyions

Sample	M_w (g/mol)[a]	M_u (g/charge)[b]	b (nm)[c]
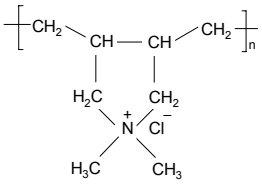 PDADMAC	240000	162.7	0.5
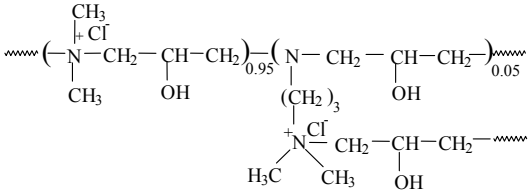 PCA_5[d], [η]= 0.46 dL/g	-	140.35	0.57
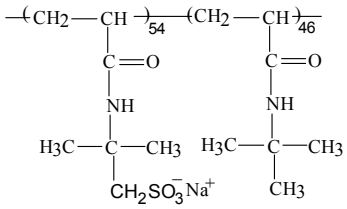 $P(AMPS_{54}\text{-co-}TBA_{46})$	175000	337	0.463
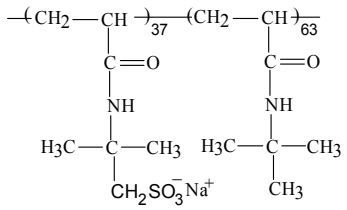 $P(AMPS_{37}\text{-co-}TBA_{63})$[d], [η]= 0.47 dL/g	-	440.66	0.667

[a] Molar mass determined by SEC;
[b] Mass per charge;
[c] Charge distance;
[d] Intrinsic viscosity determined in 1M NaCl, at 25 °C.

CONCLUSIONS

Polyions concentration strongly influenced the OD_{500} values, both before and after the complex stoichiometry; the higher the polyion concentration was, the higher OD_{500} values.

The viscometric study showed that the η_{sp} values depended on the structure of the complementary polyions and the stoichiometric point was influenced by the polyion mixing order, the ratio n^-/n^+ corresponding to the stoichiometry being pushed to higher values when the polycation was the titrant.

A good colloidal stability of the complex dispersions was found after one week of storage when the concentration of the starting solution was $5x10^{-4}$ mol/L and that of the titrant $5x10^{-3}$ mol/L. NIPECs colloidal dispersions, with a ratio n^-/n^+ of 0.6, obtained from $P(AMPS_{54}\text{-co-}TBA_{46})$ and PCA_5, had a very good storage stability up to a maximum concentration in the macromolecular components of about 3 mmol/L.

Acknowledgements: The financial support of this research by the Roumanian Ministry of Education and Research (Grant No 32953/2004) is gratefully acknowledged.

REFERENCES

1. A.S. Michaels and R.G. Miekka, *J. Phys. Chem.,* **1961**, *65*, 1765-1773.
2. E. Tsuchida and K. Abe, *Adv. Polym. Sci.*, **1982**, *45*, l-119.
3. B. Philipp, H. Dautzenberg, K.J. Linow, J. Kötz and W. Dawydoff, *Prog. Polym. Sci*., **1989**, *14*, 91-172.
4. H. Dautzenberg, *Macromolecules*, **1997**, *30*, 7810-7815.
5. S. Drăgan, M. Cristea, C. Luca and B.C. Simionescu, *J. Polym. Sci.: Part A: Polym. Chem*., **1996**, *34*, 3485-3494.
6. S. Drăgan and M. Cristea, *Eur. Polym. J.*, **2001**, *37*, 1571-1575.
7. S. Drăgan and M. Cristea, *Polymer*, **2002**, *43*, 55-62.
8. S. Drăgan and M. Cristea, "Recent Research Developments in Polymer Science", A. Gayathri (Editor), vol. 7, Research Signpost, Keralla, 2003, p. 149-181.
9. Y. Zhang and J. Binner, *Polymer*, **2005**, *46*, 10517-10522.
10. E. Tsuchida, Y. Osada and K. Sanada, *J. Polym. Sci., Polym. Chem. Ed*., **1972**, *10*, 3397-3404.
11. V.A. Kabanov and A.B. Zezin, *Pure Appl. Chem*., **1984**, *56*, 343-354.
12. V.A. Kabanov and A.V. Kabanov, *Macromol. Symp*., **1995**, *98*, 601-613.
13. J.F. Gohy, S.K. Varshney, S. Antoun and R. Jérôme, *Macromolecules*, **2000**, *33*, 9298-9305.
14. T. Anderson, S. Holappa, V. Aseyev and H. Tenhu, *J. Polym. Sci.: Part A: Polym. Chem*. **2003**, *41*, 1904-1914.
15. A. Zintchenko, G. Rother and H. Dautzenberg, *Langmuir*, **2003**, *19*, 2507-2513.
16. M. Sotiropoulou, C. Cincu, G. Bokias and G. Staikos, *Polymer*, **2004**, *45*, 1563-1568.
17. V.A. Izumrudov, M.Y. Gorshkova and I.F. Volkova, *Eur. Polym. J.*, **2005**, *41*, 1251-1259.
18. G. Petzold, A. Nebel, H.-M. Buchhammer and K. Lunkwitz, *Colloid Polym. Sci*., **1998**, *276*, 125-130.
19. D.V. Pergushov, H.-M. Buchhammer and K. Lunkwitz, *Colloid Polym. Sci*., **1999**, 277, 101-107.
20. H.-M. Buchhammer, G. Petzold and K. Lunkwitz, *Langmuir*, **1999**, *15*, 4306-4310.
21. H.-M. Buchhammer, M. Mende and M. Oelmann, *Colloids Surf. A*, **2003**, *218*, 151-159.
22. T. Reihs, M. Müller and K. Lunkwitz, *J. Colloids Interface Sci*., **2004**, *271*, 69-79.
23. L. Gärdlundm, L. Wågberg and R. Gernandt, *Colloids Surf. A*, **2003**, *218*, 137-149.
24. R.G. Nyström, J.B. Rosenholm and K. Nurmi, *Langmuir*, **2003**, *19*, 3981-3986.
25. J. Chen, J.A. Heitmann and M.A. Hubbe, *Colloids Surf. A*, **2003**, *223*, 215-230.
26. E.S. Drăgan and S. Schwarz, *J. Polym. Sci.: Part A: Polym. Chem*., **2004**, *42*, 2495-2505.
27. E.S. Drăgan and S. Schwarz, *J. Polym. Sci.: Part A: Polym. Chem*., **2004**, *42*, 5244-5252.
28. S. Schwarz and E.S. Drăgan, *Macromol. Symp*., **2004**, *210*, 185-192.
29. S. Drăgan and L. Ghimici, *Angew. Makromol. Chem*., **1991**, *191*, 199-211.
30. D. Drăgan, unpublished data.

Revue Roumaine de Chimie, **2007**, *52*(3), 275–281

TEMPERATURE DEPENDENCE OF THE ALKYL CHAIN ORDERING IN TWO LYOTROPIC SYSTEMS

Maria Nicoleta GRECU,[a] Gabriela BURDUCEA,[b] Voicu GRECU,[c]
Rodica MOLDOVAN,[d*] Traian BEICA[a] and Irina ZGURA[a]

[a] National Institute of Materials Physics P.O.Box Mg- 07, Bucureşti-Măgurele R-077125, Roumania
[b]University „Titu Maiorescu", Bucharest Str. Dionisie Lupu nr. 70, sector 1, Bucharest, Roumania
[c]Faculty of Physics, University of Bucharest P.O,Box Mg- 11, Bucureşti-Măgurele R-077125, Roumania
[d] Roumanian Academy Center for Advanced Studies in Physics Calea 13 Septembrie nr. 13, Bucharest, Roumania;
E-mail: rodi@ infim.ro

Received April 17, 2006

X-band ESR spectra of the calamitic and discotic lyotropic nematic phases in sodium dodecyl sulphate (SDS)/decanol/water system, doped with paramagnetic nitroxide free radicals are analyzed in this paper. The studied temperature range was chosen to include phase transitions of the lyotropic systems. The variation of the surfactant hydrocarbon chains ordering versus temperature is determined by the hyperfine splitting tensor ($\underline{A}$) and the spectroscopic splitting tensor ($\underline{g}$) anisotropies. The temperature dependence of the molecular order parameters for both lyotropic systems and the corresponding angular fluctuations are presented and discussed.

INTRODUCTION

Surfactant micellar organization. Ionic surfactants are amphiphilic molecules that present a polar head and a hydrophobic tail. In the presence of an appropriate solvent, under certain temperature/concentration conditions, they have the capacity to form a large variety of micellar shapes and structures as a result of a complex process of aggregation. In these conditions they are considered to be "lyotropic liquid crystals". Micellar structures, also called "phases", have been studied by X-Ray and neutron scattering and by NMR techniques that revealed the existence of the main types: lamellar, cubic, hexagonal and nematic.[1]

The nematic phase of the lyotropic liquid crystals occurs in ternary solutions when adding a long chain alcohol in the ionic surfactant aqueous solution if the amphiphilic molecule has the polar head of the sulphate, carboxylate, or alkyl ammonium type and the tail of linear hydrocarbon type with more than 8 carbon atoms, or if it is a fluorocarbon short chain derivative.[1-3] The nematic structures generally have a rather narrow temperature/concentration domain of existence.[4] The $\overline{n}$ director that defines the mean orientation of the micelles in the nematic phase is chosen to describe the mean orientation of the l_y axis for a calamitic micelle and that of the l_z axis for a discotic micelle. The common shape of the nematic micelle can be described as an ellipsoid with three distinct axes: l_x, l_y, l_z.[5] The $l_y >> l_x \cong l_z$ situation corresponds to the calamitic micelles (N_c phase) and the $l_z << l_x \cong l_y$ situation corresponds to the discotic micelles (N_d phase).

In this paper, we present the temperature dependence of the orientation degree of the amphiphilic molecules in the micelles of two nematic phases (N_c and N_d) of the lyotropic system SDS/water/decanol, determined by ESR spectroscopy studies. Liquid crystals do not generally have paramagnetic centers. ESR spectroscopy investigation supposes the insertion of that kind of centers, called "spin markers", conveniently chosen to reflect as close as possible the liquid crystal dynamics. The most appropriate

* Corresponding author.

spin markers to study lyotropic liquid crystals are fatty acids with a nitroxid radical group insertion (Fig. 1). This insertion can be made in different positions along the aliphatic chain. For example, the n-DX symbolizes the stearic acid marked with the doxyl group inserted strictly after the nth carbon atom from the hydrophilic tail.

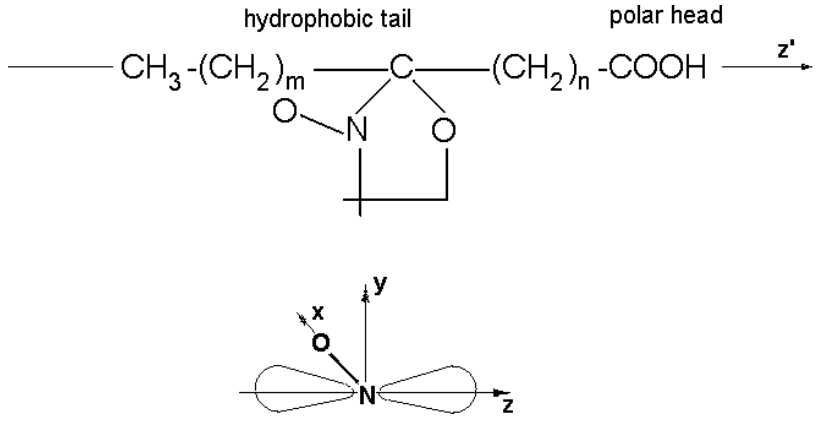

Fig. 1 – Spin marker I(*m,n*)- general structure (upward) and detail of the 2pπ orbital (downward); (*x,y,z*) is the rectangular coordinates system attached to the doxyl radical; *z′* is the long molecular axis direction of the surfactant molecule in the vicinity, initially supposed to be parallel to the *z* axis.

We denote by θ_i (i = 1, 2, 3), the angles between the three axes of a rectangular system attached to the marker molecule and the long axis *z'* of a surfactant molecule localized in the marker proximity, chosen as reference. The doxyl radical main directions are: the *x* axis corresponds to the N-O bond, *xy* being the doxyl ring plane; the *z* axis, perpendicular to the *xy* plane, corresponds to the unpaired nitrogen orbital $2p_z$ which is oriented along the fatty acid long axis (see Fig. 1). Then:

$$\cos\theta_1 = \vec{x}\cdot\vec{z}',\ \cos\theta_2 = \vec{y}\cdot\vec{z}',\ \cos\theta_3 = \vec{z}\cdot\vec{z}' \tag{1}$$

The diagonal components of the Seelig's order parameter tensor, $\underline{S}$ are expressed as the averages: [6]

$$S_{ii} = \frac{1}{2}\left\langle 3\cos^2\theta_i - 1\right\rangle \quad i = 1, 2, 3 \tag{2}$$

S_{11}, S_{22} and S_{33} are correlated to the mean angular fluctuations $\langle\theta_1\rangle$, $\langle\theta_2\rangle$, $\langle\theta_3\rangle$. Only two of the three order parameters are independent, as:

$$S_{11} + S_{22} + S_{33} = 0 \tag{3}$$

The microscopic order parameters S_{ii} are calculated using the ESR experimental data.

Analysis of ESR spectra for liquid crystalline states. The ESR spectrum of a free radical of that kind is described by a spin Hamiltonian:

$$\mathcal{H} = \beta\overline{B}\cdot\underline{g}\cdot\overline{S} + \overline{S}\cdot\underline{A}\cdot\overline{I} \tag{4}$$

where β is Bohr magneton, $\overline{S}$ is the electronic spin momentum and $\overline{I}$, the nuclear one. $\underline{g}$ and $\underline{A}$ are the tensors describing the anisotropic interaction with the magnetic field $\overline{B}$ and the hyperfine interaction with the nuclear spin of ^{14}N atom (I=1), respectively. In a rigid matrix (*e.g.* monocrystal, frozen state) the ESR spectrum is anisotropic and furnishes the values and the main directions of those tensors. For 5-DX marker used in experiments, g_x=2.0089, g_y=2.0062, g_z=2.0027 and A_x=6.4G, A_y=5.9G, A_z=33.5G.[7]

To find the $\underline{g}$ and $\underline{A}$ tensors compounds in the laboratory system, the self-system coordinates must be transformed into the laboratory system coordinates. In the laboratory reference system, the spin Hamiltonian becomes:

$$\mathcal{H} = \beta\bar{B} \cdot \underline{g}^{(L)}_{(t)} \cdot \bar{S} + \bar{S} \cdot \underline{A}^{(L)}_{(t)} \cdot \bar{I} \tag{5}$$

$\underline{A}^{(L)}_{(t)}$ and $\underline{g}^{(L)}_{(t)}$ tensors depend on the nitroxide free radical orientation in the above mentioned co-ordinate system. In their turn, these orientations are dependent of time and of molecular dynamics. There are no easy solutions to solve the dynamic problem. Approximations depending on the ratio between the calamitic dynamic correlation time $\tau_{\|}$ and the ESR spectroscopic characteristic measure time $\tau_{char} \approx 10^{-9}$ - 10^{-10} s, can be developed. The most frequently used approximation is that of rapid molecular movement $\tau_{\|} << \tau_{char}$ [8]. In this case, the rapid molecular movements partially mediate the orientation parameters and the spin Hamiltonian expression contains the mediated values:

$$\mathcal{H} = \beta\bar{B} \cdot \left\langle \underline{g}^{(L)}_{(t)} \right\rangle \cdot \bar{S} + \bar{S} \cdot \left\langle \underline{A}^{(L)}_{(t)} \right\rangle \cdot \bar{I} \tag{6}$$

So, the dynamic problem turns into a static one with values depending on mediation effects. We considered as rapid molecular movements the following ones: the rapid rotation of the n-DX molecule around its long axis (both $\underline{g}$ and $\underline{A}$ tensors are axial in the (x', y', z') reference system); the rapid diffusion in the micellar surface and the rapid rotation around the $\bar{n}$ micellar director (that coincides to the micellar rotation symmetry axis).

Due to physical considerations generated by the micellar dimensions, their dynamics towards the nematic phase $\bar{n}$ director cannot longer be treated in this approximation. Because of the axial symmetry of the molecular dynamics, the mediated tensors $\left\langle \underline{g}^{(L)}_{(t)} \right\rangle$ and $\left\langle \underline{A}^{(L)}_{(t)} \right\rangle$ have an axial symmetry and represent parameters that can be correlated to the ESR spectra shape in both nematic and isotropic phases. The molecular order parameters are expressed as:[6]

$$S_{33} = a(A_{\|} - A_{\perp}) / a'(A_{zz} - A_{xx}) \tag{7}$$

$$S_{11} = [3(g_{\|} - g_{iso}) - 2S_{33}(g_{zz} - g_{yy})] / 2(g_{xx} - g_{yy}) \tag{8}$$

where:

$$a = \frac{1}{3}(A_{xx} + A_{yy} + A_{zz}); \quad a' = \frac{1}{3}(A_{\|} + 2A_{\perp});$$

$$g_{iso} = \frac{1}{3}(g_{xx} + g_{yy} + g_{zz})$$

are isotropic parameters describing the spectrum in an isotropic medium characterized by rapid motion. Such a spectrum is a hyperfine triplet with equidistant resonance lines and intensities that can be different on account of the line width difference. The relaxation theory in isotropic liquids correlates these widths to a rotational relaxation time.

The paper is organized as follows: In the introductive chapter, essential information about the domain of the nematic liquid crystals are given and mostly of the topics in correlation with this paper interest such as physical and chemical considerations about the nematic phase, are developed. Mathematical support to understand the theory of analyzing ESR spectra applied to nematics is also given. Then, in the experimental chapter, it is presented the preparation procedure to obtain the lyotropic ternary solutions of the ionic surfactant, sodium dodecyl sulphate (SDS)/decanol/water in the calamitic phase (N_c) and the discotic phase (N_d.). The spin marker doping process is also described together with the ESR experimental measurements peculiarities. Finally, the ESR spectra shape changes with

temperature, including phase transitions, for both nematic lyotropic systems in the study are discussed, as well as the fluctuations with temperature of the three order parameters. The paper ends with some conclusions on the experimental work.

EXPERIMENTAL PART

Materials and sample preparation. To obtain lyotropic solutions we used SDS (Sigma, 99 % purity) without further purification, 1-decanol (Merck, 99 % purity) and triply distillated water. The used method was previously described.[9]

The compositions (wt %) of the two studied solutions, chosen from the phase diagram known in literature[10] in order to obtain nematic calamitic (N_c) and nematic discotic (N_d) liquid crystals at room temperature, were as follows:

N_c: 25.05(SDS) / 4.48(decanol) / 70.46(water)

N_d: 22.38(SDS) / 4.90(decanol) / 72.72(water)

For the investigation by ESR spectroscopy we used the spin marker 5-doxyl-stearic acid (5-DX) with the molar weight M=385 Kg/Kmol (Aldrich). It belongs to the so-called I(m,n) type with n=5 and is a (n + 2) doxyl derivative of the (m + n + 3)-carbon fatty acids family, with the general structure shown in Fig. 1.

The doping used (mol 5-DX/mol SDS) was 5-DX/$N_c \approx$ 1/700 and 5-DX/$N_d \approx$ 1/500. At these concentrations, the spin marker solubility was very good. When choosing the quantity of 5-DX, we had in view to minimize the spin-spin interactions in order to increase the spin-lattice interactions effect.[11,12] The high polarity of the N_d solution was also considered.

To homogenize solutions we applied both slow rotation (2 rot/min for 48 h) and ultrasonic procedures to the vessel in order to avoid the foaming of the lyotropic solutions. After preparation, we kept the samples into a thermostatted space at 23(±1)°C, to avoid degradation.

Transition temperatures for both lyotropic systems were measured directly, using the polarizing microscopy, as previously described.[13] We found that the nematic-isotropic phase transition took place at 29.7°C for the N_c sample and at 28.6°C for the N_d sample. We also found that for the N_d sample, after 30°C, the isotropic phase turned into a new anisotropic phase with a birefringent texture, probably a lamellar one.[14]

ESR measurements. To measure the ESR spectra of the nematic samples we used a JEOL spectrometer JES-ME-3 type in X-band (9.45GHz) on-line with a PC. To calibrate the magnetic field we used a MgO:Mn^{2+} standard probe. The nematic liquid crystal was sucked into capillary tubes (150 Kapilar Euroglass) at the room temperature. During the filling process, the calamitic micelles of the N_c probe orient in average with their long l_y axis parallel to the tube axis, while discotic micelles of the N_d probe orient in average with their short l_z axis perpendicular to the tube axis. During the recording of ESR spectra, the direction of the external magnetic field was perpendicular to the tube axis. ESR spectra were recorded between the 3rd and the 4th line of the manganese standard, while the external magnetic field was varied between 3200-3300G. The microwave field frequency was measured with a digital Takeda Riken 5502D. The temperature was measured with ±0.5°C precision. After modifying the temperature, we waited about 30 min. in order to reach the thermal equilibrium.

RESULTS AND DISCUSSION

As an example, the experimental ESR spectra of N_c solution are shown in Fig. 2. As a result of the ESR spectra analyses, we have obtained the experimental values in Table 1 and Table 2.

The ESR parameters analysis leads to the following observations. For the N_c sample, above the transition temperature, *a'* values decrease with a unit, indicating a decreasing polar influence in the marker vicinity. That happens only if micelle curvature modifies, so we conclude that the micellar axial ratio must decrease at the transition temperature. NMR measurements on samples having about the same composition[10] show the same phenomenon. For the N_d sample, *a'* values continue to increase above transition temperature. This remark is in complete agreement with NMR results on similar samples that indicate an increasing axial micellar ratio after transition.

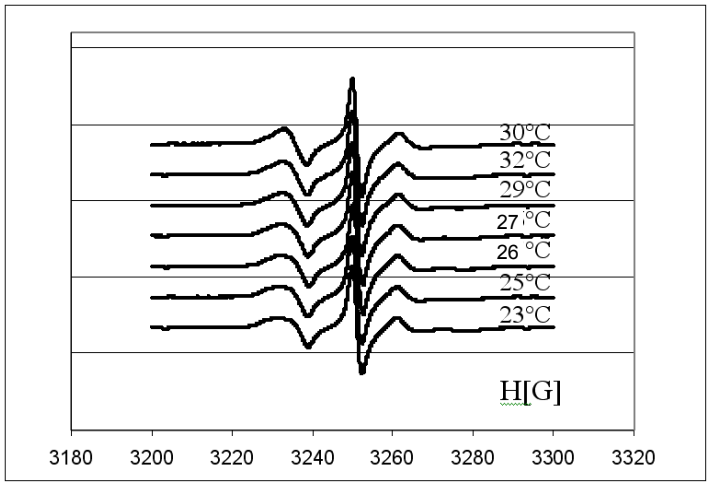

Fig. 2 – ESR spectra for the N_c sample.

The $g_{\|}$ values are lower for the N_c sample than for the N_d sample in the nematic domain and have an equalizing tendency after transition. On the other hand, we observed that $g_{\|} \neq g_{\perp}$ for each sample over all the tested temperature range, meaning that the paramagnetic centers have not an isotropic distribution in the post-transition domain. Quist[15] studied a N_c phase having a composition similar to ours and find out that it passes by a biphasic domain in a narrow temperature range (29÷32)°C before reaching the isotropic phase, instead of passing to the isotropic phase directly as the optical measurements show.[16] Our ESR results regarding the N_c solution seem to be in contradiction with the results of birefringence, which disappears at 29.7°C. To explain this we have to take into consideration that ESR spectroscopy gives information about the molecular local dynamics, while birefringence gives information about both molecular local dynamics in the micelle and micellar dynamics in the liquid crystal solution. For the N_d sample we found that our ESR experimental data, in agreement with the NMR results,[14] indicates that the N_d sample passes by a polyphase domain over 30°C, which is confirmed by optical measurements too.

Table 1

The experimental values of the ESR parameters for the N_c sample

T(°C)	$A_{\|}$ (G)	$A_{\perp}$ (G)	$g_{\|}$	$g_{\perp}$	a'
23	22.10	11.19	2.0042	2.0067	14.83
25	22.64	11.54	2.0041	2.0065	15.24
26	20.52	11.10	2.0053	2.0067	14.23
27	19.30	11.49	2.0057	2.0064	14.09
29	21.70	11.44	2.0041	2.0066	14.86
30	17.75	11.29	2.0055	2.0066	13.37
32	17.75	11.44	2.0057	2.0067	13.54

Table 2

The experimental values of the ESR parameters for the N_d sample

T(°C)	$A_{\|}$ (G)	$A_{\perp}$ (G)	$g_{\|}$	$g_{\perp}$	a'
24	17.30	11.14	2.0058	2.0069	13.19
25	16.86	11.14	2.0058	2.0067	13.05
26	16.86	11.14	2.0058	2.0066	13.05
30	17.74	11.43	2.0058	2.0066	13.53
33	18.30	11.63	2.0055	2.0066	13.85
35	18.29	11.73	2.0055	2.0066	13.92

The values of the dynamic parameters for the nematic calamitic N_c and the nematic discotic N_d solutions, calculated by applying Eqs. (2), (5), (9) and (10), are synthesized in Table 3.

The order parameters values evaluation leads to the following observations. At temperatures in the nematic phase (T<29.8° for N_c and T<29.5°C for N_d phase, as it results from the fit of the data in Fig. 3), S_{33} order parameter values for the N_c phase are about twice higher than those for the N_d phase, reflecting that the hydrocarbon chains are more confined in the calamitic micelle than in the discotic micelle. We explain that by the fact that the spin marker, which generally locates in the micellar minima curvature zone,[17] is located in a lower curvature zone in the discotic micelle than in the calamitic micelle.

Table 3

The microscopic order parameters values for the N_c and N_d samples

T°C	S_{33}		$\bar{\theta}_3$ (deg)		S_{11}		$\bar{\theta}_1$ (deg)		S_{22}		$\bar{\theta}_2$ (deg)	
	N_c	N_d	N_c	N_d	N_c	N_d	N_c	N_d	N_c	N_d	N_c	N_d
23	0.42	-	38	-	-0.40	-	75	-	-0.02	-	55	-
24	-	0.24	-	45	-	0.24	-	45	-	-0.49	-	90
25	0.41	0.24	39	45	-0.46	0.24	80	45	0.05	-0.48	53	89
26	0.37	0.24	40	45	0.12	0.24	50	45	-0.49	-0.48	85	89

Table 3 (continues)

Table 3 (continued)

29	0.39	-	40	-	-0.49	-	85	-	0.10	-	60	-
30	0.27	0.26	45	45	0.10	0.24	51	45	-0.37	-0.50	73	90
32	0.26	-	45	-	0.20	-	47	-	0.46	-	81	-
33	-	0.27	-	45	-	0.10	-	51	-	-0.37	-	73
35	-	0.26	-	45	-	0.09	-	51	-	-0.35	-	72

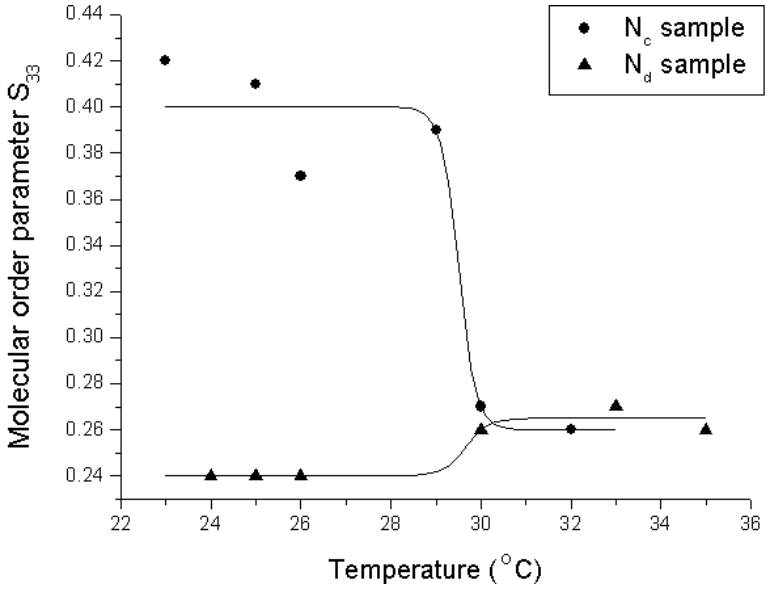

Fig. 3 – Temperature dependence of the molecular order parameter S_{33} for the liquid crystal samples. The continue line is the fit with the sigmoidal function: $S_{33} = A_2 + (A_1 - A_2)/\{1 + \exp[(T - T_0)/dx]\}$.
●- experimental results for the N_c sample; fit parameters A_1=0.24; A_2=0.26; T_0=29.8; dx=0.146;
▲- experimental results for the N_d sample; A_1=0.4; A_2=0.26; T_0=29.5; dx=0.195.

In Fig. 3 we remark the nematic – isotropic transition for the N_c sample by the abruptly reducing of the S_{33} order parameter value at 29.8°C, in accordance with the optical study. The corresponding average angular fluctuations are increasing slowly and continuously. Increasing disorder at the hydrocarbon tales level can be explained by changes in their packing shape. The lower S_{33} value after transition confirms the conclusion that micellar axial ratio decreases after transition. The two other parameters, S_{11} and S_{22} have disparate positive and negative values, while the corresponding average angular fluctuations values (bigger than 50º) show that *x* and *y* axes of the spin marker molecule are significantly inclined towards the *z'* axis.

For the N_d sample, as we can see from Tab. 3 and Fig. 3, the S_{33} order parameter is constant with temperature in the nematic phase and shows only a slight increase after transition. After transition, both S_{33} and S_{11} parameters have low values, close to the N_c sample values. The S_{22} parameter has rather high negative values in the nematic domain and decreases after transition. Because of the slight increase of the S_{33} order parameter values after transition at about 30°C, we have concluded that for the N_d sample, a bilayer-like structure continues to exist, probably lamellar fragments or discotic micelles of different dimensions than the micelles in the N_d phase. This conclusion is also concordant with NMR investigation.[14]

CONCLUSIONS

The ESR spectroscopy technique to investigate local molecular ordering degree for the lyotropic ternary system sodium dodecyl sulphate/ decanol/ water in the nematic calamitic and discotic phases was able to evidence the nematic to isotropic phase transition. From the final ESR parameters comparative analysis data we formulate the following remarks:

For the N_c solution the micellar axial ratio decreases after transition, while for the N_d solution it increases after transition, in concordance with

NMR investigations[14,15] for nematics with compositions close to ours;

For both solutions, the post-transition domain is not an isotropic one from the paramagnetic centers distribution point of view, in agreement with NMR studies[14,15];

In the nematic phase, S_{33} order parameter values for the N_c phase are about twice higher than those for the N_d phase, reflecting that the hydrocarbon chains are more confined in the calamitic micelle than in the discotic micelle.

The totality of the average angular fluctuations values demonstrates that the ionic surfactant hydrocarbon chain dynamics for both N_c and N_d solutions are similar and are generated by small angle torsions and C-C bond flexions with activation probabilities and energies depending on pre- and post-transition thermodynamic conditions and on the samples structures. We must not minimize the fact that the spin marker molecule may have a slightly different behavior from the surfactant molecules in the vicinity, because of the larger space around its long chain axis. The ring at which N-O is attached is asymmetric and that asymmetry may be a reason for the nonlinearity of the fatty acid chain, probably also induced to the surfactant chains in the vicinity.

Experimental data demonstrate that modifications in the thermodynamic conditions generate a variation of the disorder at the level of the surfactant molecule hydrocarbon chain for both N_c and N_d solutions, but this is manifested in a different way.

Acknowledgements: Some of the authors (R.M., T.B., I.Z.) thank the Roumanian Ministry of Education and Research for financial support under the CEX Project D11-76.

REFERENCES

1. C. Fairhurst, S. Fuller, J. Gray, M. C. Holmes and G. J. T. Tiddy, in "Handbook of Liquid Crystals", D. Demus, J. Goodby, G. W. Gray, H-W. Spiess and V. Vill (Eds.), Willey-VCH, Weinheim, New York, 1998, vol. 3, p.341-392.
2. K. W. Lawson and T. J. Flaut, *J. Am. Chem. Soc*., **1967**, *89*, 5489-5491.
3. L. Q. Amaral and A. M. F. Neto, *Mol. Cryst. Liq. Cryst.*, **1983**, *98*, 285-290.
4. A. S. Sonin, *Usp. Fiz. Nauk*, **1987**, *153*, 274-310.
5. P. Toledano and A. M. F. Neto, V. Lorman, B. Mettout, V. Dmitriev, *Phys. Rev. E*, **1995**, *52*, 5040-5052.
6. J. Seelig, *J. Am. Chem. Soc.*, **1970**, *92***,** 3881-3887.
7. T. Risse, T. Hill and J. Schmidt, G. Abend, H. Hamann, H.-J. Freund, *J. Phys. Chem. B*, **1998**, *102*, 2668-2676.
8. P. V. Shui, G. B. Birrell and G. O'Hayes, *J. Magn. Res.*, **1974**, *15***,** 444-449.
9. T. Beica, R. Moldovan, M. R. Puica and S. Frunza, *Liq. Cryst.*, **2002**, *29*, 1275-1278.
10. P. O. Quist, B. Halle and I. Furo, *J. Chem. Phys.*, **1992**, *96*, 3875-3891.
11. A. Arcioni, C. Bacchiocchi, L. Grossi, A. Nicolini and C. Zannoni, *J. Phys. Chem. B*, **2002**, *106*, 9245-9252.
12. Z. Liang, G. Wikander and P-O. Westlund, *J. Chem. Phys.*, **1995**, *102*, 1471-1480.
13. T. Beica, R. Moldovan, M. Tintaru, M. R. Puica, I. Enache and S. Frunza, *Liq. Cryst.*, **2004**, *31*, 325-332.
14. I. Furo, B and Halle, *Phys.Rev. E*, **1995**, *51* , 466-476.
15. P. O. Quist and B. Halle, I. Furo, *J. Chem. Phys.* **1991,** *95*, 6945-6951.
16. T. Beica, R. Moldovan, M. Tintaru, I. Enache and S. Frunza, *Cryst. Res. Technol.* **2004**, *39*, 151-156.
17. Y. Hendrix, J. Charvolin and M. Rawiso, *J. Colloid Interface Sci.* **1984**, *100*, 597-601.

Revue Roumaine de Chimie, **2007**, *52*(3), 283–291

ÉTUDE DE L'OXYDESHYDROGENATION NON CATALYTIQUE DE L'ISOBUTANE DANS UN REACTEUR INTEGRAL

STUDY OF NON CATALYTIC OXIDEHYDROGENATION OF ISOBUTANE IN AN INTEGRAL REACTOR

Mădălina-Nicoleta COBÂRLIE, Adriana IORDĂCHESCU, Ioan SĂNDULESCU et Ioan-Cezar MARCU*

Département de Chimie Technologique & Catalyse, Faculté de Chimie, Université de Bucarest, 4-12, Blv. Regina Elisabeta, 030018 Bucarest, Roumanie
Tél: 0040214103178x138, Télécopie: 0040213159249

Reçu le 4 Avril 2006

L'oxydéshydrogénation non catalytique de l'isobutane dans un réacteur intégral vide, totalement et partiellement rempli de quartz, a été étudiée. Dans le réacteur vide, une transformation importante de l'isobutane est observée. En remplissant le réacteur avec du quartz, une importante diminution de conversion est observée. De plus, ce fait est accompagné d'un changement dramatique de la distribution des produits ce qui suggère que la surface du quartz modifie les radicaux libres dans une certaine direction. Pour comparaison, la déshydrogénation non catalytique a également été étudiée. Les énergies d'activation pour les transformations oxydante et non oxydante de l'isobutane en présence du quartz sont identiques ce qui suggère que l'étape déterminante de vitesse et identique dans les deux réactions.

Non-catalytic oxidehydrogenation of isobutane was studied in an empty, partially and totally filled with quartz-particles integral reactor. In the empty reactor an important transformation of isobutane is observed. Packing the reactor with quartz leads to an important decrease of conversion. Moreover, this fact is accompanied by a drastic change of product distribution which suggests that quartz surface modifies the free radicals in some way. For comparison, the non catalytic dehydrogenation was also studied. The activation energies for oxidative and non oxidative transformations of isobutane in the presence of quartz are identical which suggests that the rate limiting step is the same in both cases.

INTRODUCTION

Etant donnée son importance à la fois pratique et théorique, l'oxydéshydrogénation des alcanes aux alcènes correspondants est une réaction beaucoup étudiée et un grand nombre d'articles de revue lui ont été consacrés.[1-10] Par contre, à la différence de l'oxydéshydrogénation des butènes ou l'ammoxydation du propène, deux exemples d'applications industrielles d'activation catalytique d'une molécule de réactif à basse température,[6] l'activation de la molécule d'alcane, de par son inertie chimique, se réalise à des températures beaucoup plus élevées. C'est ainsi qu'on explique les données de littérature qui indiquent le fait que la transformation catalytique des alcanes en général, et des alcanes C_4 en particulier, a lieu à des températures supérieures à 500°C. Dans ces conditions, la transformation catalytique est toujours accompagnée par des réactions thermiques, à savoir craquage et déshydrogénation, et la présence de l'oxygène détermine oxydations en phase gazeuse homogène. De plus, le matériau, considéré inerte, présent dans les volumes libres du réacteur, tel que le quartz, pourrait, par sa surface qu'il expose aux réactifs, intervenir dans la réaction thermique.

Le mécanisme de l'oxydation thermique des alcanes est un mécanisme radicalaire bien connu.[11] Il est évident que la présence d'un catalyseur dans ce processus complique le problème, notamment parce que la plupart des mécanismes catalytiques ne sont pas radicalaires. Dans ces conditions, il est difficile d'apprécier quelle est la contribution des réactions en phase gazeuse homogène, des réactions de paroi et des réactions catalysées, aux processus global. La connaissance de ces

* Auteur à qui la correspondance doit être adressée. Mél : marcu.ioan@unibuc.ro

contributions pourrait permettre le choix de certains catalyseurs qui accélère les réactions amorcées en phase gazeuse. Si le profil de température le long du réacteur est également pris en considération, on pourrait établir la position optimale du catalyseur dans le réacteur de façon à ce qu'on obtienne l'effet décrit ci-dessus.

Au niveau de la littérature, il y a peu d'études prenant en considération ces aspects.[12-15] Nous nous sommes donc proposés de faire une étude qui mette en évidence ces phénomènes et que nous présentons par la suite.

RÉSULTATS ET DISCUSSION

Étude de la réaction dans le réacteur vide

Nous avons, dans un premier temps, réalisé la réaction de l'isobutane dans le réacteur vide. Les résultats obtenus pour un débit du mélange réactionnel de 7000 mL/h et un rapport molaire isobutane/air de 1/2,5 (isobutane/oxygène = 1/0,5), sont résumés dans le Tableau 1.

Tableau 1

Résultats obtenus pour la transformation oxydante de l'isobutane dans le réacteur vide, pour un débit du mélange réactionnel de 7000 mL/h et un rapport molaire isobutane/air de 1/2,5

Température (°C)	Conversion (%)	Sélectivités (%)			
		Isobutène	Craquage	CO	CO_2
555	46	34,6	43,9	19,7	1,8
610	53	35,6	46,6	15,9	1,9

Il est évident qu'avec une conversion de 46% à 555°C et de 53% à 610°C, la transformation de l'isobutane est très importante. Les processus de craquage, qui s'intensifient légèrement avec la température, sont plus importants que l'oxydéshydrogénation, cette dernière n'étant pas affectée par la température dans le domaine de travail. D'autre part, les quantités de CO, qui diminuent lorsque la température augmente, sont beaucoup plus grandes que celles de CO_2. Ces observations sont caractéristiques pour les réactions d'oxydation en phase gazeuse homogène par l'intermédiaire des radicaux peroxyde.

Étude de l'effet combiné du quartz et du volume libre

Un volume du réacteur, correspondant à une hauteur de 130 mm, a été rempli de débris de quartz de granulométrie comprise entre 3 et 7 mm. Cette couche de quartz, dont la porosité vaut 50,6%, centrée sur la zone de température maximale, recouvre complètement la partie du réacteur chauffée à des températures supérieures à 400°C. Nous avons balayé cette couche de quartz le long du réacteur de façon à ce que elle occupe successivement chacune des positions illustrées sur la figure 1, tout en mesurant la conversion de l'isobutane et les sélectivités à une température de réaction de 620°C. A partir de ce moment nous appellerons température de réaction, la température maximale du réacteur correspondant à la région chaude dont la hauteur vaut 30 mm (voir figure 1).

Lorsque la couche de quartz se trouve dans les positions 4 à 8, la région chaude du réacteur est complètement recouverte.

Les résultats ainsi obtenus, pour un débit du mélange réactionnel de 7000 mL/h ce qui correspond à une vitesse linéaire du gaz de 6 mm/s environ dans la couche de quartz et de 3 mm/s environ dans le volume libre, sont présentés sur la figure 2.

On observe sur la figure 2 qu'avec une conversion de l'isobutane qui dépasse 40%, la transformation de l'isobutane est très importante quelle qu'elle soit la position de la couche de quartz dans le réacteur. Lorsque la couche de quartz se trouve dans les positions de 4 à 8, les conversions sont minimales, les sélectivités pour l'isobutène étant maximales, soit supérieures à 44%. Ceci s'explique par le fait que dans ces situations la région chaude du réacteur est complètement recouverte par la couche de quartz où la vitesse linéaire du gaz est élevée et où les réactions de craquage sont minimisées (figure 2). Au fur et à mesure que la région chaude du réacteur est remplie par la couche de quartz, c'est-à-dire lorsque cette dernière passe de la position 1 à 4, on observe une diminution de la conversion de l'isobutane et une augmentation de la sélectivité pour l'isobutène. En fin, lorsque la couche de quartz découvre la région chaude du réacteur en passant de la position 8 à 11, une variation inverse de la conversion et de la sélectivité pour l'isobutène est observée.

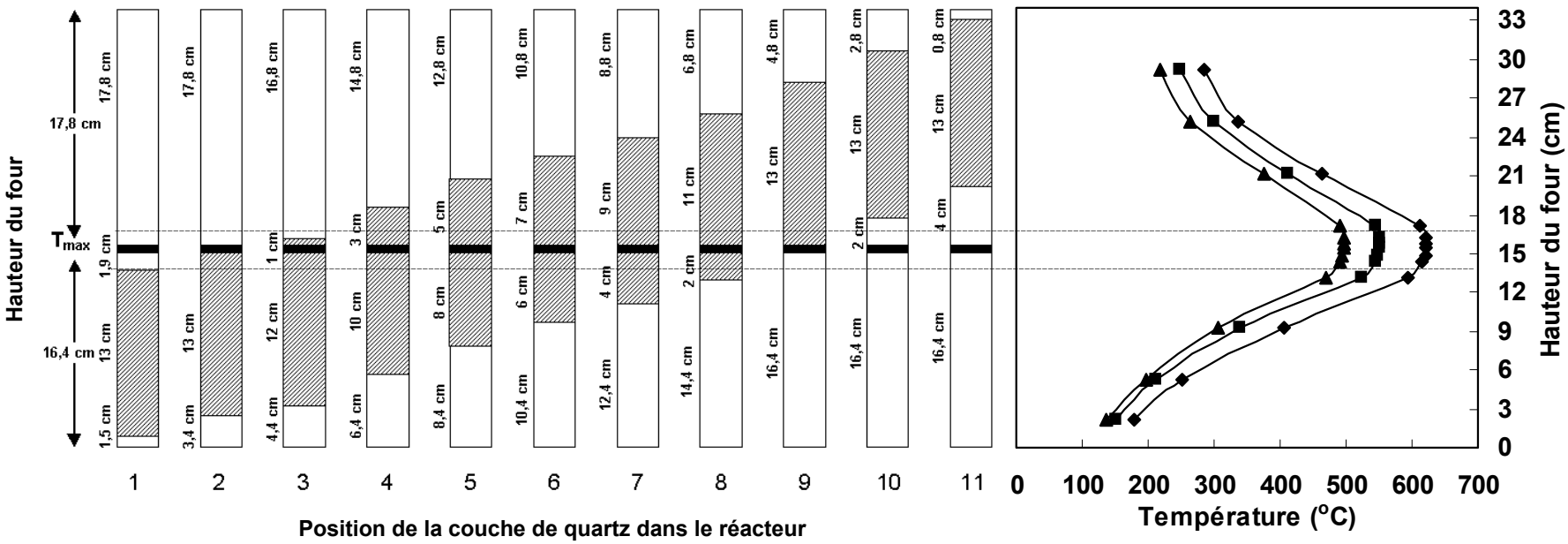

Fig. 1 – Position de la couche de quartz par rapport à la région chaude du réacteur et le profil de température sur la hauteur du réacteur: ◆ – Tmax 620°C, ■ – Tmax 550°C, ▲ – Tmax 500°C (Tmax – température maximale).

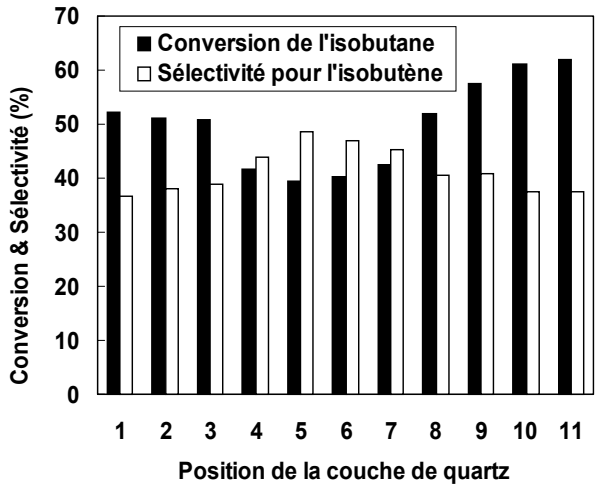

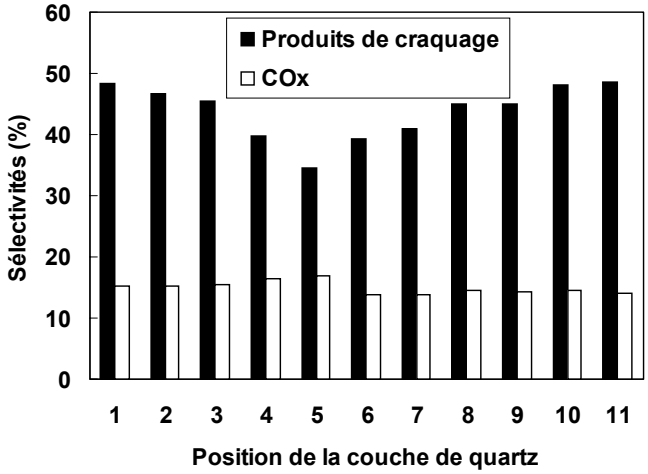

Fig. 2 – Effet de la position de la couche de quartz dans le réacteur sur la transformation oxydante de l'isobutane à 620°C (rapport molaire isobutane/air = 1/2,5, débit du mélange réactionnel 7000 mL/h).

On observe sur cette même figure que le profil de la sélectivité pour produits de craquage est similaire à celui de la conversion ce qui rends compte du fait que responsables pour l'augmentation de la conversion dans le volume libre du réacteur sont les réactions de craquage. D'autre part, le profil de la sélectivité pour oxydes de carbone est similaire à celui de la sélectivité pour l'isobutène ce qui suggère que, lorsque la région chaude est remplie de quartz, les réactions de craquage laisse la place à l'oxydéshydrogénation et à l'oxydation, ce qui a d'ailleurs été observé.[15] Cette modification de la distribution des produits par rapport à la situation où la région chaude était vide, suggère que la surface du quartz modifie les radicaux libres dans une certaine direction.

Comme attendu, une diminution de la température de réaction est accompagnée d'une diminution de conversion et une augmentation de la sélectivité pour l'isobutène aux dépens des produits de craquage. Ces faits peuvent être observés sur la figure 3 où l'effet de la température de réaction sur la transformation de l'isobutane est représenté pour la position 5 de la couche de quartz dans le réacteur. Par contre, la variation de la conversion et la distribution des produits en fonction de la position de la couche de quartz dans le réacteur ne changent pas, comme on peut voir sur la figure 4 où seules la conversion et la sélectivité pour l'isobutène sont représentées pour la réaction à 570°C.

Nous avons étudié l'effet du temps de résidence en modifiant le débit du mélange réactionnel à 620°C. Les résultats obtenus pour la réaction avec la couche de quartz placée de façon à ce qu'elle recouvre totalement la région chaude du réacteur, sont présentés sur la figure 5.

Fig. 3 – Effet de la température de réaction sur la transformation oxydante de l'isobutane lorsque la couche de quartz rempli la région chaude du réacteur: conversion de l'isobutane (■), sélectivités pour isobutène (◆), craquage (●) et oxydes de carbone (▲); (rapport molaire isobutane/air = 1/2,5, débit du mélange réactionnel 7000 mL/h).

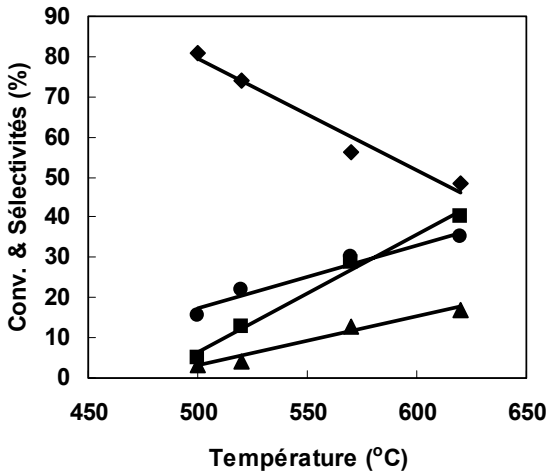

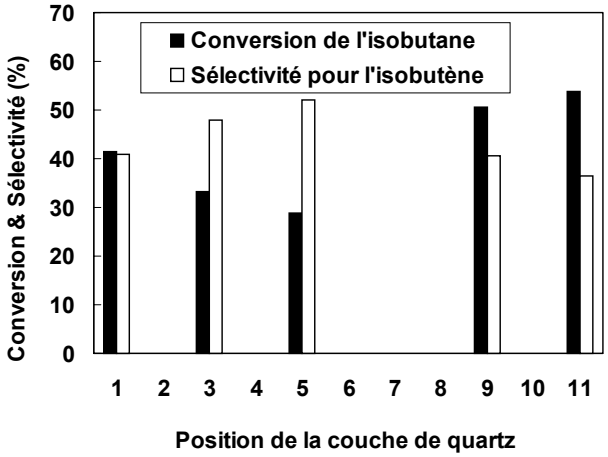

Fig. 4 – Effet de la position de la couche de quartz dans le réacteur sur la conversion de l'isobutane et la sélectivité pour l'isobutène à 570°C (rapport molaire isobutane/air = 1/2,5, débit du mélange réactionnel 7000 mL/h).

Fig. 5 – Effet du débit du mélange réactionnel sur la transformation oxydante de l'isobutane à 620°C lorsque la couche de quartz rempli la région chaude du réacteur: conversion de l'isobutane (■), sélectivités pour isobutène (◆), craquage (●) et oxydes de carbone (▲); (rapport molaire isobutane/air = 1/2,5).

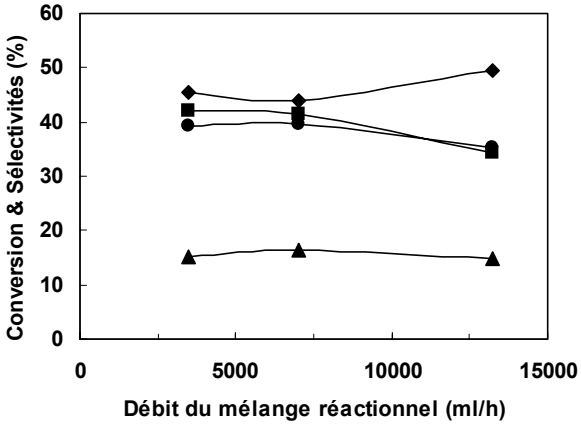

On observe que le temps de résidence, dans le domaine de débits choisi, n'influe pas la réaction d'une manière importante. Ainsi, lorsque le débit passe de 3600 mL/h à 7000 mL/h, la conversion de l'isobutane et la distribution des produits restent pratiquement inchangées. Une faible diminution de conversion accompagnée d'une augmentation de la sélectivité pour l'isobutène aux dépens de la sélectivité pour produits de craquage est observée lorsque le débit du mélange réactionnel passe de 7000 mL/h à 13200 mL/h. Vraisemblablement, la transformation chimique, dans le domaine de débits choisi, est tellement rapide que le temps de résidence des réactifs dans la région chaude du réacteur n'a aucune influence sur celle-ci.

En fin, nous avons comparé les résultats obtenus pour la même vitesse linéaire du gaz, lorsque la région chaude du réacteur est vide et,

respectivement, remplie de quartz. Pour un débit de gaz de 7000 mL/h, la vitesse linéaire du gaz est de 6 mm/s environ dans la couche de quartz et de 3 mm/s environ dans le volume libre. Un débit de gaz de 3600 mL/h nous permet d'obtenir une vitesse linéaire dans la couche de quartz de 3 mm/s et un débit de 13200 mL/h, une vitesse linéaire dans le volume libre de 6 mm/s. Les résultats obtenus sont présentés dans le Tableau 2.

Tableau 2

Comparaison de la transformation oxydante à 620°C, en présence du quartz et dans le réacteur vide dans la région chaude, pour la même vitesse linéaire du gaz.

Vitesse linéaire du gaz (mm/s)	Région chaude	Conversion (%)	Sélectivités (%)		
			Isobutène	Craquage	CO_x
3	vide	62	37,4	48,6	14,0
	avec quartz	43,7	47,9	38,4	13,7
6	vide	58,2	40,0	48,7	11,3
	avec quartz	40,3	46,9	39,2	13,9

Il est bien évident qu'à la même vitesse linéaire du mélange réactionnel dans la région chaude, la présence du quartz a pour effet une diminution de conversion ce qui indique le fait que la surface du quartz termine les processus des radicaux libres. Cette diminution de conversion va de pair avec une augmentation de sélectivité pour l'isobutène aux dépens des produits de craquage.

Étude de l'oxydéshydrogénation et de la déshydrogénation simple dans le réacteur rempli de quartz ayant deux granulométries dans la région chaude

Nous avons étudié la transformation oxydante et non oxydante de l'isobutane avec le réacteur rempli de débris de quartz et avec, dans la région chaude, 2 cm^3 de quartz de granulométrie comprise entre 1 et 1,25 mm, comme schématisé sur la figure 7. Cette couche de quartz fin, dont la porosité vaut 40%, sera, dans les études catalytiques ultérieures, remplacée par une couche de catalyseur de même granulométrie. La transformation oxydante de l'isobutane est négligeable en dessous de 490°C et les résultats obtenus au dessus de cette température pour un débit du mélange réactionnel de 7000 mL/h et un rapport molaire isobutane/air de 1/2,5 (rapport isobutane/oxygène 1/0,5), sont résumés dans le Tableau 3.

Notons que la conversion de l'isobutane est légèrement plus faible et la sélectivité plus élevée que celles observées dans l'expérience où une couche de quartz remplissait seulement la région chaude du réacteur (figure 3). Cette différence est vraisemblablement liée à la granulométrie du quartz placé dans la région chaude.[14, 15] Il est intéressant de remarquer que la transformation de l'isobutane est très importante par rapport à celle du n-butane dans les mêmes conditions,[16] ceci étant probablement due à la différence de réactivité entre les deux alcanes.

Tableau 3

Résultats obtenus pour la transformation oxydante de l'isobutane dans le réacteur rempli de quartz, pour un débit du mélange réactionnel de 7000 mL/h et un rapport molaire isobutane/air de 1/2,5.

Température (°C)	Conversion (%)	Sélectivités (%)			Vitesse de transformation (10^6 mol/s)
		Isobutène	Craquage	CO_x	
490	4,8	83,6	9,2	2,7	1,1
530	12,5	77	19,3	3,7	2,9
570	23,5	69,8	27,7	2,5	5,4
600	28,1	68,7	28,8	2,6	6,5

D'autre part, on observe une forte augmentation de la conversion avec la température, accompagnée d'une diminution de la sélectivité pour l'isobutène au profit des produits de craquage. A des températures élevées, la conversion augmente sans une modification notable de la distribution de produits. A noter que la sélectivité pour l'isobutène reste à un niveau élevé à haute température. La sélectivité pour oxydes de carbone reste à un niveau bas et pratiquement constant dans le domaine de température choisi.

En remplaçant l'air par l'azote, la transformation de l'isobutane change dramatiquement, comme l'on peut observer dans le Tableau 4. Ainsi, on n'observe une conversion mesurable qu'à des températures supérieures à 500°C. La conversion, très faible par rapport à celle obtenue en présence d'oxygène, augmente toujours avec la température et la sélectivité pour l'isobutène, relativement élevée, diminue au profit des produits de craquage.

Tableau 4

Résultats obtenus pour la transformation non oxydante de l'isobutane dans le réacteur rempli de quartz, pour un débit du mélange réactionnel de 7000 mL/h et un rapport molaire isobutane/azote de 1/2,5.

Température (°C)	Conversion (%)	Sélectivités (%)		Vitesse de transformation (10^7 mol/s)
		Isobutène	Craquage	
530	2,3	92	8	5,3
570	3,8	78	22	8,7
600	6,7	68,2	31,8	15,5

Nous avons représenté les droites d'Arrhenius sur la figure 6 et calculé les énergies apparentes d'activation pour la transformation de l'isobutane dans les deux réactions, en présence et en absence de l'oxygène. Les valeurs obtenues sont 21,6 kcal/mol et, respectivement, 20,9 kcal/mol, donc pratiquement les mêmes. Ce résultat nous suggère que l'étape déterminant la vitesse est identique dans les deux cas, probablement la rupture homolytique de la première liaison C – H.

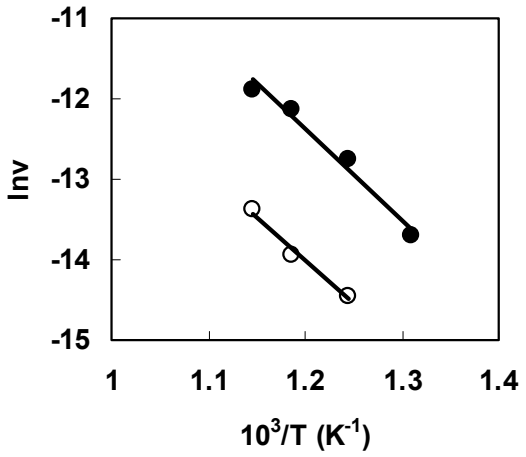

Fig. 6 – Droites d'Arrhenius pour la transformation oxydante (●) et non oxydante de l'isobutane (○).

EXPERIMENTAL

Les réactions ont été effectuées à la pression atmosphérique, dans un réacteur tubulaire en quartz placé dans un four, en utilisant un courant descendant du mélange réactionnel. Le diamètre intérieur du réacteur est de 29 mm, le diamètre extérieur de l'étui pour thermocouple est de 8 mm et la hauteur du four 342 mm. Le schéma du réacteur utilisé est présenté sur la figure 7.

Le mélange réactionnel est constitué de l'isobutane et d'air ou de l'isobutane et d'azote pour l'étude de la déshydrogénation simple. Les débits ont été contrôlés par des valves fines et mesurés, à la température ambiante, avec des débitmètres capillaires. La température de réaction a été mesurée avec un thermocouple chromel-alumel placé dans un étui centré dans la zone de température maximale, le profil de température en réacteur, en l'absence dés réactifs, étant présenté sur la figure 1. La température du four a été contrôlée avec un thermocouple chromel-alumel fixé à l'extérieur du réacteur.

Le réacteur est chauffé de la température ambiante à la température désirée avec une vitesse de 10°/min sous courant de réactifs. Après une heure environ de stabilisation à la température de réaction, la première analyse des produits est faite. Le rapport molaire air/isobutane est égal à 2,5 (rapport oxygène/isobutane 0,5) et la température de réaction varie de 450 à 620°C. Trois valeurs du débit du mélange réactionnel ont été choisis: 3600, 7000 et 13200 mL/h. Les produits de réaction observés sont isobutène, produits d'oxydation totale, soit CO et CO_2, et produits de craquage, soit éthane, éthylène, méthane et propène. Ils ont été analysés par chromatographie en phase gazeuse. Les bilans carbone sont supérieurs à 96 %.

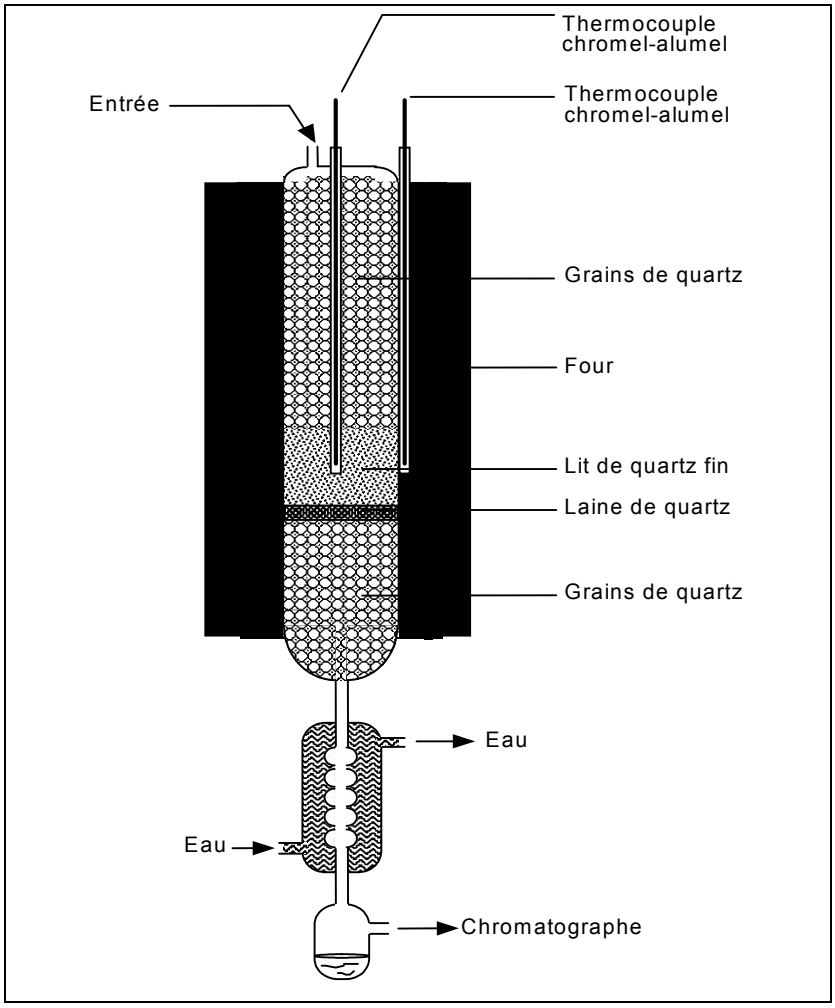

Fig. 7 – Schéma du réacteur utilisé.

Le calcul de la conversion et des sélectivités a été effectué de la façon suivante:

Conversion de l'isobutane:

$$C\,(\%) = \frac{\sum_i n_i C_i}{4\,C_4 + \sum_i n_i C_i} \times 100$$

Où n_i = nombre d'atomes de carbone dans le produit *i*,
C_i = concentration du produit *i* dans l'effluent,
C_4 = concentration de l'isobutane dans l'effluent.

Sélectivité d'un produit *i*:

$$S_i\,(\%) = \frac{n_i C_i}{\sum_i n_i C_i} \times 100$$

CONCLUSION

Les conclusions de cette étude peuvent être résumées de la manière suivante:

La transformation oxydante de l'isobutane en phase gazeuse homogène est très importante à des températures supérieures à 500°C, avec des sélectivités élevées pour l'isobutène.

Lorsque la région chaude du réacteur est remplie de quartz, la transformation oxydante de l'isobutane diminue avec une augmentation de la sélectivité pour l'isobutène, mais reste à un niveau élevé contrairement à ce qui a été rapporté dans la littérature.[15]

La surface du quartz termine les processus des radicaux libres, d'une part, et modifie les radicaux libres dans une certaine direction, d'autre part.

La déshydrogénation simple de l'isobutane en présence du quartz n'est observée qu'à des températures supérieures à 500°C.

Les énergies apparentes d'activation pour les transformations oxydante et non oxydante de l'isobutane en présence du quartz sont identiques ce qui suggère que l'étape déterminante de vitesse

et la même dans les deux réactions, soit la rupture homolytique de la première liaison C – H.

BIBLIOGRAPHIE

1. H. H. Kung, *Adv. Catal.*, **1994**, *40*, 1.
2. E. A. Mamedov et V. Cortés-Corberán, *Appl. Catal. A*, **1995**, *127*, 1.
3. M. M. Bettahar, G. Costentin, L. Savary et J. C. Lavalley, *Appl. Catal. A*, **1996**, *145*, 1
4. M. A. Bañares, *Catal. Today*, **1999**, *51*, 319.
5. F. Cavani et F. Trifirò, *Catal. Today*, **1999**, *51*, 561.
6. B. Grzybowska-Swierkosz, *Topics Catal.*, **2000**, *11/12*, 23.
7. F. Cavani et F. Trifirò *dans* R. K. Grasselli, S. T. Oyama, A. M. Gaffney, J. E. Lyons (Eds.), "Third World Congress on Oxidation Catalysis", *Stud. Surf. Sci. Catal.*, **1997**, *110*, 19.
8. J. Haber *dans* R. K. Grasselli, S. T. Oyama, A. M. Gaffney, J. E. Lyons (Eds.), "Third World Congress on Oxidation Catalysis", *Stud. Surf. Sci. Catal.*, **1997**, *110*, 1.
9. H. H. Kung, *Ind. Eng. Chem. Prod. Res. Dev.*, **1986**, *25*, 171.
10. G. Busca, E. Finocchio, G. Ramis et G. Ricchiardi, *Catal. Today*, **1996**, *32*, 133.
11. Kirk-Othmer, "Encyclopedia of Chemical Technology" vol. 13, John Wiley & Sons, 1995, p. 682.
12. D. J. Driscoll, K. D. Campbell et J. H. Lunsford, *Adv. Catal.*, **1987**, *35*, 139.
13. M. Y. Sinev, L. Y. Margolis et V. N. Korchak, *Uspekhi Khimii (Russ. Chem. Rev.)*, **1995**, *64*, 373.
14. M. Y. Sinev, L. Y. Margolis, V. Y. Bychkov et V. N. Korchak, *dans* R. K. Grasselli, S. T. Oyama, A. M. Gaffney, J. E. Lyons (Eds.), "Third World Congress on Oxidation Catalysis", *Stud. Surf. Sci. Catal.*, **1997**, *110*, 327.
15. V. P. Vislovskiy, T. E. Suleimanov, M. Y. Sinev, Y. P. Tulenin, L. Y. Margolis et V. Cortés Corberán, *Catal. Today*, **2000**, *61*, 287.
16. I. C. Marcu, A. Urdă et I. Săndulescu, *Anal. Univ. Buc. – Chimie*, **2005**, *XIV*, 57.

Revue Roumaine de Chimie, **2007**, *52*(3), 293–297

QSAR STUDY FOR CLASSES WITH A BROAD RANGE OF BIOLOGICAL ACTIVITY USING ELECTRONEGATIVITY DESCRIPTORS FOR OMO – UMO QUANTUM STATES. CLOTRIMAZOLE IMIDAZOLE DERIVATIVES WITH ANTIFUNGAL ACTIVITY

Paul Gabriel ANOAICA[a*] and Costinel I. LEPĂDATU[b]

[a]Faculty of Pharmacy, University of Medicine and Pharmacy Craiova, 1 Mai nr. 66, cod 200638
[b]Institute of Physical Chemistry "I. Murgulescu", Romanian Academy, Sp. Independentei 202, 060021, Bucharest, Roumania

Received August 4, 2006.

The class of clotrimazole imidazole derivatives having a broad spectrum of antimycotic activity has been studied using fingerprint descriptors based on electronegativity of the occupied molecular orbitals (OMO) and unoccupied molecular orbitals (UMO).
The Hansch equation $Kd = a_0 + a_1X_1$, where X_1 = OMO / UMO electronegativity allows us to identify the nature of the atoms involved in ligand (drug) – receptor interactions, as well as the nature of those interactions.

INTRODUCTION

The QSAR studies are usually performed[1] in order to obtain a linear equation $A = a_0 + \Sigma_k a_k X_k$ (Hansch equation) between the biological activity "A" values for a class of molecules and the descriptors X_k representing their chemical structures. Such an equation is useful for CADD (Computer Assisted Drug Design) techniques, where new candidates with predictable "A" activity can be designed by chemical modulation.

Due to the linear form of the Hansch equation, the molecules from a class must have their activity "A" comprised in a reasonable domain of values. The molecules from the class are chosen in such a way that their chemical structures do not differ too much.

The aim of the present paper is the study of a class of drugs having on one hand quite different chemical structures and on the other hand a broad range o values for their biological activity. As we shall see in the following, the use of fingerprint - descriptors for the valence shell of the molecules (electronegativity, hardness) allows us to get information regarding the nature of interactions taking place between ligand (drug) and biological receptor. In addition, the descriptors presented in this paper allow the identification of the atoms contributing to these interactions. The localization of these atoms on each chemical structure makes possible the identification of those molecular fragments or chemical groups which are involved in the biological response. A new way in CADD technique can be opened for the design of chemical structures incorporating the found fragments or chemical groups.

RESULTS AND DISCUSSION

For the set of 22 clotrimazole derivatives, their antifungal activity (see Table 1) by inhibition of the P450 enzyme is already known.[2]

As may be seen in Table 1, the activity –logKd assumes very broad range of values comprised between –logKd = 7.7 – 4.6 (*i.e.* Kd= 20 – 25,000 nM). The chemical structures of these derivatives are quite different.

The chemical structures contained in Table 1 have been modelled and their molecular geometries optimized using the Molecular Mechanics (MM+) and MOPAC 7 [3] packages. The descriptors have been obtained using original programs and the output data from quantum molecular ab initio calculations using GAMESS (RHF, STO 6, MP=4).[4]

* Corresponding author: gabriel@umfcv.ro

Table 1

The antifungal activity of 22 clotrimazole derivatives

Derivative	R_1	R_2	R_3	$-\log K_d$
1a	Cl	H		7.1549
1c	Cl	CH_3		5.9208
2a			OH	6.2840
3a			NH_2	6.0000
3e			$NHCOCH_3$	5.9208
3h			$NHNONH_2$	5.3010
3m			$CH(COOC_2H_5)_2$	6.3979
5a	o-Cl			7.2218
5b	o-Fl			7.1549
5c	p-Cl			6.1249
5d	p-Fl			6.0969
6a	H	H	H	5.6021
6b	o-Cl	H	H	7.6990
6c	o-Fl	H	H	7.3979
6d	p-Cl	H	H	7.0458
6e	p-Fl	H	H	6.6990
6f	o-CF_3	H	H	5.4202
6g	p-CF_3	H	H	5.8239
6h	o-Cl	CH_3	H	5.9586
6i	o-Cl	CH_3	CH_3	4.9208
6j	o-Cl	CF_3	H	5.6990
6k	o-CF_3	CF3	H	4.6021

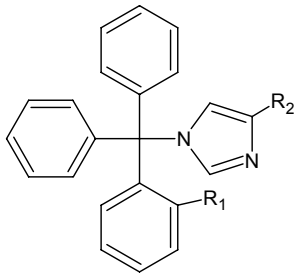

1a-c

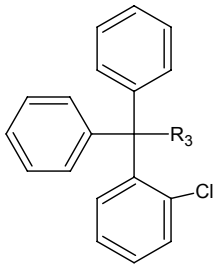

2a, 3a, 3e, 3h, 3m

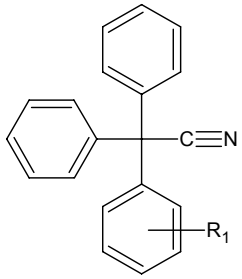

5a-d

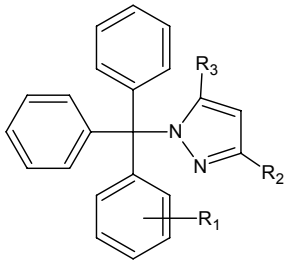

6a-k

The fingerprint descriptors used in this paper regard the valence shell of the molecule, i.e. OMO (Occupied Molecular Orbitals) and UMO (Unoccupied Molecular Orbitals).

The OMO and UMO quantum states are characterized (LCAO approach) by the molecular orbitals $\Psi_i = \sum_j c_{ij}\varphi_j$ built from atomic orbitals φ_j, c_{ij} being their mixing coefficients. These molecular wavefunctions are useful to calculate the partition of the electron population as well as the electric charges on atoms in the molecule. One may in this way calculate the molecular electronegativity EL_i from the contribution of each atom to the corresponding quantum state (atomic electronegativity χ_j, weight p_{ij}), according to the expression:

$$EL_i = \langle \Psi i | \mathbf{EL} | \Psi_i \rangle = \sum \chi_j p_{ij} \quad (1)$$

The atomic electronegativity can be estimated from the following formulas derived from the Slater Type Orbitals and the Parr's definition of the atomic electronegativity[5]:

$$\chi(Q) = \chi_0 + \eta(Q)Q \; ; \; \eta(Q) = \eta_0 + \frac{3}{2}\frac{b^2 Q}{n^2}, \quad (2)$$

where Q is the electric charge of the atom in molecule, "n" the principal quantum number and b= 0.3 a screening constant. Formulas 1 and 2 allow us to define the following fingerprint descriptors:

For OMO states: OELN = $\sum_i^{occ} EL_i$ is the electronegativity of all OMO states.

As one can see, OELN = OELAT + OELH, where OELAT represents the sum of all electronegativities of the "heavy" atoms, other than the hydrogen ones and OELH the contributions of the hydrogen atoms. In the same way, OELAT = OEC + OEO + OEN + OEX, where the four terms represent the contributions to OELAT from different heavy atoms: OEC (carbon), OEO (oxygen), OEN (nitrogen) and OEX the contribution of the heavy atoms other than C, O and N.

For UMO states: LELN = $\sum_i^{unocc} EL_i$ is the electronegativity of the UMO quantum states. One may define in the same way the following quantities:

LELN = LELAT + LELH, where LELAT = LEC + LEO + LEN + LEX, the meaning of these quantities being the same as for OMO states substituting the prefix O by L.

The use of these descriptors in the QSAR analyses can give valuable information about the nature of the atoms involved in ligand (drug) – receptor interaction. The values of these descriptors summarized in Table 4, have been estimated from MOPAC and GAMESS outputs by using our own programs.

Table 2

OMO electronegativity descriptors

Derivative	-logKd	OELN	OELAT	OELH	OEC	OEN	OEX
1a	7.1549	141.229	81.373	59.856	65.108	9.534	6.731
1c	5.9208	151.586	84.523	67.063	68.257	9.557	6.710
2a	6.2840	121.111	68.246	52.865	56.965	0.000	6.706
3a	6.0000	124.259	67.712	56.548	56.741	4.344	6.627
3e	5.9208	142.564	78.905	63.659	63.274	4.296	6.919
3h	5.3010	140.389	80.283	60.105	60.382	8.827	6.742
3m	6.3979	193.180	104.589	88.591	79.751	0.000	6.649
5a	7.2218	120.433	71.044	49.390	59.941	4.347	6.756
5b	7.1549	122.715	73.315	49.400	60.277	4.345	8.693
5c	6.1249	120.318	70.938	49.380	59.965	4.333	6.640
5d	6.0969	122.610	73.239	49.371	60.223	4.338	8.678
6a	5.6021	138.044	74.593	63.452	65.338	9.255	0.000
6b	7.6990	141.209	81.305	59.904	65.340	9.247	6.717
6c	7.3979	143.467	83.567	59.900	65.630	9.255	8.682
6d	7.0458	141.116	81.226	59.891	65.334	9.246	6.645
6e	6.6990	143.401	83.520	59.881	65.594	9.249	8.678
6f	5.4202	163.667	103.789	59.877	69.328	9.128	25.334
6g	5.8239	163.711	103.838	59.873	69.267	9.233	25.338
6h	5.9586	151.518	84.416	67.102	68.475	9.230	6.710
6i	4.9208	161.808	87.512	74.296	71.576	9.214	6.723
6j	5.6990	167.208	110.845	56.364	69.152	9.652	32.040
6k	4.6021	189.710	133.373	56.337	73.109	9.572	50.691

Table 3

The values of UMO electronegativity descriptors

Derivative	-logKd	LELN	LELAT	LELH	LEC	LEN	LEX
1a	7.1549	145.348	69.046	76.302	61.991	5.992	1.063
1c	5.9208	155.553	72.216	83.337	65.146	6.015	1.055
2a	6.2840	123.931	57.186	66.745	54.902	0.000	1.053
3a	6.0000	127.443	57.936	69.507	54.389	2.524	1.023
3e	5.9208	143.821	66.055	77.766	61.296	2.477	1.134
3h	5.3010	139.552	65.913	73.640	58.559	5.182	1.067
3m	6.3979	190.565	84.778	105.787	78.878	0.000	1.032
5a	7.2218	123.241	61.357	61.884	57.759	2.526	1.072
5b	7.1549	123.834	62.054	61.780	58.408	2.525	1.121
5c	6.1249	123.323	61.336	61.987	57.794	2.513	1.028
5d	6.0969	124.002	61.928	62.074	58.296	2.518	1.114
6a	5.6021	148.216	68.163	80.053	62.390	5.773	0.000
6b	7.6990	145.046	69.211	75.835	62.395	5.759	1.058
6c	7.3979	145.727	69.845	75.882	62.959	5.771	1.116
6d	7.0458	145.152	69.175	75.977	62.385	5.759	1.030
6e	6.6990	145.839	69.762	76.077	62.885	5.762	1.114
6f	5.4202	152.148	76.030	76.118	67.380	5.592	3.058
6g	5.8239	152.222	76.071	76.152	67.274	5.737	3.060
6h	5.9586	155.306	72.311	82.994	65.525	5.732	1.055
6i	4.9208	165.625	75.369	90.257	68.580	5.729	1.059
6j	5.6990	148.948	77.407	71.541	67.132	6.164	4.111
6k	4.6021	156.043	84.228	71.816	72.054	6.048	6.125

These descriptors have been individually correlated with -lokKd, according to the linear equation $-\log Kd = a_0+a_1X_1$. We can identify in this way the contribution of OMO – UMO electronegativities to the formation of the biological response. The regression data are summarized in Table 4, where $R^2\%$ is the correlation coefficient of the regression.

Table 4

Regression data for OMO- UMO electronegativities

Descriptor X_1:	$-\log Kd = a_0 + a_1X_1$	$R^2\%$
OELN	8.83 - 0.0180 OELN	21.1
OELAT	8.27 - 0.0242 OELAT	23.0
OELH	7.31 - 0.0185 OELH	4.1
OEC	9.08 - 0.0439 OEC	8.9
OEN	6.50 - 0.0417 OEN	2.6
OEX	6.60 - 0.0342 OEX	23.1
LELN	8.34 - 0.0148 LELN	8.6
LELAT	9.04 - 0.0409 LELAT	14.2
LELH	7.36 - 0.0153 LELH	3.6
LEC	9.14 - 0.0466 LEC	10.6
LEN	6.48 - 0.0640 LEN	2.5
LEX	6.66 - 0.292 LEX	23.1

As may be seen in Table 4, the total electronegativity OELN (21.1%) of the quantum states occupied with electrons (OMO) participate to a greater extent to the activity -logKd, than that of the unoccupied quantum states (UMO), LELN (8.6%). The result pleads for the existence of electrostatic interactions between ligand and receptor, inasmuch the electric charges of the atoms are due to the partition of the electron population on the OMO states.

Because the hydrogen atoms contribute almost equally in OMO and UMO states to –logKd

(OELH: 4.1%, LELH: 3.6%), the difference between OELN and LELN contributions must be due to the heavy atoms. Indeed, as may be seen in Table 4, the contribution of all heavy atoms to –logKd is different (OELAT: 23.0%, LELAT: 14.2%).

If the heavy atoms are taken separately, their contribution to -logKd is in the order: N: LEN (2.5%), OEN (2.6%); C: LEC (10.6%), OEC (8.9%); X= (halogen atoms, Figure 1): LEX (23.1%), OEX (23.1%).

Note that the halogen atoms have a significant and almost equal contribution to the biological activity: LEX (23.1%) ≈ OEX (23.1%). This result reveals the nature and the contribution of these atoms from the molecular quantum states able to donate (OMO) or to accept (UMO) electronic densities during their interactions with the receptor.

Such information can be helpful for rational drug design by chemical modulation of new chemical structures. The QSAR analysis performed using fingerprint descriptors herein presented allows the identification and localization of those atoms involved in the drug – receptor interaction. One may identify those fragments or chemical groups responsible for the biological activity. These groups or molecular fragments can be used to "build" new chemical structures with predictable activity.

REFERENCES

1. C. Hansch and A. Lec, "Exploring QSAR: Fundamentals and Applications in Chemistry and Biology", American Chemical Society, 1995.
2. H. Wulff, M. J. Miller, W. Hansel, S. Grissmer, M. D. Calahan and K. G. Chandy, *Proc. Natl. Acad. Sci. U.S.A.*, **2000**, *97*, 8151.
3. MOPAC 7.0 for UNIX, Quantum Chemistry Program Exchange, Project 688.
4. M. W. Schmidt, K. K. Baldrige, J. A. Boatz, S. T. Elbert, M. S. Gordon, J. H. Jensen, S. Koseki, N. Matsunaga, K. A. Nguyen, S. J. Su, T. L. Windus, M. Dupuis and J. A. Montgomery, *J. Comput. Chem.*, **1993**, *14*,1347.
5. C. I. Lepădatu, *Rev. Roum. Chim.*, **1985**, *30*, 111.

Revue Roumaine de Chimie, **2007**, *52*(3), 299–300

NOTE

QUANTUM CHEMISTRY COMPUTATION OF STABILITY CONSTANT OF COBALTHEXAMINE ION IN AQUEOUS SOLUTION. AN ATTEMPT

Ludovic SAYTI, Valentin CAREJA, Simona MUNTEAN, Ramona TUDOSE*, Otilia COSTIŞOR and Zeno SIMON

Institute for Chemistry Timişoara of Romanian Academy, 24 M. Viteazu Bv., RO-300223, Timisoara, Roumania, Tel: +40-256-491818; fax: +40-256-491824;

Received August 3, 2006

Free enthalpy for formation of the cobalthexamine cation in aqueous solution was calculated by an ab initio method at the 3-21G level, with a polarisable continuum method (BemCalc) for hydration free enthalpies. The calculated ΔG = -21.25 kcal/mol compares favourably with ΔG = -31.8 kcal/mol from the experimental stability constant.

Computation of stability constants for transition metal complexes imply calculations of in vacuo formation energies of participants to the corresponding equilibrium, of hydration energies and of various entropy effects. Here we attempt to compute the ΔG corresponding to the stability constant of cobalthexamine cation in aqueous solution, i.e. to the equilibrium:

$$Co(OH_2)_6^{3+} + 6\ NH_3 \rightleftharpoons Co(HN_3)_6^{3+} + 6\ H_2O \quad (1)$$

The experimental value of the stability constant (25^0C),[1] K = 1.34 . 10^{23}, corresponds to ΔG = -31.8 kcal/mol for the abovementioned equilibrium. Ab initio method at the 3-21G level[2] was used for internal energy calculations of the participants and the BemCalc method[3-6] for hydration free energies; the last yields good results for higher valence cation hydrations.

Although modern computational chemistry methods are rather successful in calculation of molecular stability and hydration effects, applications to stability constants of complex ions are rather rare. Stabilities of cobalt complexes were evaluated with a second order perturbational method based upon calculated electronic energy levels,[7] solvation of metal complexes was discussed on hand of relativistic effects in ZDO methods,[8] and, more recently, DFT-methods were used to calculate stability of spin states for some Co(II)- complexes.[9]

METHODS

Internal energies, U_i, of the participants to equilibrium (1) are calculated by an ab initio method at the 3-21G level[2]. These U_i values, listed in kcal/mol in Tab. 1, are energies of formation out of free nuclei and electrons (at 0^0K).

Hydration energies, G_i, were calculated by the BemCalc method[3-6] with a dielectric constant D_{ext} = 78.5 for the exterior polarisable continuum (water) and D_{int} = 4 for the polarising particles. Geometries, for BemCalc, are these calculated by our ab initio method, with Van der Waals radii 1.20Å, 1.54 Å and 1.40 Å for the H, N and O atoms[10.11] and 0.61 Å, 0.645 Å for the Co^{3+} and Fe^{3+} cations. These central cations are actually not in direct contact with the polarisable continuum.

No corrections for zero point energies or translational, rotational and vibrational entropy effects were performed. As numbers of particles on both sides equilibrium (1) are equal and their

* Corresponding author: ramona_tudose@yahoo.com

structures similar, such corrections are expected largely to cancel. The ΔG for equilibrium was equated to the algebric sums of internal energies, ΔU_i, and hydration free enthalpies, ΔG_i^h:

$$\Delta G = \Delta U_i + \Delta G_i^h \quad (2)$$

Table 1

Results of internal energy and hydration free enthalpy calculations

Particle	ΔU_i	ΔG_i^h
H_2O	-47430.90	**-8.915**
NH_3	-35060.00	**-1.600**
$Co(NH_3)_6^{3+}$	-1072481.05	**-428.81**
$Co(H_2O)_6^{3+}$	-1146688.33	**-467.59**
$Fe(NH_3)_6^{3+}$	-998207.41	**-423.60**
$Fe(H_2O)_6^{3+}$	**-1072416.07**	**-464.22**

U_i - internal energies (vacuum), G_i^h - hydration free enthalpies, kcal/mol

RESULTS

According to equation (2) and Tab. 1, the result for equilibrium (1) is ΔG = -21.25 kcal/mol which compares favourably to the experimental ΔG = -38.8 kcal/mol. For the corresponding equilibrium for the, unstable in water, ferihexammine cation $Fe(NH_3)_6^{3+}$, the computed value, ΔG = -18.03 kcal/mol, yields an about 200 times lower predicted stability constant than for the stable cobalthexamine cation.

For the in vacuo dissociation, $ML_6^{3+} \leftrightarrow M^{3+}$ + 6 L, our ab initio 3-21G computations yield 847.8 kcal/mol for $Co(NH_3)_6^{3+}$ and 822.4 kcal/mol for $Fe(NH_3)_6^{3+}$. The difference, 24.5 kcal/mol is in agreement with expectation for both electrostatic effect (smaller radius for Co^{3+} than for Fe^{3+}) and the classic ligand field effect (Co^{3+} - d^6 electronic structure, Fe^{3+} - d^5 electronic structure).

CONCLUSIONS

The calculated free enthalpy, ΔG, for the stability constant of $Co(NH_3)_6^{3+}$ in aqueous solution compares favourably with the ΔG corresponding to the experimental stability constant, albeit the rather low degree of sophistication of our theoretic calculations. This encourages us to develop more exact methods for such computations, including the zero point energy and entropy corrections.

Acknowledgements: are due to Dr. M. Mracec, from our institute, for the permission to use the HyperChem™ Release 5.11.

REFERENCES

1. J. A. Plambeck, "Chemical" Data Tables. Stability constants of aqueous complex ions, 1996, http:/www.ualberta.ca/~jplambeck/che/data/p00408.htm
2. HyperChem™ Release 5.11 Professional for Windows, Hypercube, Inc. 1999, Gainsville FL, USA, www.hyper.com
3. E. D. Purisima and S. H. Nilar, *J. Comput. Chem*., **1995**, *16*, 681.
4. E. D. Purisima, *J. Comput. Chem*., **1998**, *19*, 494.
5. S. L. Chan and E. O. Purisima, *J. Comput. Chem*., **1998**, *19*, 1268.
6. T. L. Sulea and E. O. Purisima, *J. Phys. Chem*., **2001**, *105*, 889.
7. V. E. Sahini, V. Tufoi and A. Ivanov, *Rev. Roum. Chim*., **1972**, *17*, 617.
8. R. Boca, *Internat. J. Quant. Chem*., **1988**, *33*, 159.
9. A. M. SchmiedeKamp, M. D. Ryan and R. J. Deetk, *Inorg. Chem*., **2002**, *41*, 5739.
10. Y. Marcus, *Chem. Rev*., **1988**, *88*, 1475-1498.
11. ISPT Periodic Table, http:/www.qivx.com/ispt/ptw_st.php